ACCELERATED TESTS OF ENVIRONMENTAL DEGRADATION IN COMPOSITE MATERIALS

by

Tom George Reynolds

B.Eng (Hons), Aeronautical Engineering
University of Bristol, United Kingdom (1995)

Submitted to the Department of Aeronautics and Astronautics
in Partial Fulfillment of
the Requirements for the Degree of

Master of Science
in Aeronautics and Astronautics

at the

Massachusetts Institute of Technology

September 1998

Signature of Author_____
Department of Aeronautics and Astronautics
14 August 1998

Certified by_____
Professor Hugh L. McManus
Associate Professor
Thesis Supervisor

Accepted by_____
Jaime Peraire
Associate Professor
Chairman, Department Graduate Committee

ACCELERATED TESTS OF ENVIRONMENTAL DEGRADATION IN COMPOSITE MATERIALS

by

Tom G. Reynolds

Submitted to the Department of Aeronautics and Astronautics
on 14 August 1998 in Partial Fulfillment of the Requirements for the
Degree of Master of Science in Aeronautics and Astronautics

ABSTRACT

High temperature polymer matrix composites are key candidates for the structural components of proposed supersonic transport aircraft. The operational environment of these vehicles exposes the airframe to harsh conditions, including temperature extremes and moisture. These environments have been seen to cause visible damage in polymer matrix composites in timescales much less than the lifetime of the vehicle. Therefore, there is an urgent requirement for accelerated testing of the key components of the environment. A first step to this goal is to identify the components of the environment responsible for the damage. The effects of a realistic moisture and thermal environment on two high temperature polymer matrix composites (PETI-5 and PIXA-M) have been investigated in this work. An extensive test program was developed to test the response of the materials to this baseline environment and its individual components: time at moisture, moisture cycling, time at temperature and thermal cycling. Mechanism-based models were used to design accelerated moisture cycles and acceler ed thermal cycles in an attempt to speed up the response to these environmental factors. These accelerated cycles were also used in the test program. The results showed visible damage in the form of cracking in both materials. The PIXA-M material was found to show more damage than the PETI-5. Cracking was confined to a thin layer of material next to the exposed edge. This suggests that the environmental exposure is reducing the effective fracture toughness of the material in this layer more than in the interior. Analysis suggests that this layer is exposed to more of the environmental components and fluctuations than the material in the interior. The individual components of time at moisture and thermal cycling were seen to cause cracking, while time at temperature did not, and moisture cycling did not appear to accelerate moisture damage. The combined environments in the baseline cycle caused more damage than any one component of the cycle on its own. Evidence points to the combined effects of time at moisture and thermal cycling as being the dominant parameters causing damage, while moisture cycling controls the extent of the damaged region. Although the designed accelerated cycles were not successful in accelerating the damage from the baseline cycle, they were instrumental in establishing what *were* the dominant parameters. It is suggested that a promising way of accelerating the damage observed under the realistic conditions is by combining an isomoisture environment with a cyclical stress environment, which can be achieved either thermally or mechanically.

Thesis Supervisor: Hugh L. McManus
Title: Associate Professor
Department of Aeronautics and Astronautics
Massachusetts Institute of Technology

ACKNOWLEDGEMENTS

It is not often that you are forced to sit down and think about who you want to thank when work such as this is complete. It was only when I did that I realised just how many people have influenced and supported me, both professionally and personally. This is my humble attempt at recording my gratitude to those people.

Firstly, I would like to thank my advisor, Prof. Hugh McManus. He has an enviable ability to find the important results in a sea of data and always pointed me in the right direction. I will also be eternally grateful to him for having the faith to hire me as a Research Assistant in TELAC two years ago, which provided the financial support which enabled me to come to MIT. My sincere thanks to Prof. Paul Lagace and Prof. Mark Spearing for their constructive inputs to my work and for always supporting me in my educational endeavours. It means a great deal to have two people I admire so much on my side. Thanks also to Prof. Carlos Cesnik and Prof. John Dugundji for always finding the right questions to ask during presentations (or the wrong ones if you are the one having to answer!) and for their support. Of course, I am also extremely grateful to Deb for all her help (and wise comments!) and to Ping for making sure my accounts were in order.

It is often said that UROPs are key elements of many of the research programs here at MIT. My UROPs were no exception and it has been a privilege to work with four extremely bright people. In the early days, Phil Ogston toiled for hours on the polishers to track the progress of damage. Ryan Peoples counted about as many cracks as I did and, believe me, that's too many for any sane person! In the latter stages of the work, I was very ably assisted by Thad Matuszeski, who has a unique ability to solve any problem you throw at

him. The final round of testing and the really fun job of preparing this thesis was made a whole lot more pleasant and efficient thanks to the help of Kim Murdoch. My sincerest gratitude goes to them all.

My thanks to Eric Sager of The Boeing Company in Renton for being my point of contact and coordinating the testing conducted there. It made my job a whole lot easier. Thanks are also due to Ron Zabora at Boeing for his support in this work. Invaluable technical assistance was provided primarily by John Kane of TELAC. Thanks also to Lenny Rigione of DMSE and Don Weiner of the Aero/Astro workshop.

Before I came to MIT, I was told that the people I would meet would be as important as the technical knowledge that I gained. And so it has turned out to be. Thanks to all the graduate students in TELAC for creating a very friendly atmosphere in the lab. Particular thanks go to my 'second big sister' Lauren for always lending me an ear for my whining (and pretending to care!) and to my throwing buddy Mike. Maybe one day I'll be able to throw a consistent tight spiral. In the greater Aero/Astro community I have made some good friends. But I particularly look forward to 'working' with Cyrus and Paulo over the next x years (x=3??) since we all went through the hell they call the Doctoral Qualifying exam and managed to come out the other side smiling.

Finally, none of this would have been possible without the love and support of my family. My brother Jim and sister Kate have always blazed a trail for me to follow and taught me that second best was never good enough. There are not enough words to express my gratitude and love to my parents. They have sacrificed so much to enable their children to have the best possible opportunities in life. This is all thanks to them.

FOREWORD

This work was conducted in the Technology Laboratory for Advanced Composites (TELAC) of the Department of Aeronautics and Astronautics at the Massachusetts Institute of Technology.

The program manager for the funding was Ron Zabora of the High Speed Civil Transport Structures Group, The Boeing Company, Renton, WA, and was conducted under the Hygrothermal Microcracking Research Program.

Partial financial assistance for the academic year 1996/7 was provided by a Fulbright Scholarship sponsored by the British-American Foundation of the British-American Chamber of Commerce. Their support is gratefully acknowledged.

TABLE OF CONTENTS

LIST OF FIGURES

LIST OF TABLES

NOMENCLATURE

CLPT	Classical Laminated Plate Theory
HSCT	High Speed Civil Transport
HSR	High Speed Research
PMC	Polymer Matrix Composite
a	thicknesses
A	constant fit to data
A_{ni}	amplitude of each mode at time i
c	(subscript) cracking ply group
$C_o(z)$	initial state of moisture through laminate
C_{eq}	internal equilibrium moisture concentration
C_m	concentration of moisture in laminate
$C_\infty(t)$	ambient far field condition of moisture concentration
d	depth of 'thrashed zone'
D	moisture diffusivity
$D_{ij}^{\ m}$	anisotropic diffusivity tensor for moisture
$D_o^{\ m}$	moisture diffusivity constant
$D_z^{\ m}$	component of moisture diffusivity corresponding to z
e	depth from exposed edge
f	material constant
g	material constant
G_c	effective critical strain energy release rate (toughness)
G_o	initial toughness
h	thickness of laminate
E	material stiffness in x' direction
$E_A^{\ m}$	moisture activation energy
l	length of exposed depth gage
n	index of the mode
N	number of cycles
o	(subscript) entire laminate
r	(subscript) smeared properties of the laminate
R	universal gas constant
RH	relative humidity
T	absolute temperature
T_o	stress free temperature
x_i, x_j	material directions
x', y', z'	local coordinate system of crack
z	through thickness direction
α	coefficient of thermal expansion in the x' direction
Δt^*	modified time step
ΔT	maximum difference between environment temperature and T_o
ρ	crack density
σ_a	applied stress to laminate
ξ	shear lag parameter

CHAPTER 1

INTRODUCTION

1.1 THE PROBLEM

Polymer matrix composite materials (PMCs) are well suited to the aerospace industry, primarily because of their high specific strength and stiffness. Reduced structural weight equates to better performance, greater payload or increased range. The usage of composites is increasing for primary aircraft structures: the Boeing 777 airframe is about 10% composite (compared to only 3% for the 767) while the F-22 airframe is 30% composite. Future applications are proposing extensive use of composite materials to meet demanding performance requirements. Examples include gas turbine engine structures, reusable launch vehicles (such as the X-33) and supersonic commercial aircraft. In all of these applications, the material is exposed to harsh cyclic environments (including moisture, thermal, mechanical and chemical components) for extended periods of time. These environments have been shown to cause degradation and damage to polymer matrix composites.

It is the latter application, that of the supersonic commercial airliner, which is the focus of this study. Boeing has established the High Speed Civil Transport (HSCT) program with the goal of developing a 300 passenger, 5000+ nautical mile range, Mach 2.4 aircraft within the next two decades (see Figure 1.1). The program goals require an advanced airframe to be developed which significantly outperforms (in terms of mass fraction) the conventional aluminum skin-stringer designs we see today. It is likely that advanced polymer matrix composites will be used extensively in the airframe of the HSCT to meet the challenging performance requirements. In order to choose suitable materials for the

airframe, an understanding of the effects of the harsh environment on candidate materials needs to be gained.

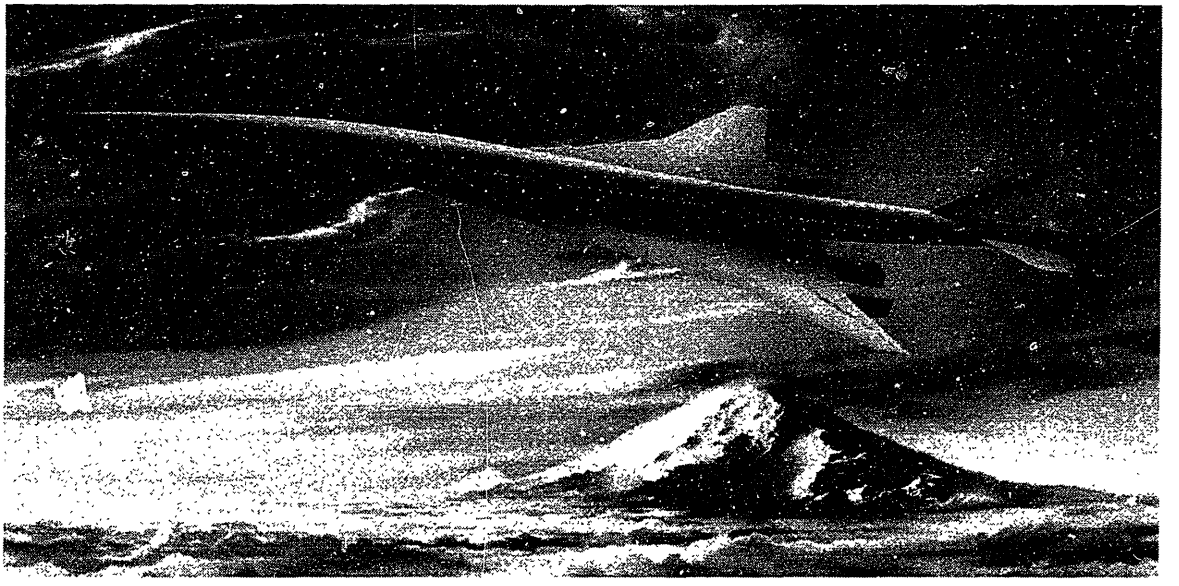

Figure 1.1: An artist's impression of Boeing's High Speed Civil Transport (HSCT) [*courtesy of The Boeing Company*]

1.2 THIS WORK

The focus of this work is the environmental response of potential PMCs for the airframe of the HSCT. The airframe material is exposed to high temperatures (up to 350°F at Mach 2.4 cruise) and low temperatures (down to -65°F in subsonic flight), moisture and a spectrum of mechanical stresses over the entire design lifetime of 20,000 flight cycles. These environmental factors have been seen to significantly degrade even advanced high temperature PMCs. To assess the suitability of a material to the HSCT application, a 'baseline' test cycle has been defined by Boeing (Figure 1.2). Although it is not identical to the conditions that the airframe will encounter during a flight, the baseline cycle captures the main elements of the actual environment. A short 'cold/dry' segment represents a subsonic phase of flight, while a longer 'hot/dry' segment represents a typical supersonic

cruise phase. Moisture is introduced via a 'warm/wet' segment. Moisture is encountered by the airframe in a number of different operational environments, such as low altitude flight, maintenance and airport gate times.

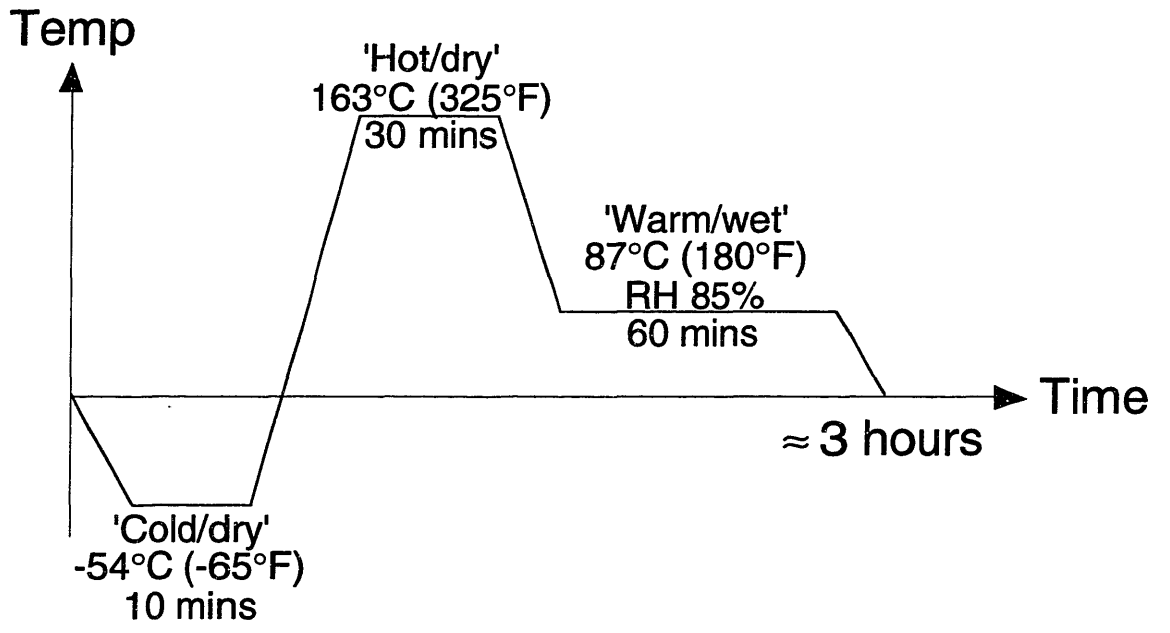

Figure 1.2: Baseline test cycle for material evaluation

Degradation in the form of edge crazing and through-laminate microcracking is observed when some materials are exposed to this baseline environment (Figure 1.3). However, different materials show different damage responses. For some materials, the observed damage is restricted to a very thin edge layer (about 1 mm in depth - Figure 1.4), while others show damage (particularly through-thickness 'microcracks') to much deeper levels (Figure 1.5).

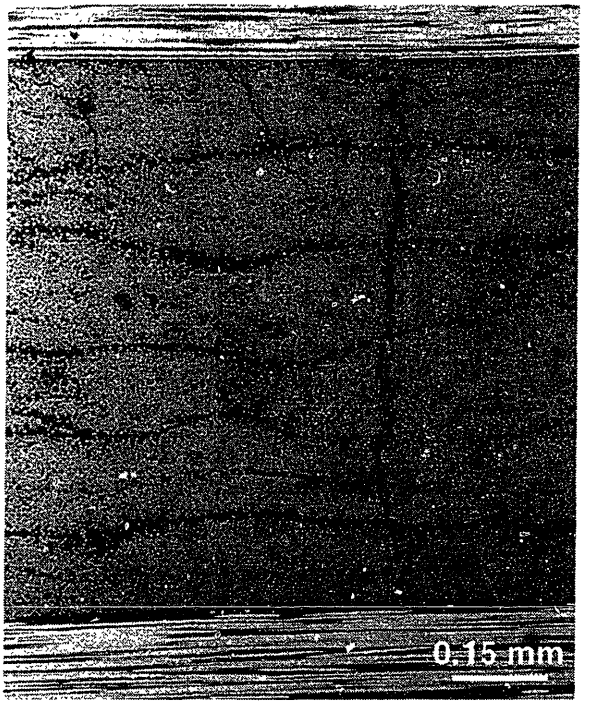

Figure 1.3: Edge damage in a cross-ply laminate exposed to 500 baseline cycles

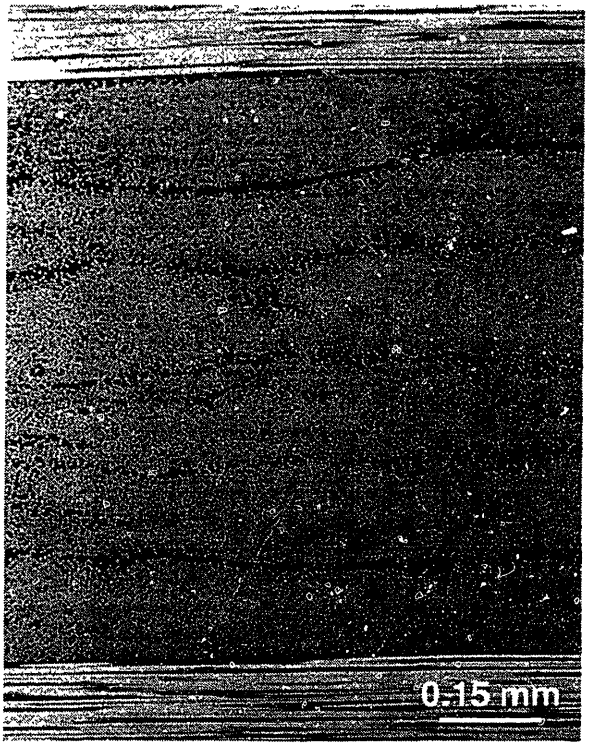

Figure 1.4: 1 mm below exposed edge of a material where damage does not progress beyond a thin layer

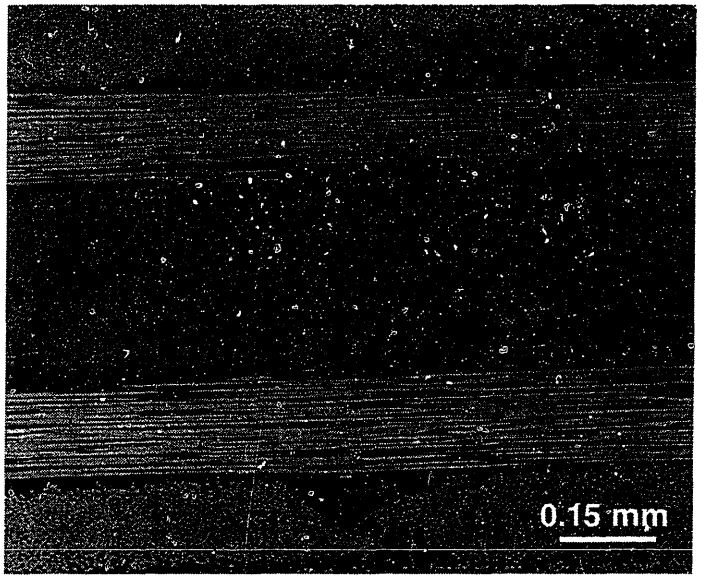

Figure 1.5: Interior of a material that exhibits through-cracks away from the exposed edge

Different materials respond in different ways when exposed to the same environment. There are a number of different components of the environment which could be responsible for the different types of damage observed, including moisture cycling, thermal cycling, time at moisture, time at temperature or interactions of any of these. Since the airframe has a service life of twenty thousand cycles, it is unrealistic to test the environmental response of candidate materials in real time. The baseline cycle is approximately 3 hours in length, so 20,000 cycles equates to almost 7 years of continuous testing. Hence, it is highly desirable to use accelerated test methods which expose the materials to environmental conditions which bring the same degradation response from the material as the baseline cycle (or some other, more realistic test environment), but in a much shorter time. To do this, it is necessary to understand which mechanisms are causing the observed damage.

In this work, previously-developed mechanism-based models (see Section 2.5) are used to investigate the mechanisms believed to be behind the observed degradation phenomena. An

experimental test matrix was designed to isolate each of the mechanisms to determine which was responsible for the damage behavior of each material under investigation. The models were used to devise accelerated test methods for moisture cycling and thermal cycling, two of the possible mechanisms causing the damage. Baseline hygrothermal, accelerated hygrothermal and isothermal testing were carried out at Boeing. Accelerated thermal cycling tests and all damage assessment and data reduction were conducted at MIT. These tests provided a wealth of data on the response of two candidate materials to different components (and combination of components) of the service environment and enabled identification of the most important mechanisms causing damage.

When the overall damage mechanisms have been isolated, it is possible to design accelerated tests which enable more timely evaluation of materials for the HSCT application. This should also produce significant savings in both cost and manpower.

1.3 THESIS OUTLINE

Background for this research in terms of relevant prior work in environmental effects on PMCs is given in Chapter 2. Chapter 3 provides a focused problem statement and the approach for its solution. A review of the models used in this work and the design of the accelerated tests is given in Chapter 4. The experimental test matrix and procedures are outlined in Chapter 5, with results and discussions given in Chapters 6 and 7 respectively. Conclusions from this work are given in Chapter 8.

CHAPTER 2

BACKGROUND

2.1 SUPERSONIC TRANSPORTS AND THEIR OPERATIONAL ENVIRONMENT

Supersonic transports were first developed in the 1960s in the USA (SST), USSR (Tu-144) and Britain/France (Concorde). The SST program was canceled following significant weight and environmental problems with preliminary designs. The Tu-144 was the first supersonic transport to fly commercially, but service soon ceased and it is now used only as a research vehicle. Only the Concorde has survived in commercial service, but it is an economic and environmental failure. Not until recently has technology evolved sufficiently to solve most of the shortcomings of these 'first generation' designs. Active research is ongoing around the world, particularly in America (HSCT), Europe (Alliance) and Japan [1].

Supersonic transports are only permitted to fly above Mach 1.0 when over water. Almost three quarters of international routes are 85% or more over water. Over half of the current international routes are in excess of 2000 nautical miles. As a result, more than 300 potential HSCT city pairs exist, and traffic is predicted to at least double by 2015. All these factors combined have led to market forecasts for supersonic transports ranging from 900 to 1300 aircraft through 2025. This is far in excess of the minimum market size of 300-500 aircraft required for a program launch. The potential returns include 140,000 new jobs and an estimated $500 billion in positive trade [2].

NASA's High Speed Research (HSR) program is directing 'focused technology development' [3], the results of which should enable the aerospace industry to develop a high speed commercial airplane. The HSR program has a stated vision to "establish the technology foundation by 2002 to support the US transport industry's decision for a 2006 production of an environmentally acceptable, economically viable, 300 passenger, 5000 nautical mile range, Mach 2.4 cruise speed aircraft". The 5000 nautical mile range was chosen as being the minimum necessary for the high volume Los Angeles/Tokyo trans-Pacific route.

Many challenges still exist, particularly in the areas of propulsion (supersonic and subsonic efficiency with low noise and emissions), aerodynamics (sonic boom mitigation) and structures. This study is focused on the structural problems. The required structural mass fraction (compared to operating weight empty) for a supersonic commercial transport is much smaller (<20%) than that for a subsonic aircraft (25%), requiring innovative structural concepts to be developed and advanced materials to be used.

One of the biggest challenges faced by the structural designers is the selection of the materials to withstand the aerothermal loads (particularly aerodynamic heating) experienced by the aircraft [4]. The skin of the aircraft will be exposed to temperatures as high as 350°F at Mach 2.4 [5] and as low as -65°F in subsonic flight, while moisture both in flight and while on the ground is also experienced. The structure will be exposed to these environments for extended periods of time—the HSCT has a design life of 20,000 flight cycles or over 60,000 flight hours. By setting a cruise speed of Mach 2.4, the HSR program is pushing the state of the art of materials technology. Different families of materials are required for use at sustained temperatures above 250°F (which is the skin temperature at Mach 2.2) than for use at below 250°F. Aluminum is suitable below 250°F,

but titanium or high temperature PMCs are required for sustained use above this temperature.

Over 140 different materials have been analyzed to assess their suitability to the HSCT application. Unlike aluminum alloys, titanium alloys are stable up to 350°F and are not susceptible to environmental degradation at these temperatures. But an all-titanium HSCT structure would be too heavy to be economically viable. It is likely that titanium will be used in parts of the structure (particularly for high temperature areas such as the wing and tail leading edges) but not throughout. New hybrid materials made out of alternating layers of titanium and graphite composite material (TiGr) show significant promise as they combine the attractive properties of both materials. The titanium provides compressive strength and protection from the environment, while the graphite composite provides stiffness, tensile strength and fatigue resistance [6]. However, from a materials technology viewpoint, there are still major obstacles to overcome with regard manufacturability, maintainability and repairability.

Hence, it is likely that more conventional (but advanced, high temperature-capable) polymer matrix composites will be used extensively in the airframe of the HSCT. It is, therefore, necessary to investigate the behavior of PMCs when exposed to conditions they will meet in service. The environment includes cyclical exposure to moisture and temperature, and the impact of these on PMCs is reviewed next.

2.2 MOISTURE

2.2.1 Behavior of PMCs exposed to moisture environments

A great deal of work has been performed in the last few decades on various aspects of moisture effects on PMCs. Reviews are included in Weitsman [7] and Wolff [8]. Much of the early work established the fundamental behavior of PMCs exposed to moisture. When moisture and temperature are constant throughout a test, it was found that the maximum moisture content depends primarily on the ambient relative humidity, while the speed of diffusion of moisture into the laminate is controlled by temperature and not humidity [9,10]. Investigations into transient cyclic moisture conditions concluded that the moisture *content* of the material approaches a steady state after prolonged exposure, while most of the moisture *distribution* changes occurred in a narrow 'boundary layer' near the exposed surface [10]. A complete transient analysis needed to be performed before equivalent constant conditions could be substituted to accelerate the transient effects. An early attempt at simulating a 'realistic' supersonic service environment was made by McKague *et al.* [11]. They used a cycle comprising -65°F 'subsonic' and 300°F 'supersonic dash' components, together with simulated periods of rainfall. They found that the supersonic dash component constituted a thermal spike which significantly increased the moisture diffusivity (measured by weight increase) over the materials not experiencing the spike. This phenomenon was later analyzed in more detail to investigate the effect of spike temperature and material layup [12]. It was suggested that the enhanced moisture absorption was due to the increase in the free volume of the matrix at the spiking temperature.

DeIasi, *et al.*, [13] attempted to simulate operational environments by incorporating 'realistic' tropical and temperate climates, plus periods of typical sub- and supersonic flight conditions. They compared the material response in these use environments to those under

simpler environmental conditions (plain thermal and moisture cycling). They found that the latter tests gave much insight into the observed anomalies in the results from the full tests. Based on these observations, they concluded that good prospects existed for the substitution of accelerated tests for real time tests to predict the response of materials to the service environment.

Experiments performed by immersing material in various kinds of liquids [14] showed that moisture uptake depended on time and temperature for immersion in distilled water and salt water. This was not the case for diesel fuel, jet oil and aviation oil, where only time seemed to be important. Techniques for tracking moisture distribution through a laminate with a nuclear probe were demonstrated by Whiteside *et al.* [15] using labeled hydrogen atoms (in heavy water, D_2O). Effects of the composite manufacturing techniques [16] were shown to have a significant effect on moisture uptake. Oven cured composites were shown to have more voids than those autoclave cured, leading to greater moisture absorption/diffusivity and a concomitant reduction in glass transition temperature and properties. In the same work, kevlar fiber was shown to be strongly hygroscopic, providing an easy route for moisture ingress.

2.2.2 Moisture diffusion

Models of moisture (and oxygen) diffusion based on Fick's law have been widely used to describe the process [17]. The diffusivity of the material is usually assumed to be exponentially temperature dependent and may also depend on degradation and damage. A review of the applicability of Fick's equation to diffusion of moisture in PMCs is given in Shirrell & Halpin [18]. Significant deviation from Fickian diffusion occurs primarily when damage such as microcracking provides alternative mechanisms for moisture ingress into the material. Fick's equation is generally used as the exclusive governing equation for

moisture diffusion into a material. Highly efficient numerical schemes have been developed to compute moisture distributions with Fick's law under time-varying ambient conditions of temperature and relative humidity [19]. Truncated infinite series solutions obtained extremely high accuracy with only a small number of terms. Similar schemes have been incorporated into computer codes, such as W8GAIN [20] which simplify the process of predicting the moisture (and temperature) distribution in a laminate. It is the code developed by Foch [21,53] called MODCOD which is the foundation for the moisture study in this work. It will be fully described in Chapter 4. These codes predict that in a transient moisture environment, much of the moisture level fluctuations occur in a thin boundary layer near the surface. The interior moisture concentration is shielded from the moisture transients and approaches an equilibrium level (depending on the ambient conditions) as the number of cycles increases.

2.2.3 Degradation and damage from moisture

Long term moisture exposure, especially at elevated temperatures and extreme high or low pH, has been shown to cause both reversible and irreversible degradation effects [22]. Short exposures to moisture at low temperatures tends to only cause effects which are reversed on drying. However, long term moisture exposure, especially at temperatures above the glass transition temperature for the material, is seen to irreversibly degrade a composite material.

Water plasticizes epoxy resins by interruption of the Van de Waals bonds in the matrix [8]. This reduces the glass transition temperature of the matrix material by as much as 10-20°C for every 1% weight gain due to moisture [23], which has a significant effect on the mechanical properties. Humid environments have been seen to cause reductions in

transverse and shear strengths [24] and decreases in mode II fracture toughness of the material [25].

Moisture and elevated temperatures over extended periods of time can cause viscoelastic response changes [26]. Moisture causes the matrix to swell, which can introduce significant stresses into a material with wet surface plies and dry interior [18]. When the stresses exceed the matrix *in situ* strength, cracking can occur. Moisture also causes mechanical damage from moisture-induced swelling affecting the fiber/matrix interface region [27]. This can cause fiber debonds, thus reducing the mechanical properties [7]. Initial crescent-shaped fiber debonds coalesce on drying and/or cyclic moisture exposure to form discrete continuous cracks [28,29]. This introduces new pathways for moisture to enter the material, altering the moisture uptake and making the diffusion non-Fickian. Since the moisture diffusivity is low, only the material immediately surrounding a crack will experience noticeably non-Fickian diffusion. The bulk of the material still sees diffusion which is close to being Fickian, at least until cracking becomes very extensive or long periods of time have elapsed allowing significant moisture ingress from cracked areas.

2.3 TEMPERATURE

2.3.1 Diffusion of temperature

The temperature distribution in a material is controlled by conduction, with the rate of heat flow being governed by Fourier's law. Typically, the in-plane conductivity along the fibers is greater than the through-thickness conductivity, leading to increased heat flow to/from the edges of specimens. This often makes a one dimensional heat flow analysis inadequate, requiring two and three dimensional analyses to be performed [30]. Parametric studies by

Crews [31] have developed metrics for when one dimensional analyses of heat flow are adequate. These metrics can also be applied to moisture and oxygen diffusion. Typically, though, heat conductivities are orders of magnitude greater than moisture diffusivities. Hence specimens reach thermal equilibrium long before they reach moisture equilibrium. It is valid when studying moisture diffusion, therefore, to assume that temperature in a specimen is everywhere equal to the current ambient temperature. Linear theory of coupled heat and moisture effects has verified that coupling becomes significant only as the ratio of thermal conductivity to moisture diffusivity approaches unity [32]. Hence, only moisture transients are considered in this work.

2.3.2 Degradation and damage from temperature and oxygen

Elevated temperatures over long periods of time will degrade PMCs, either directly or via enhanced temperature-dependent diffusions of moisture, oxygen or other substances. Direct degradation includes thermally-driven reactions which chemically and physically alter the properties of the material [33], physical aging [34] and burning/charring when exposed to very high temperatures [31]. Models of these phenomena have been developed, and are presented in the references cited. A coupled diffusion-reaction model has been incorporated into the same code as used in the moisture analysis [21]. Used to analyze material susceptible to oxygen at high temperatures, it shows severe degradation can happen near the edge of the material in certain environments. This damage grows slowly inwards with time.

Effects of these degraded matrix states, plus laminate geometry, loads, temperature and moisture states, have been used to find stresses, strains and deformations in laminates and to see if failure occurs [36]. Degraded surface layers are often quite highly stressed due to matrix shrinkage [21,33]. The effect of degraded surface layers on overall laminate material

properties is somewhat harder to determine. In work by Tsuji [37], mechanical and thermal bend tests have been used to extract material properties. The radii of curvature of specimens with thin degraded layers were used to quantify the shrinkage and mechanical property changes of material in the surface layer.

Promising work with protective coatings has been conducted [e.g. 35]. In this work, silicon nitride was applied to the surface of the composite material by chemical vapor deposition (CVD). The material was protected from oxidation for 500 hours at 371°C, but the effectiveness was found to be highly dependent on surface finish. Complex coating technologies (e.g. CVD) are expensive, and cheaper coatings (such as spreadable polymers) have similar problems to the composite resins themselves.

New, high temperature-resistant resin systems are being developed which are capable of surviving (and being usable) at high temperatures for extended periods of time [38,39]. Many of these developmental materials, although having impressive high temperature properties, have major disadvantages that reduce their potential for operational use. Problems include manufacturability, cost and toxicity concerns. However, a number of new materials do show significant promise, such as PETI-5, PIXA, PIXA-M and K3B. These are the focus for much of the HSR work, and Boeing is particularly interested in PETI-5 and PIXA-M for the HSCT application. The chemistry, synthesis and behavior of the NASA Langley-developed PETI (phenylethynyl-terminated imide) family of polyimide materials is fully described in Hou *et al.* [40]. PETI-5 is a new variant which combines the excellent thermo-oxidative stability and mechanical performance at elevated temperatures of a polyimide, together with superior processability [41]. PIXA-M is an amorphous form of the thermoplastic polyimide PIXA material, which promises thermal and chemical resistance, toughness, good processability and cost-effectiveness [42].

2.4 MICROCRACKING

Microcracks are cracks that appear in the matrix and run parallel to the fibers, often through the entire laminate. They are generally confined to ply groups (a number of plies together with the same orientation). Microcracks are often the most obvious form of damage seen in PMCs.

'Classical thermal microcracking' arises due to the mismatch in the coefficient of thermal expansion (CTE) between plies in a laminate when exposed to a temperature other than the stress free (nominally the cure) temperature. This mismatch induces stresses in the plies, which cause matrix cracks when these stresses exceed the strength of the matrix material. The physical mechanism is explained more fully in Chapter 4. A thorough review of thermal microcracking literature is given in Maddocks [43]. A large experimental database of thermally-induced microcracking for a number of material systems and laminate configurations has been developed [e.g. 44,45]. The prediction of thermal microcracking, usually based on a shear lag analysis and simple fracture mechanics crack formation criteria, is well established and incorporated into a computer code known as CRACKOMATIC [46,47]. This will be discussed in the next section and Chapter 4.

A number of extensions to the basic code have also been developed. Reduced stresses at free edges for certain ply angles have been analyzed [48] and used to explain some of the observed cracking behaviors. An extension by Michii, which incorporates a Monte Carlo simulation method [49], accounts for much of the observed statistical nature of microcracking. The method 'seeds' effective flaws at random places on the edge of the specimen to act as crack initiation sites, while material property variations are modeled to vary about a mean value. The gradual appearance of cracks, data scatter, partial through-

cracks and delayed appearance of cracking seen in thick ply groups have all been captured with this method.

Microcracking can also be caused by factors other than temperature and temperature cycling. Degraded layers due to oxidation have been observed to microcrack [33]. Moisture and solvents (such as dye penetrants [50]) have also been shown to cause or accelerate microcracking.

2.5 MECHANISM-BASED MODELS

The models which will be used in this study, incorporated into the MODCOD and CRACKOMATIC codes, are two of a group of mechanism-based models which have been developed in the Technology Laboratory for Advanced Composites (TELAC) at MIT. A summary of the overall modeling effort is provided in McManus *et al.* [51]. Mechanism-based models attempt to directly capture the relevant isolated physical mechanisms. Simple models are developed based on these mechanisms and tests are conducted to confirm the applicability of each individual model. The simple models for each mechanism are combined in order to replicate the complex behavior seen when a material is exposed to a realistic environment.

2.5.1 Physics

The environmental factors which lead to degraded performance were described in the preceding sections: they are shown schematically in Figure 2.1.

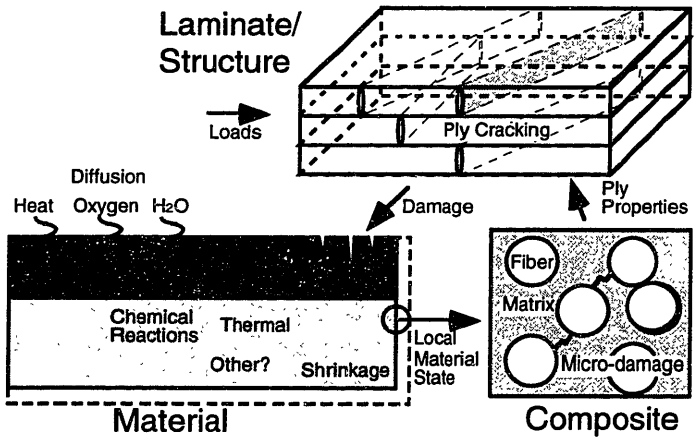

Figure 2.1: Events leading to degraded performance

Moisture enters the material as described by Fickian diffusion at a speed determined by the material's moisture diffusivity. Moisture affects the composite material both physically (e.g. swelling and fiber/matrix bond interference) and chemically (e.g. plasticization). Cyclic variations in the moisture environment are mirrored by significant variations in the moisture content in a very thin layer of material next to the edge or surface which is exposed. The interior of the specimen, on the other hand, slowly approaches an equilibrium moisture concentration determined by the ambient relative humidity.

Heat enters the material governed by Fourier's law. Temperature affects the composite both physically (e.g. shrinkage and thermal mismatch in plies leading to microcracking) and chemically (e.g. thermal reactions and oxidation coupled with oxygen diffusion into the material). Temperature conductivity for the materials under consideration are typically orders of magnitude higher than the moisture diffusivities. Hence, temperature gradients can generally be ignored when studying moisture effects.

Temperature and moisture can affect the properties of the material, either reversibly or irreversibly via chemical reactions. Figure 2.1 shows microdamage such as fiber-matrix debonding (due to stresses created by all of the above combined with material property

changes), and ply cracking (also caused by stresses and possibly aided by microdamage). Most discussion here will concentrate on the thermal and moisture states, as these are believed to be the drivers of the observed damage.

2.5.2 Modeling framework

The framework for the mechanism-based modeling effort in TELAC is shown in Figure 2.2. Environmental inputs of both temperature and moisture affect the thermal response and diffusion/reaction processes. Physical and chemical changes which result change the properties of the composite and hence its response to loads. Damage may occur depending on this response, which in turn affects the thermal/diffusion behaviors. Hence the model is coupled as seen in Figure 2.2.

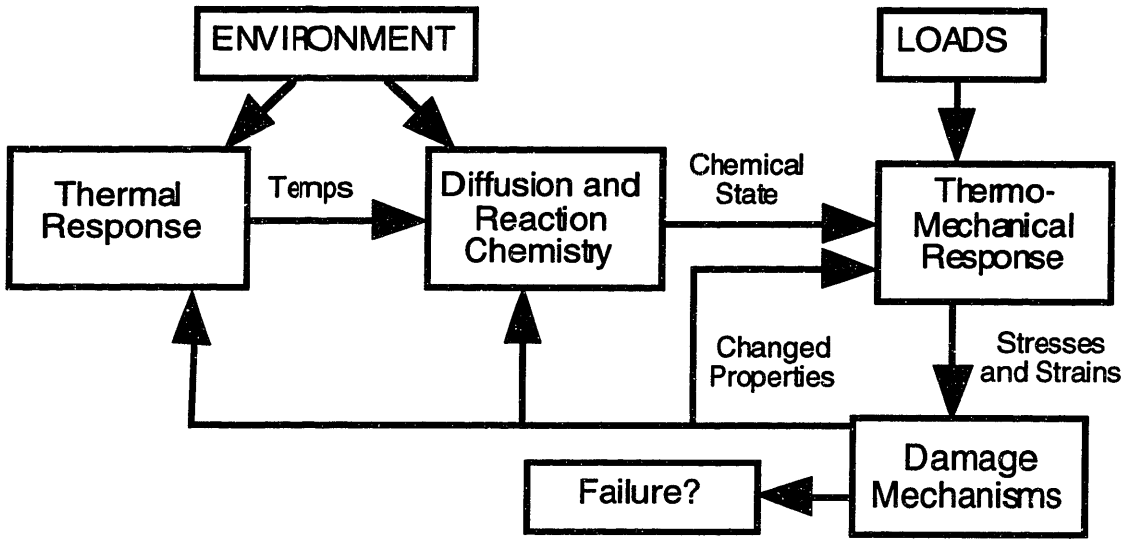

Figure 2.2: Mechanism-based modeling framework

2.5.3 Implementations of models

The diffusion and reaction chemistry elements are part of the MODCOD code, while thermomechanical response and damage mechanisms are incorporated into

CRACKOMATIC. The other components of the framework are complemented by other models as described in McManus *et al.* [51]. When combined together, they form a set of models which can realistically analyze most complex environments to which a material can be exposed.

MODCOD uses an efficient modal solution to the governing Fickian diffusion equation to model the moisture distribution through the laminate both within and between any number of cycles of a predefined moisture and thermal environment. It is fully described in Section 4.2.

CRACKOMATIC predicts crack density (number of cracks per unit length) and the resulting degradation in elastic material properties (stiffness and CTE) for both monotonically decreasing temperatures and temperature fatigue cycling. Thermal fatigue (cycling) effects have been modeled in CRACKOMATIC using an effective material toughness reduction criterion. Material toughness is assumed to decrease with number of cycles. This technique has been utilized elsewhere for related fatigue work [52]. The CRACKOMATIC code is used extensively in this work and so is discussed more fully in Section 4.4.

2.6 SUMMARY

As composite materials find wider application in the aerospace industry, more and more effort is being expended on characterizing their long term behavior in the environments to which they are exposed. It has been established that transient moisture environments cause fluctuating moisture conditions for a thin layer of material just below the surface which is exposed, while the interior approaches an equilibrium level as more cycles are experienced. This response has been modeled in efficient computer codes based on Fickian diffusion.

Moisture can cause both temporary and permanent material property changes, as well as inducing stresses. This combination can cause damage, which can in turn cause complications in establishing the moisture distribution within a laminate by making the diffusion non-Fickian.

Temperature effects include oxidation, aging, enhanced moisture diffusion and microcracking. The primary temperature concerns in this study are the enhanced moisture diffusion effects and thermally-induced microcracking. Models handle both effects.

This work utilizes the MODCOD and CRACKOMATIC models (which are based on much of the work included in this section) to better understand the environmental effects that are observed when candidate HSCT materials are subjected to the baseline and accelerated conditions.

CHAPTER 3

PROBLEM STATEMENT & APPROACH

Given that the operational environment of the HSCT causes damage to PMCs, there is a need to characterize and quantify this damage to assess the suitability of any given material for the HSCT application over the lifetime of the aircraft. This requires that the nature and causes of damage are thoroughly understood. It also requires that accelerated tests be developed so that data on material suitability can be obtained in a much shorter time frame than real time testing would allow.

Different materials may be damaged by different components of the use environment. A list of 'suspect' mechanisms has been developed from previous work: moisture cycling, temperature cycling, time at moisture, time at temperature, mechanical stress and interactions of some or all of these.

It was suspected prior to this work that it is the moisture cycling component of the baseline cycle which is responsible for observed surface damage, and the thermal cycling component which is responsible for observed interior cracking. Design of accelerated test cycles for moisture and thermal cycling environments is achieved by using two of the mechanism-based models developed in TELAC: the moisture effects code MODCOD and the thermal microcracking code CRACKOMATIC. An accelerated moisture cycle is designed which is predicted to cause a very similar moisture response in the material as the baseline environment, but in a much shorter time. Similarly, the accelerated thermal cycle is

predicted to cause thermal microcracking damage equivalent to that caused by the baseline environment in a much smaller number of more severe thermal cycles.

An experimental test program is designed which subjects the candidate materials to the baseline environment, the individual components of that environment and the accelerated moisture and thermal environments just discussed. This experimental program allows us to establish whether (and which of) the 'suspect list' of individual mechanisms is causing the damage for each material and to confirm whether the accelerated tests do indeed accelerate the damage mechanisms, as postulated. The test program allows us to rule out those mechanisms shown not to be responsible for the damage in the materials under investigation. This will also allow us to direct future studies in acceleration testing to the true causes of damage.

CHAPTER 4

ANALYSIS

4.1 MECHANISM-BASED MODELING FRAMEWORK

As discussed in Section 2.5, a group of mechanism-based models have been developed in TELAC over the last few years. These simple models are combined together into a framework (Figure 2.2) which can analyze many complex environments. The two models which we used in this work were the moisture code MODCOD and the thermal microcracking code CRACKOMATIC. These models will be reviewed in detail in the following sections, along with how the models were used in this study. Complete descriptions of the development of the models are given in [53] and [43] respectively.

4.2 MOISTURE DISTRIBUTION MODELING

4.2.1 Analytical development

This analytical development is the work of Foch [53]. Moisture effects have been modeled assuming Fickian diffusion, which is described by the equation:

$$\frac{\partial C_m}{\partial t} = \frac{\partial}{\partial x_i}\left(D_{ij}^m \frac{\partial C_m}{\partial x_j} \right) \tag{4.1}$$

where C_m is the concentration of moisture in the laminate, x_i and x_j denote material directions and D_{ij}^m is the anisotropic diffusivity tensor for moisture. The assumed geometry is of an infinitely long/wide flat plate, subjected to the same environment on the top and bottom surfaces. Given this, only through-thickness moisture gradients need be considered

and the further assumption of orthotropic diffusivity reduces the above equation to its one-dimensional form:

$$\frac{\partial C_m}{\partial t} = \frac{\partial}{\partial z}\left(D_z^m \frac{\partial C_m}{\partial z} \right) \tag{4.2}$$

where z represents through-thickness direction and D_z^m is the corresponding component of moisture diffusivity. This is assumed to increase exponentially with temperature as described by an Arrhenius equation:

$$D_z^m = D_0^m \exp\left[\frac{-E_A^m}{RT} \right] \tag{4.3}$$

D_o^m is the moisture diffusivity constant, E_A^m the moisture activation energy, R the universal gas constant and T the absolute temperature. All of these are taken as constant in z, so the rate of moisture ingress can be described by (dropping the z and m):

$$\frac{\partial C}{\partial t} = D\frac{\partial^2 C}{\partial z^2} \tag{4.4}$$

Initial and boundary conditions to solve Eqn. 4.4 are given by:

$$C(z) = C_0(z) \quad \text{for } t \leq 0 \tag{4.5}$$

$$C(0) = C(h) = C_\infty(t) \quad \text{for } t > 0 \tag{4.6}$$

The value of $C_0(z)$ is simply the initial state of moisture through the laminate, while $C_\infty(t)$ is the ambient far field condition of moisture concentration. Here, h is the thickness of the laminate. The boundary conditions are set by the assumption that the exposed edge or surface is always in equilibrium with the environment, and that the equilibrium can be expressed by the relation

$$C_\infty = f(RH)^g \tag{4.7}$$

where RH is the relative humidity and f and g are material constants. The material properties used for all analyses are given in Table 4.1. They are taken from PETI-5 data [21].

Table 4.1: Moisture diffusion properties for PETI-5 [21]

D_o (mm^2/s)	E_A (kJ/mol)	f	g
0.8	42	0.018	1

A very efficient modal solution to the above system of equations for cyclic environments has been obtained, as fully described in [53]. Cyclic environment profiles that include relative humidity segments that remain constant over time (Figure 4.1) and temperatures that remain constant or change at a constant rate (Figure 4.2) can be analyzed.

A modal solution to Eqn. 4.4 in the time interval starting at t_i is:

$$C(z,t) = C_{\infty i} - \sum_{n=0}^{\infty} A_{ni} sin\left(\frac{n\pi z}{h}\right) exp\left[\frac{-n^2\pi^2 D\Delta t}{h^2}\right] \tag{4.8}$$

where the change in time $\Delta t = t - t_i$, and $C_{\infty i}$ is calculated from RH_i with Eqn. 4.7. In Eqn. 4.8, A_{ni} represents the amplitude of each mode at time i, and n the index of each mode. In order to find the first set of modal amplitudes from the initial conditions, use is made of a Fourier series expansion:

$$A_{n1} = \frac{2}{h}\int_0^h (C_{\infty 1} - C_0(z)) sin\left(\frac{-n\pi z}{h}\right) dz, \tag{4.9}$$

where the subscript *1* represents values at the first time step. The first set of calculations for A_{ni} can be performed and these values used in Eqn. 4.8 to find the concentration levels in the first time interval, $C(z,t)$. In order to calculate subsequent modal amplitudes, $A_{n(i+1)}$, and thus new concentrations, substitute $C(z,t_i)$ (from Eqn. 4.8) for $C_0(z)$ and $C_{\infty(i+1)}$ for $C_{\infty 1}$ in Eqn. 4.9, simplify, integrate, and exploit the orthogonality of the sine function to get the general form:

$$A_{n(i+1)} = \frac{4}{n\pi}\left(C_{\infty_{(i+1)}} - C_{\infty_i}\right) + A_{ni} exp\left(\frac{-n^2\pi^2 D\Delta t_i}{h^2}\right) \tag{4.10}$$

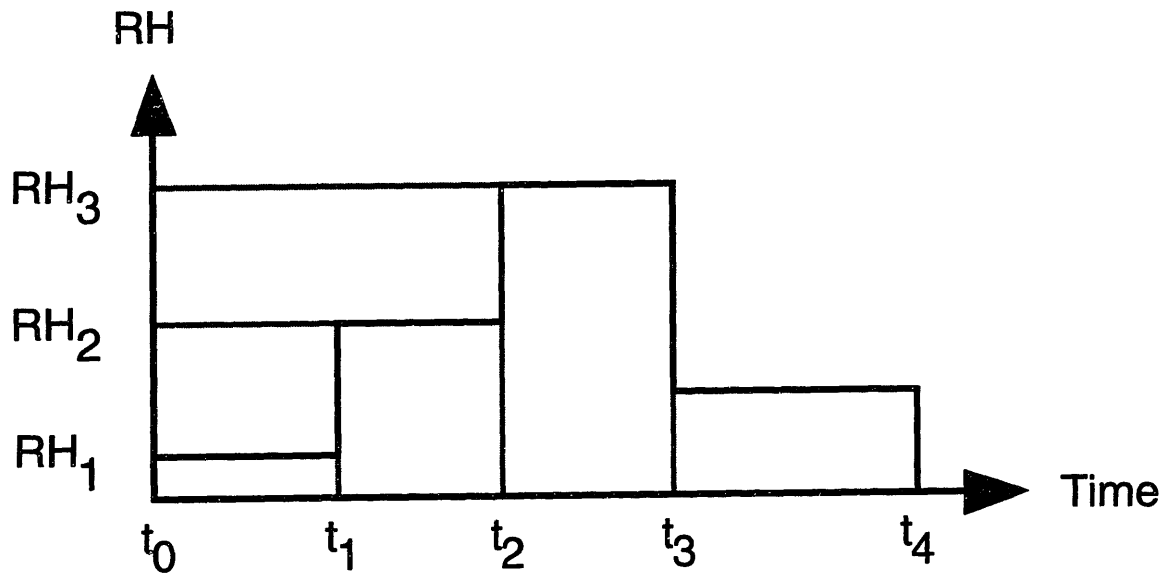

Figure 4.1: Representative moisture profile

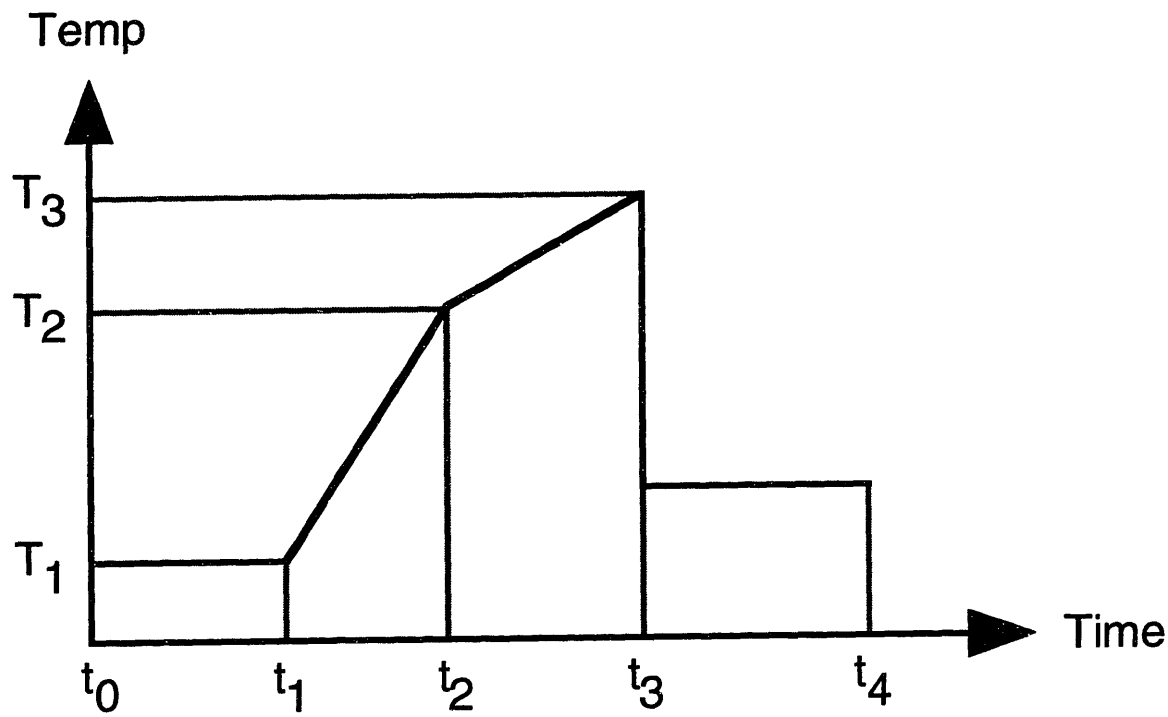

Figure 4.2: Representative temperature profile

where $\Delta t_i = (t_{i+1} - t_i)$. For the geometry of interest, only odd values of n need to be calculated. This form is useful in that it does not require the evaluation of the integrals of the form of Eqn. 4.9 except at the initial time step.

This development is appropriate for periods of constant temperature, as the moisture diffusivity, D, is constant, and can be calculated via Eqn. 4.3. For the segments with ramped temperature changes, however, this calculation is complicated by the time dependence of temperature. The resulting variation in D invalidates the solutions above. This problem is solved by substituting Eqn. 4.3 into 4.8 and defining a modified time step, Δt^*. This yields a new form of Eqn. 4.8 for the calculation of the current moisture concentration following a temperature ramp:

$$C(z,t) = C_{\infty_i} - \sum_{n=0}^{\infty} A_{ni} \sin\left(\frac{n\pi z}{h}\right) exp\left[\frac{-n^2\pi^2 D_o \Delta t^*}{h^2}\right] \tag{4.11}$$

where

$$\Delta t^* = \int_{t_{i-1}}^{t} exp\left[\frac{-E_A}{RT(t)}\right] dt \tag{4.12}$$

If the moisture and temperature profiles are repeated (cycled), the values of Δt_i^* can be calculated for each segment prior to doing the cyclical calculations.

$$\Delta t_i^* = \int_{t_{i-1}}^{t_i} exp\left[\frac{-E_A}{RT(t)}\right] dt \tag{4.13}$$

and Eqn. 4.10 becomes

$$A_{n(i+1)} = \frac{4}{n\pi}\left(C_{\infty_{(i+1)}} - C_{\infty_i}\right) + A_{ni} exp\left(\frac{-n^2\pi^2 D \Delta t_i^*}{h^2}\right) \tag{4.14}$$

This allows repeated calculations of moisture concentration for each segment. The coefficients A_{ni} are found by progressive application of Eqn. 4.14, and then the

concentration at any time can be found from Eqn. 4.11. The calculations are repeated for as many cycles as desired. The mathematical procedure just outlined was coded into a FORTRAN program known as MODCOD (MOisture Diffusion, Chemical reactions and Oxygen Diffusion). Similar procedures were developed to analyze oxidative diffusion and reactions as well (see [53]). An algorithm giving the computation sequence is shown in Figure 4.3.

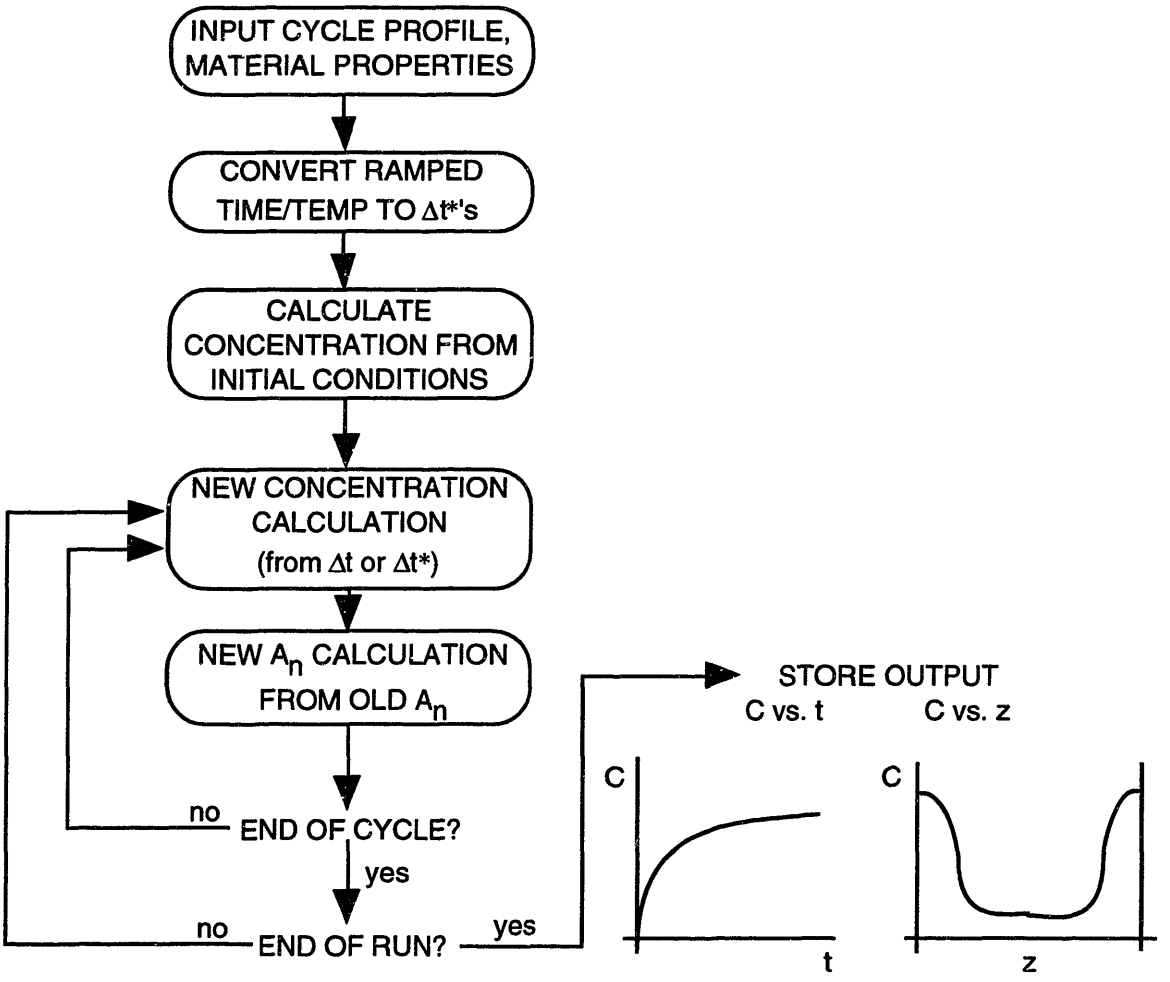

Figure 4.3: MODCOD algorithm (from Foch [53])

4.2.2 Modeling the effects of the baseline environment

Figure 4.4 shows the model output for a 16 ply laminate exposed to the baseline environment (shown in Figure 1.2). During the warm/wet part of the baseline cycle, moisture is driven into the exposed edge of the material but the absorbed moisture drops off quickly away from the edge due to the low moisture diffusivity of the material. The moisture 'spike' is confined to a volume of material about one ply thickness from the exposed surface. As the cycle goes to the cold/dry segment, the exposed surface dries out, but the cold temperature does not provide enough energy to drive the moisture out from just below the surface, and a 'moisture bubble' results. However, the temperature of the hot/dry part of the cycle is sufficient to drive the moisture out of this spike, most being removed out of the material but some being driven into the center of the material. This is the origin of the internal equilibrium moisture concentration.

This modeled behavior is confirmed indirectly in two ways: the overall moisture uptake of the entire laminate is correctly predicted by this model, and the depth of the observed damaged zones (Figures 1.3 and 1.4) in most materials exposed in the screening tests corresponds to the predicted depth over which the moisture concentration varies greatly with each cycle (the so-called 'moisture-thrashed' zone).

It is observed that two metrics are relevant in analyzing the moisture distribution in the material: depth of this 'thrashed zone', d and the internal equilibrium moisture concentration, C_{eq} (see Figure 4.5). These metrics were used when designing the accelerated moisture cycle, as discussed later in this chapter.

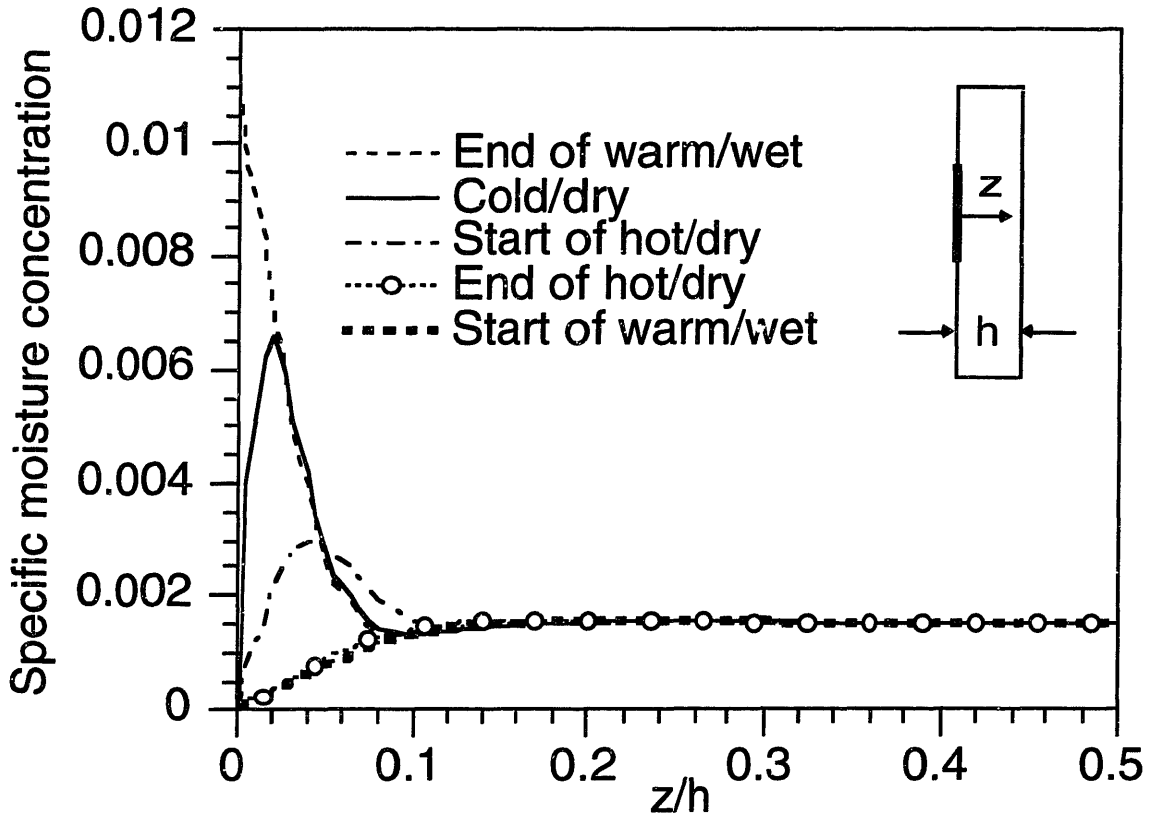

Figure 4.4: Moisture absorption through the material at different points of the cycle after 100 baseline cycles

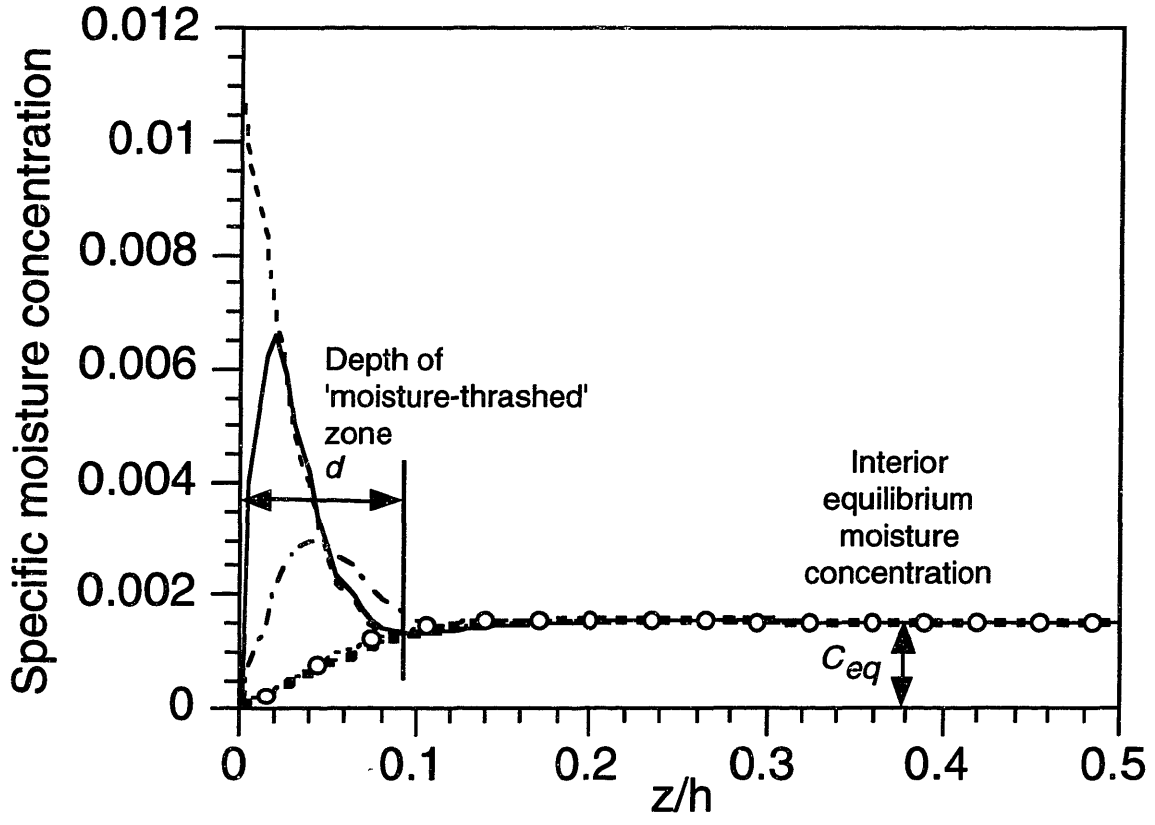

Figure 4.5: Moisture distribution metrics

4.3 DESIGNING ACCELERATED MOISTURE CYCLES WITH MODCOD

4.3.1 Parametric studies

There are a number of components of the baseline environmental cycle which can be varied to accelerate the cycle and which affect the moisture response to the environment. These include:

- warm/wet hold temperature
- warm/wet hold time
- relative humidity of warm/wet hold
- dry hot and cold hold times
- ramp rates between segments

It was desired to keep the temperature extremes in the accelerated cycle the same as in the baseline cycle, so hot and cold dry temperature variations were not investigated.

Parametric studies were undertaken to investigate the sensitivity of the moisture response of the material to each of these components. Each of the above were altered in the cycle separately, while all other parameters were kept as in the baseline cycle. The following studies compare the response of the material at the cold/dry part of the cycle after 100 cycles. The cold/dry part of the cycle was chosen here as it captures both d and C_{eq} characteristics and the moisture concentration at the peak of the moisture bubble trapped beneath the surface at the exposed edge of material.

4.3.1.1 Warm/wet hold temperature

The effect of varying the warm/wet hold temperature is shown in Figure 4.6. This parameter has the largest effect on the moisture response of the material. A 50°C (90°F) increase in the warm/wet temperature significantly increases both C_{eq} (up about 200%) and d (up about 67%). A 50°C decrease in the temperature reduces C_{eq} to virtually zero (the modality of the moisture distribution solution becomes visible at these very low moisture values), while d is also significantly reduced (by about 50%).

Increasing the temperature increases the moisture diffusivity of the material in an exponential manner (Eqn. 4.3). Hence, more moisture enters the material in a given time at increased temperatures, and thus cause the increases in C_{eq} and d seen in the response.

4.3.1.2 Warm/wet hold time

The effect of varying the warm/wet hold time is shown in Figure 4.7. The effect of this parameter on C_{eq} is linear. Increasing the hold time by 50% increases C_{eq} by 50% (and d by 20%), while decreasing the hold time by 50% causes an equal and opposite effect on C_{eq} and d. As we have assumed that the temperature through the laminate is the same as the ambient temperature, doubling the hold time allows double the amount of moisture to diffuse into the material.

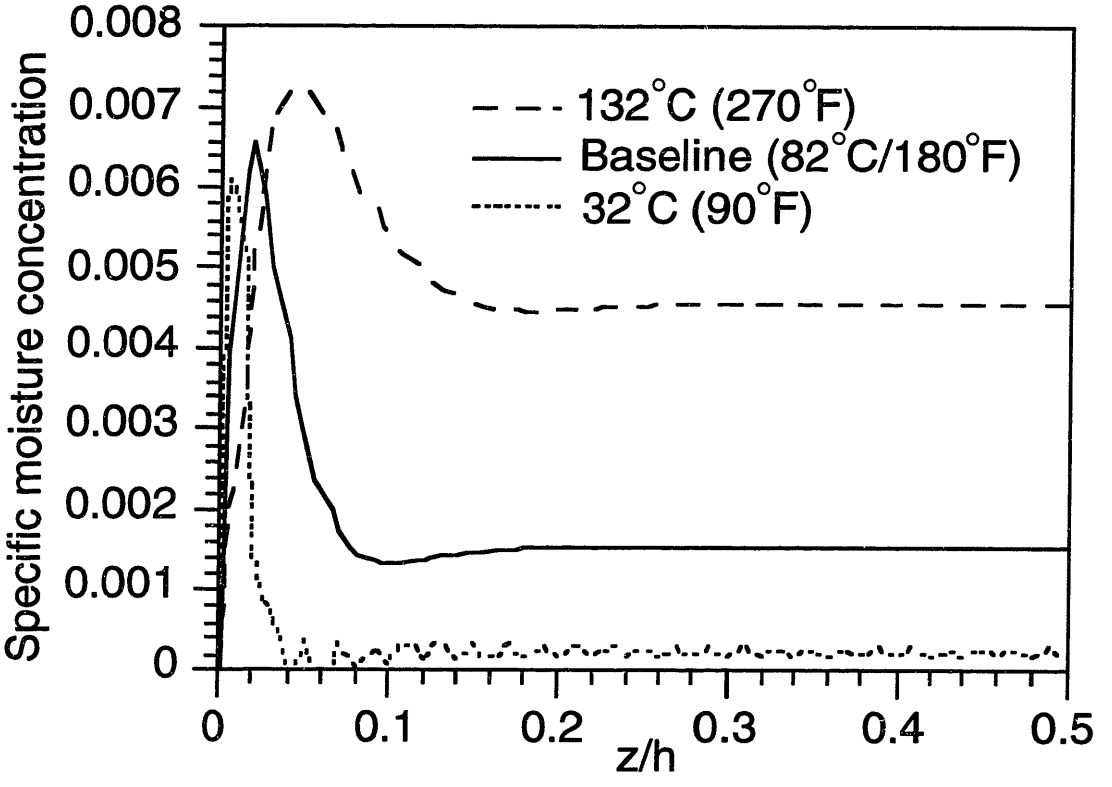

Figure 4.6: Effect of varying warm/wet hold temperature

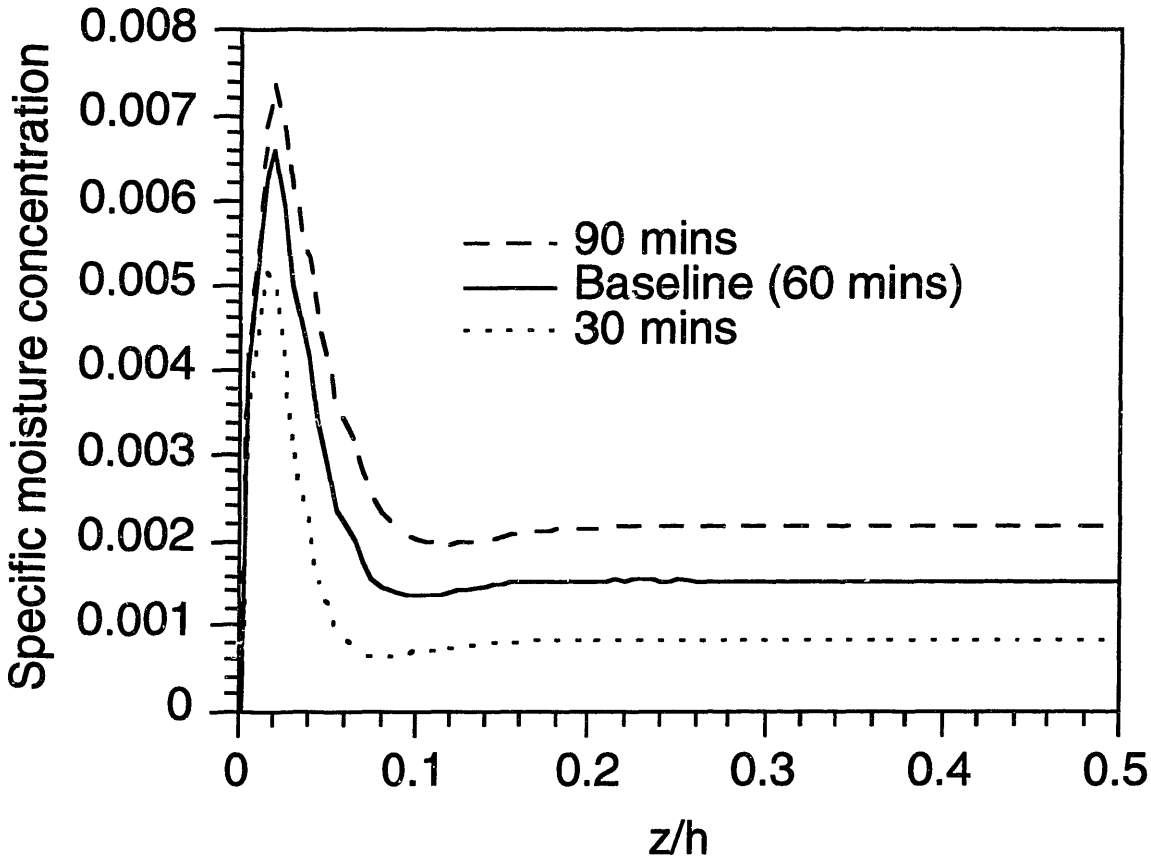

Figure 4.7: Effect of varying warm/wet hold time

4.3.1.3 Relative humidity of warm/wet hold

The effect of varying the relative humidity by 10% above and below the baseline value of 85% is show in Figure 4.8. The effect is linear due to the g parameter in Eqn. 4.7 being unity. A higher ambient relative humidity allows more moisture to diffuse into the material in a given amount of time.

4.3.1.4 Dry hot and cold hold times

Changing the hot dry hold times has an effect as seen in Figure 4.9. A 50% increase or decrease in the hot hold time has a minor effect on d, but a somewhat larger effect on C_{eq}. The hot dry segment of the cycle provides thermal energy which indirectly affects the moisture distribution in the material. When the hold time is increased, the elevated temperature has more time to cause enhanced diffusion out of the surface, hence reducing C_{eq}. The reverse is the case when the hold time is decreased.

The effect of changing the cold dry hold time is not noticeable (Figure 4.10). This is because virtually no diffusion occurs when the temperature is at the low point of the cycle (at least in the time frame of minutes to hours). The curves of moisture responses with hold times of 5, 10 and 30 minutes sit on top of each other (the 30 mins curve is just distinguishable at low z/h values).

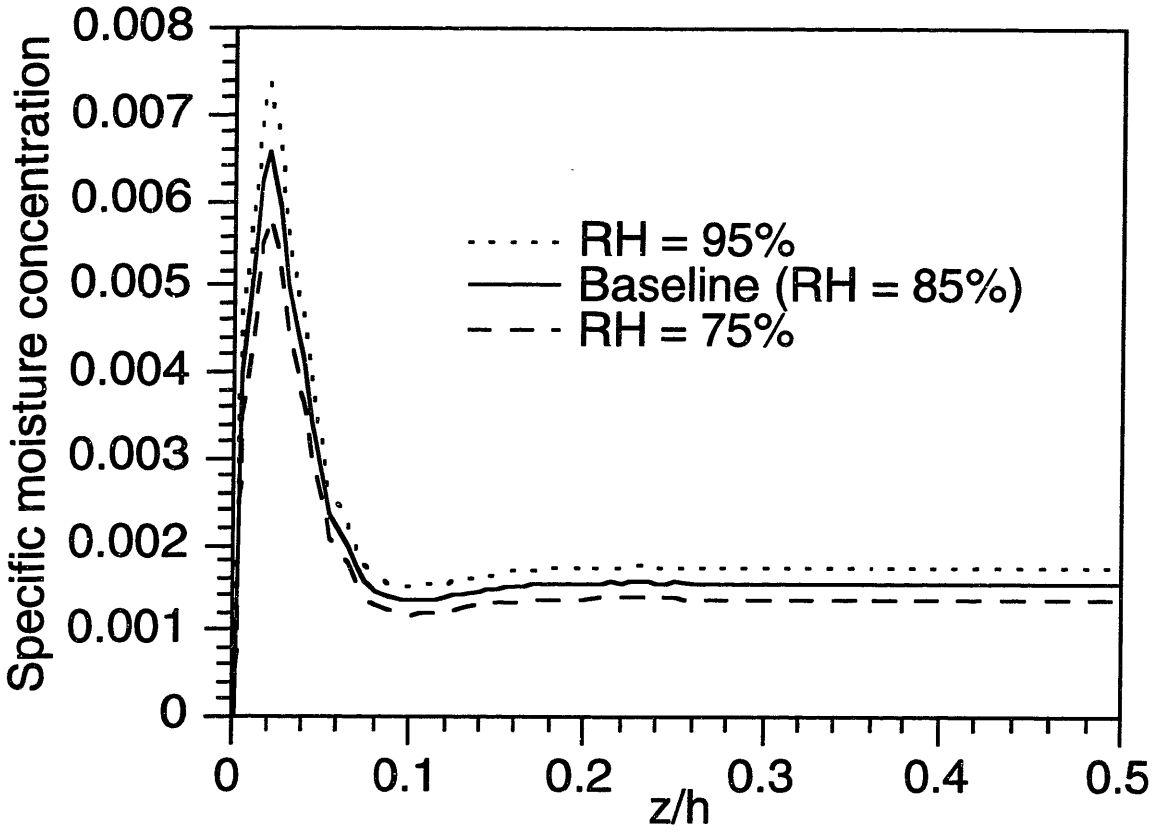

Figure 4.8: Effect of varying warm/wet relative humidity

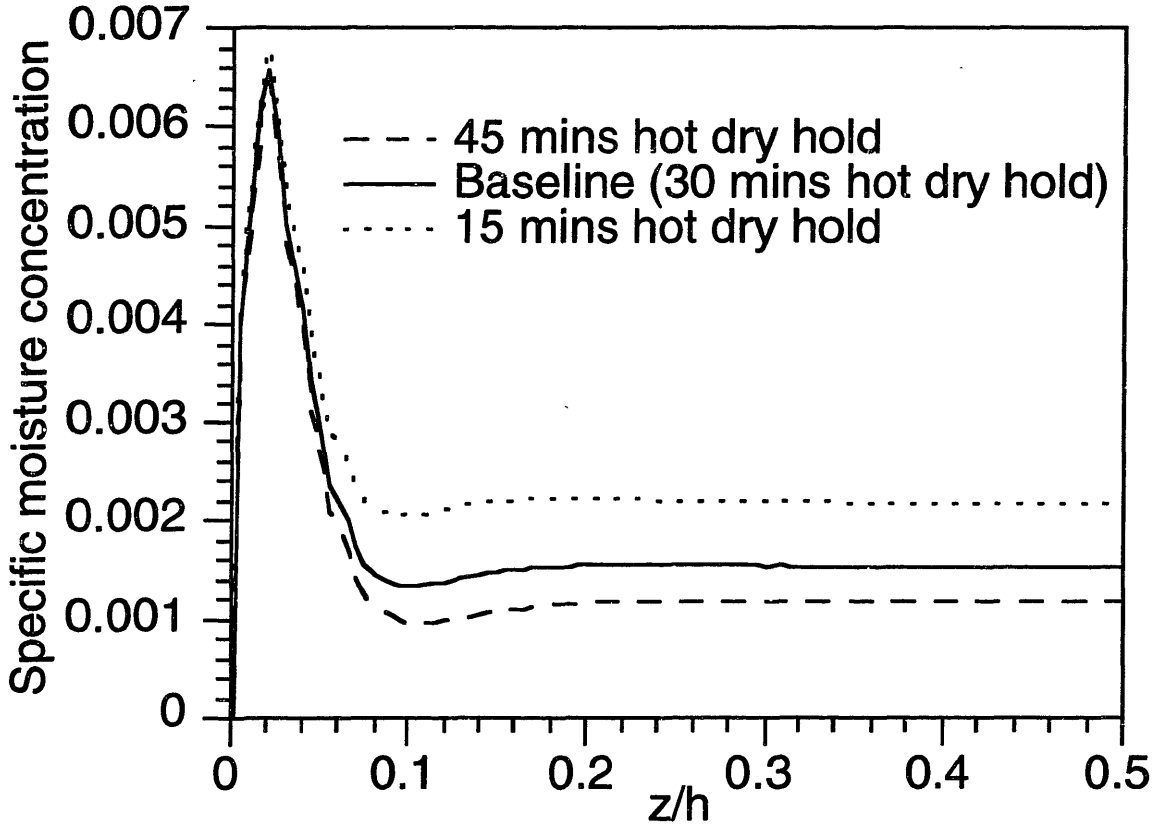

Figure 4.9: Effect of varying hot dry hold time

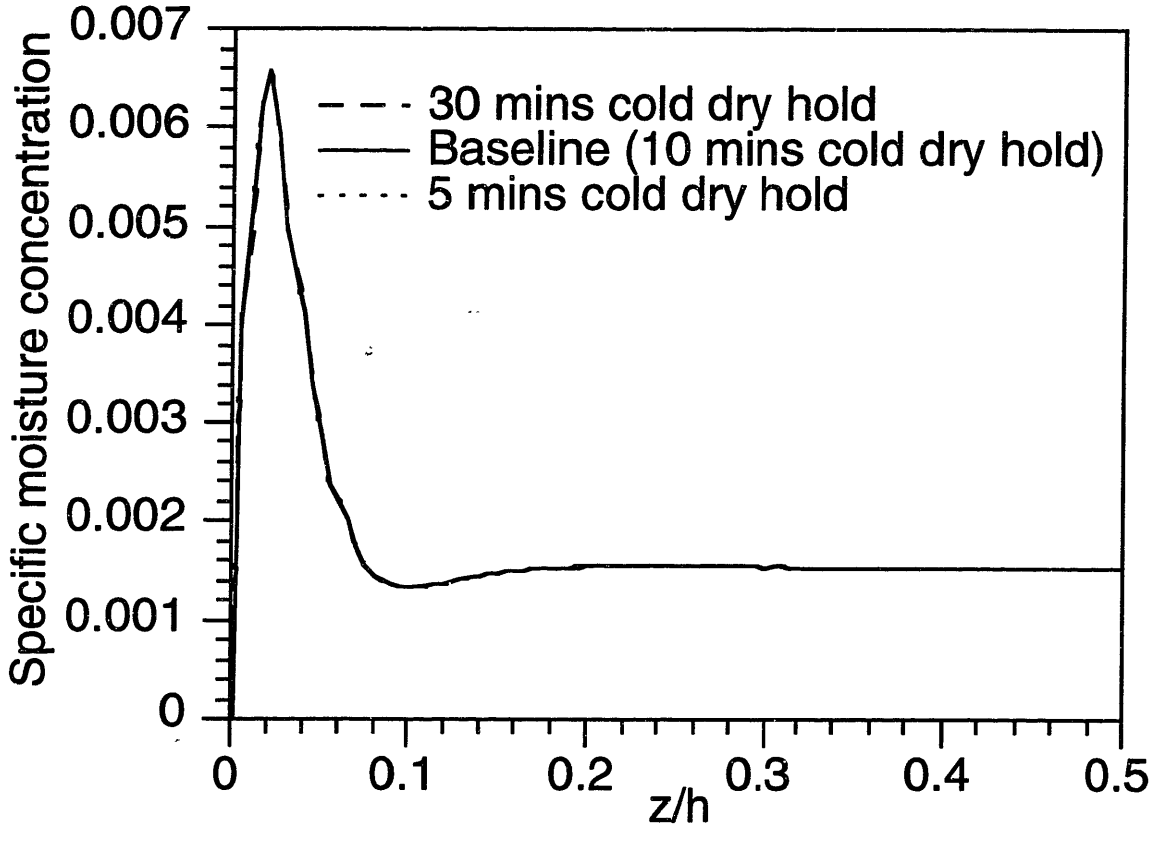

Figure 4.10: Effect of varying cold dry hold time

4.3.1.5 Ramp rates between segments

The baseline cycle ramp rates are 11°C/min heating and 5.5°C/min cooling. The effects of changing these rates by +5°C/min and -5°C/min are seen in Figure 4.11. Increasing the rates has a negligible effect on the overall moisture response. The moisture peak is somewhat higher in magnitude, but C_{eq} and d are virtually unaffected from the baseline response. It is the hold time segments of the cycle which dictate the general appearance of the response in this case. However, the effect of reducing the rates is more dramatic. Now it is the ramp segments of the cycle which dominate the moisture response in the laminate, as they take up proportionately more time of the cycle compared with the fixed hold times. The moisture peak is much lower in magnitude. As the cooling rate is very low, the cycle spends a long time at high temperatures after the warm/wet segment, so more moisture diffusion occurs from the trapped bubble and hence d is increased from the baseline. The slow cool from the hot dry hold means more time is spent in hot dry conditions and this leads to a reduced C_{eq}.

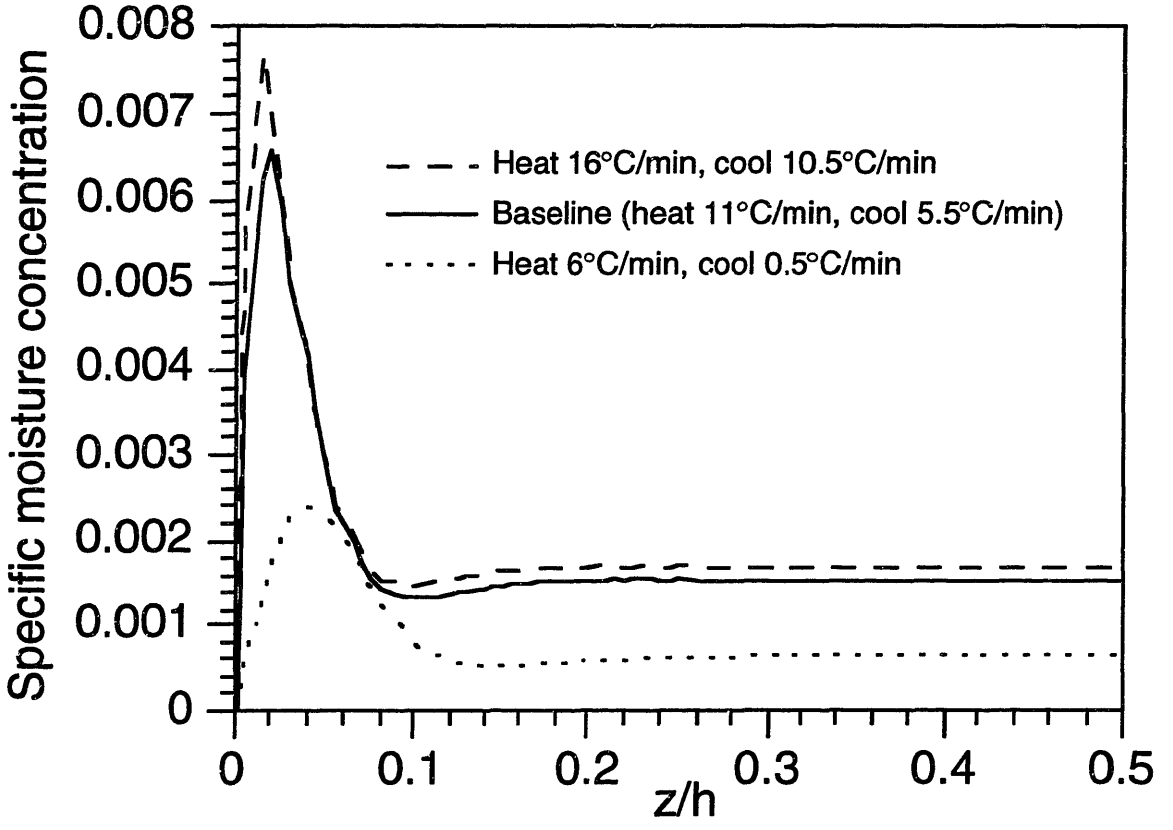

Figure 4.11: Effect of varying heating and cooling ramp rates

4.3.2 Accelerated moisture cycle design

The objective in designing a good accelerated test cycle is to match the metrics of d and C_{eq} as closely as possible to the metrics for the baseline cycle, both throughout and between cycles, but doing so in a cycle which takes less time.

Based on the results of the parametric studies, it is possible to design accelerated cycles to match these two metrics very closely. This can be achieved by varying the parameters in a number of different ways, although the response is more sensitive to changes in some parameters than others.

Most time saving can be achieved by increasing the ramp rates between the hold points and by using slightly more aggressive conditions in the warm/wet phase. It is desirable not to change the conditions too drastically so as not to enter a new type of damage response.

The accelerated cycle which was used had the following philosophy behind its design. The heating rate of 11°C/min was the maximum rate that the testing equipment could achieve, so could not be increased. However, the cooling rate was increased from the -5.5°C/min in the baseline cycle to -14°C/min in the accelerated cycle. This value was chosen as it was not so great that any thermal shock effects would be encountered, but was a significant increase over the baseline cooling rate. This rate is also consistent with similar successful cooling experiments which have been carried out in the laboratory. It was decided that the warm/wet phase relative humidity should be maintained at 85% for ease of equipment setup relative to the baseline apparatus. It is difficult to maintain RH values much greater than this for the extended periods of time which were required for these tests, and a 5-10% increase does not have a dramatic effect on the moisture response in any case (Figure 4.8). To shorten the cycle, the warm/wet temperature was made more aggressive (increased by 11°C

(20°F) to 93°C (200°F)), and thus enabling the warm/wet hold time to be reduced from 60 minutes to 30 minutes. Temperatures higher than 93°C were avoided as the conditions become very hard to maintain for extended periods of time as 100°C is approached in a humid environment. With these warm/wet conditions, the dry hot and cold hold times were adjusted by trial and error to get a best fit. It was found that the C_{eq} and d metrics were very closely matched to the baseline response when the hot dry and cold dry times were 20 minutes and 5 minutes respectively (compared with 30 minutes and 10 minutes respectively for the baseline cycle).

These comparative conditions are summarized in Table 4.2 and Figure 4.12. The accelerated cycle cuts the total cycle time from 160 minutes for the baseline cycle, to 90 minutes for the accelerated cycle, a saving of 44%.

Table 4.2: Baseline vs. accelerated moisture cycle parameters

Cycle	Ramp rates heat/cool °C/min (°F/min)	Dry hot/cold hold times (mins)	Warm/wet hold conditions	Cycle time (mins)
Baseline	+11/-5.5 (20/-10)	30/10	60 mins 82°C (180°F) RH 85%	160
Accelerated moisture	+11/-14 (+20/-25)	20/5	30 mins 93°C (200°F) RH 85%	90

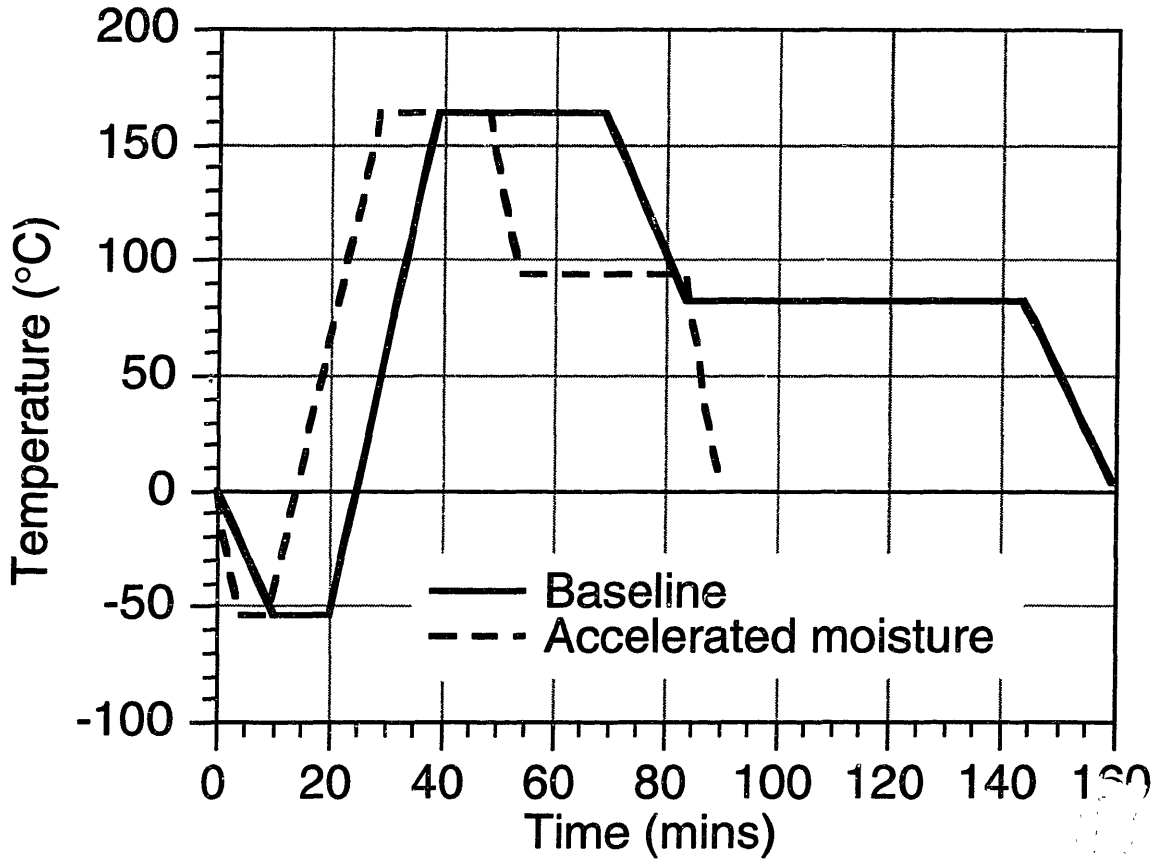

Figure 4.12: Temperature/time plot for the baseline and accelerated moisture cycles

A comparison of the theoretical material response to the baseline and accelerated moisture environments after 100 cycles is shown in Figure 4.13. As can be seen, the C_{eq} and d metrics are very similar for the two environments. Hence, the moisture history through the material should be equivalent for both cycles after any number of cycles. Since the accelerated moisture cycle is significantly shorter, the objective of duplicating the moisture response in the material in a shorter amount of time should be met.

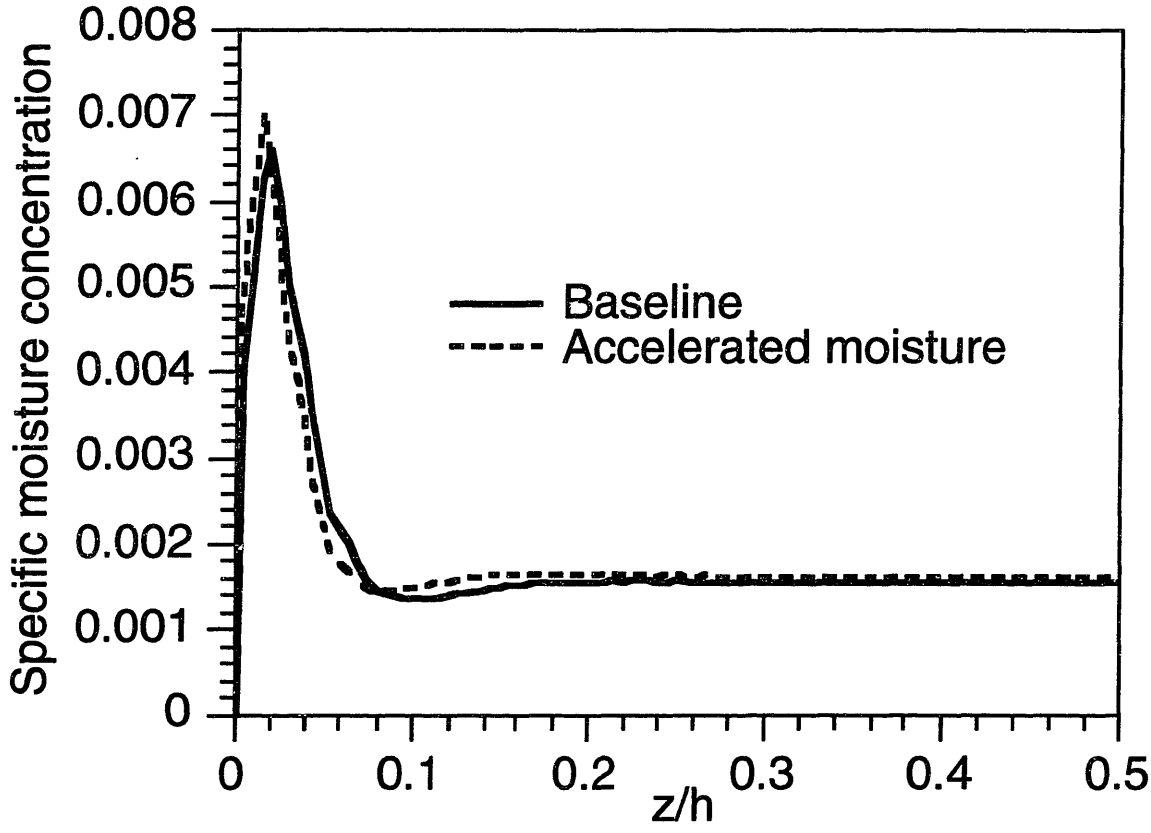

Figure 4.13: Comparison of material response to baseline and accelerated moisture environments in cold/dry phase after 100 cycles

4.4 THERMAL EFFECTS MODELING

A simple shear lag solution of the stresses around a crack was used by McManus and Maddocks [47] combined with a strain energy release model of crack appearance. Much of this analytical development can be found in this reference, and in Maddocks [43]. A ply or ply group (stack of plies with the same orientation) embedded in a laminate is considered. Cracks form parallel to the fibers with geometry as shown in Figure 4.14.

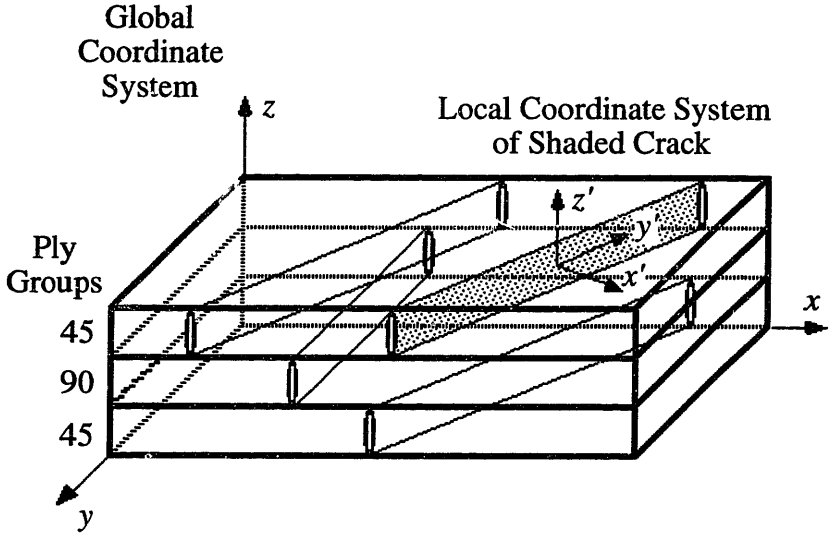

Figure 4.14: Laminate and crack geometry

The laminate is modeled as being made up of two regions: a cracking ply group (subscript *c*) and the rest of the laminate (subscript *r*): see Figure 4.15.

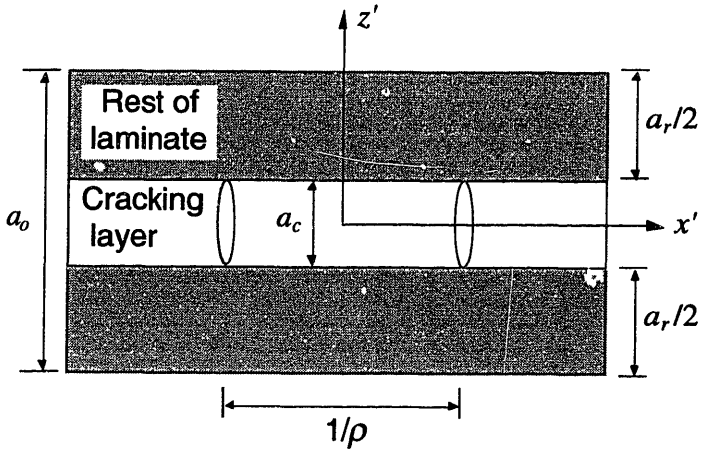

Figure 4.15: Geometry of microcracking problem

A one dimensional shear lag model is used to determine the stress and displacements in the vicinity of a crack in its local *x'y'z'* coordinate system: see Figure 4.16.

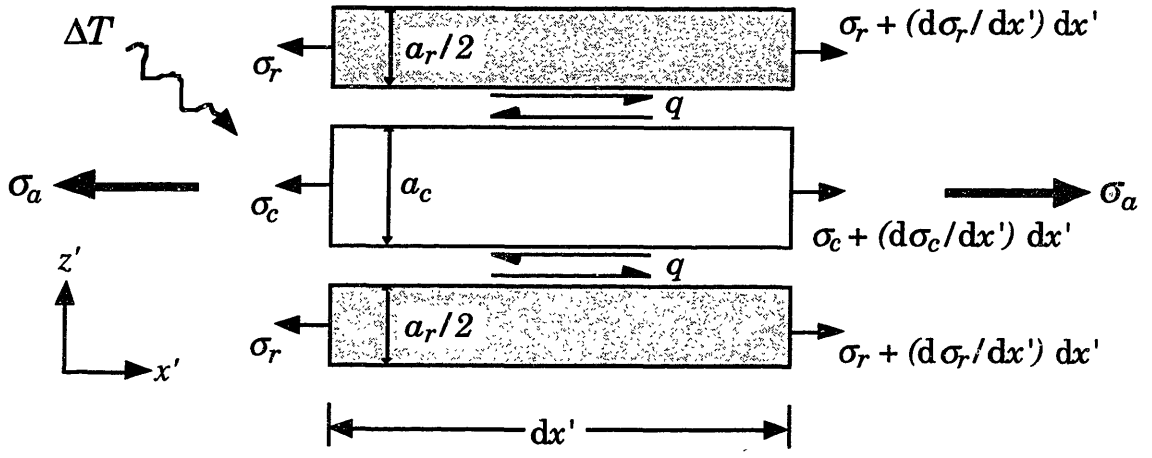

Figure 4.16: Shear lag stress model

Figure 4.17 shows the stress distribution around two crack configurations. The stresses cause strain energy to be stored in the material due to elastic deformation. A new crack forms when the strain energy released due to new crack formation is greater than the critical strain energy release rate (the energy required to form the new crack surfaces).

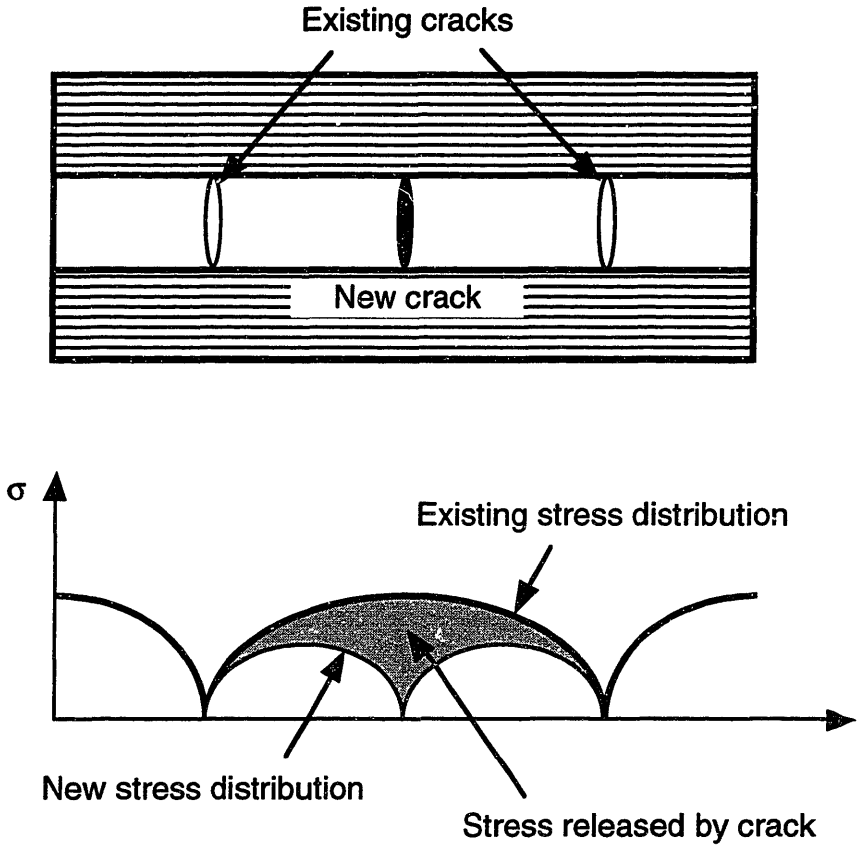

Figure 4.17: Stress distribution around cracks

A complete analysis of the model is not duplicated here, but can be found in [47]. This method allows the following relation to be derived for the cracking of a ply or ply group within a laminate under thermal stresses:

$$G_c = \frac{a_c a_0 E_0}{2\xi a_r E_r E_c}\left[\frac{E_c}{E_0}\sigma_a - E_c(\alpha_c - \alpha_0)\Delta T\right]^2 \times \left\{2tanh\left(\frac{\xi}{\rho a_c}\right) - tanh\left(\frac{2\xi}{\rho a_c}\right)\right\} \qquad (4.15)$$

Here, a's are thicknesses, E's are the stiffnesses in the x' direction of Figure 4.14, and α's are the x' coefficients of thermal expansion (CTE's), with the subscripts identifying properties of the cracking ply group (c), the smeared properties of the rest of the laminate (r) or the entire laminate (o). G_c is the effective critical strain energy release rate (toughness)

of the material when microcracking, ΔT is the maximum difference between the environmental temperature and the effective stress free temperature T_o, ξ is a shear lag parameter, and ρ is the crack density, expressed in cracks/unit length, in the cracking ply group. σ_a is the applied stress to the laminate, which is zero in this case. The stiffnesses and CTE's used in Eqn. 4.15 are calculated by classical laminated plate theory (CLPT). The relation is an implicit one; the desired quantity ρ must be solved for numerically or graphically.

As fully described in [43] and [47], thermal loads (and mechanical if they are being considered also) are considered incrementally. At every temperature/load increment, the crack formation analysis is carried out for all ply groups. A numerical solution of Eqn. 4.15 is used to determine the crack density in the cracking ply group under consideration. The properties of the ply group under consideration and the properties of the rest of the laminate are calculated using CLPT relations. Cracking which does occur degrades the properties of the laminate, and this is accounted for by the use of 'knockdown factors' applied to those properties affected once all of the ply groups have been examined at this load increment.

The above process is repeated for each load increment until the entire load history has been completed. This iterative damage progression model is implemented by the computer code CRACKOMATIC. This code utilizes material properties, laminate geometry, and thermomechanical load history and outputs crack densities and degraded laminate properties: see Figure 4.18.

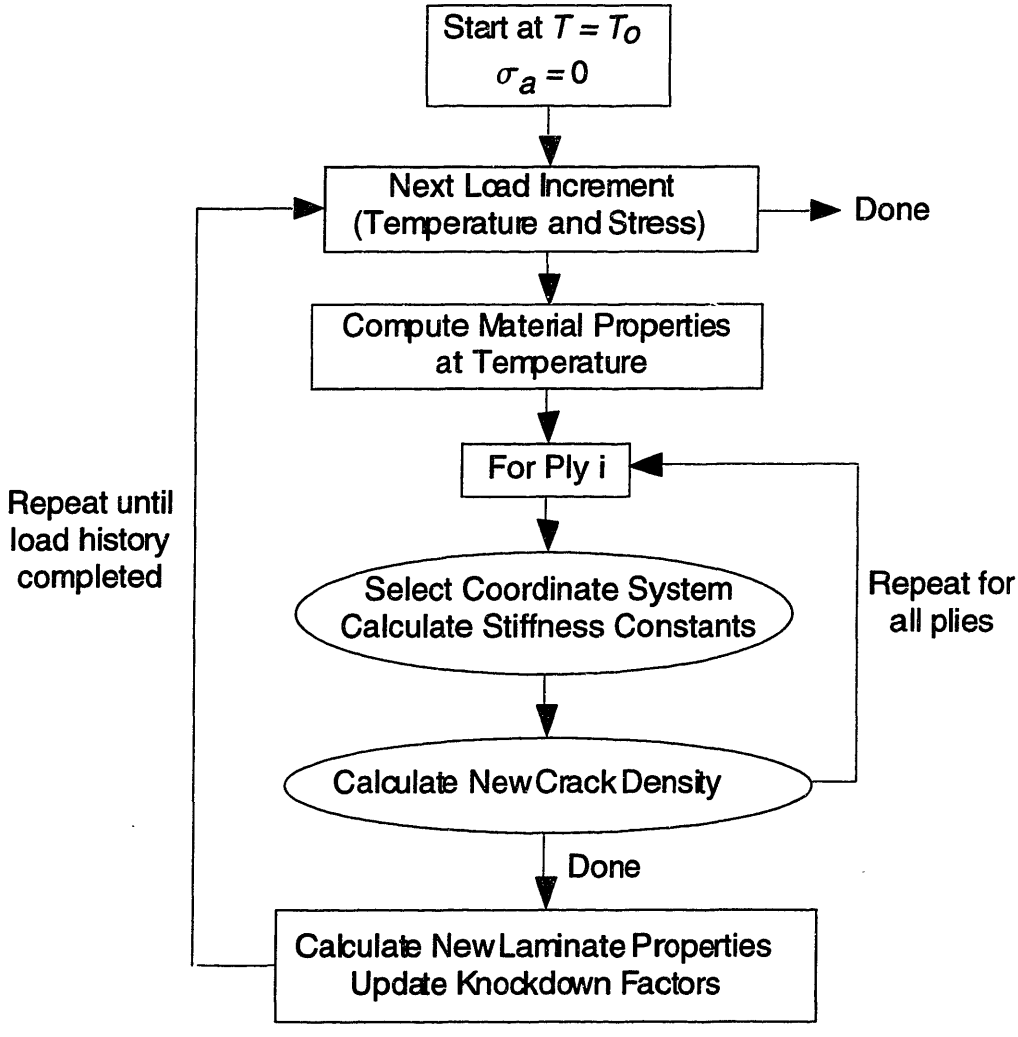

Figure 4.18: CRACKOMATIC code algorithm (from Maddocks [43])

If the material undergoes numerous thermal cycles, the material gets progressively more damaged. This 'thermal fatigue' is accounted for by an effective toughness reduction method. The effective toughness is assumed to drop with cycles according to the following (strictly empirical) relation:

$$G_c = G(N) \tag{4.16}$$

where N is the number of cycles. For convenience in reducing data, the G-N relation is sometimes expressed as:

$$G_c = G_0 A^{log10(N)} \tag{4.17}$$

where G_o is the initial toughness and A is a constant fit to data. This relation has been used by other researchers [52] and experimental evidence exists to justify its application to this problem [54]. On running the code, the user inputs the (empirical) shear lag factor, ξ, the greatest ΔT (which is the temperature difference between the cure temperature and the lowest temperature in the cycle) and a 'G-N curve', in addition to the mechanical properties required by CLPT (Appendix C).

Some of the material properties are very difficult to obtain for the materials under investigation and only approximate values are known. This is particularly true for the zero cycle and degraded fracture toughness properties. Hence, it is necessary to fit these parameters to existing data for a given material and layup, and then use these 'backed-out' parameters to predict other damage behaviors for the same material.

4.5 DESIGNING ACCELERATED THERMAL CYCLES WITH CRACKOMATIC

4.5.1 Parametric studies

The only component of the baseline environment which strongly affects the thermal microcracking response of the material is the low temperature point in the cycle. The lower this temperature, the greater the ΔT is from the stress free (cure) temperature in the laminate. This directly affects the thermal load in the composite: the greater the ΔT, the greater the thermal load. As the low temperature is decreased, microcracking initiates sooner and is more severe for a given number of cycles: see Figure 4.19. These curves were produced using parameters in CRACKOMATIC which were consistent with microcracking data found from the first round of testing with the high temperature material K3B. Input requirements for the CRACKOMATIC code and input values used in these analyses can be found in Appendix C.

This kind of microcracking response is typical: cracking is suppressed until a certain number of cycles have been experienced (when the fracture toughness of the material has fallen below the critical value for cracking). The onset of cracking is sudden and crack density rises rapidly. As more cycles are experienced, the crack density approaches an equilibrium value determined by the low temperature in the cycle. The rate of increase of microcrack density is reduced after the initial onset because stress in the material is reduced as cracks form (see Figure 4.17).

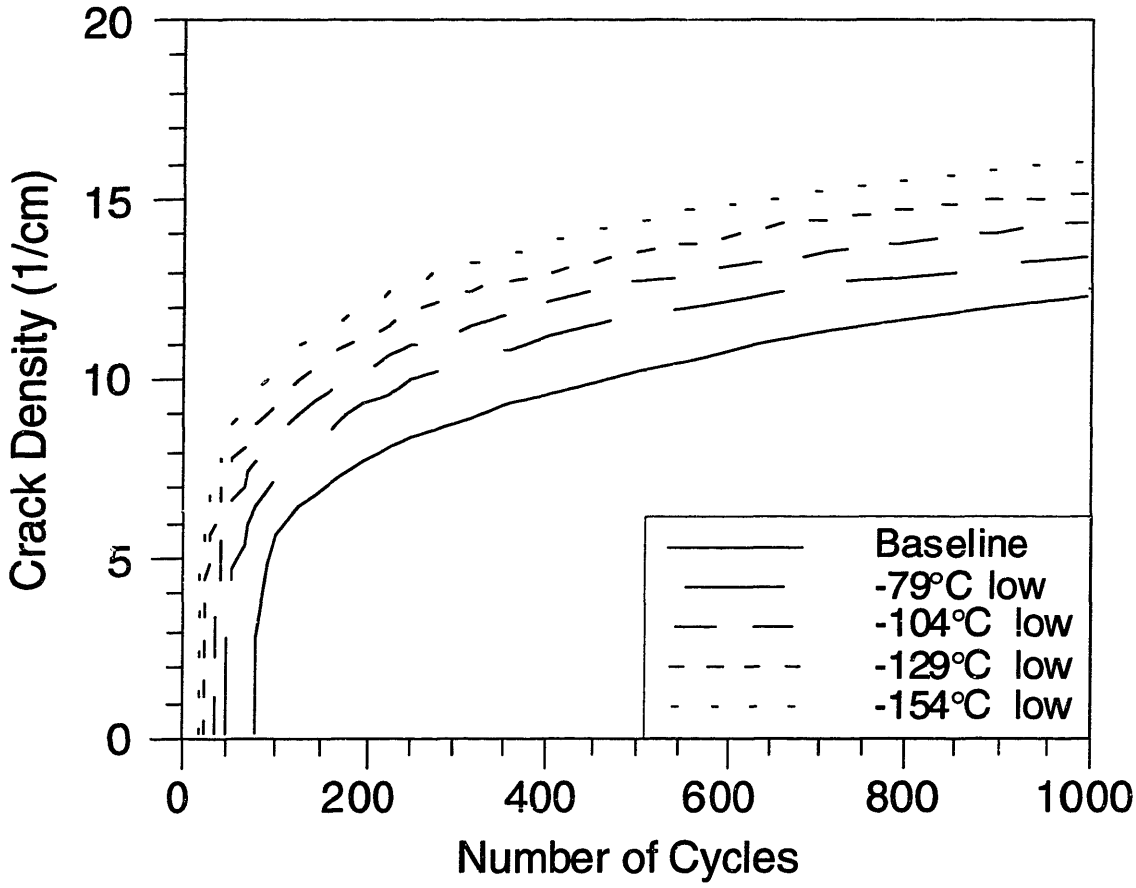

Figure 4.19: Effect of varying cold temperature

4.5.2 Accelerated thermal cycle design

When designing the accelerated moisture cycle, the two metrics of d and C_{eq} were matched to get the same moisture distribution in the material after a certain number of cycles, but those cycles took much *less time* to complete compared to the baseline. For the design of the accelerated thermal cycle, the same predicted level of microcracking damage was obtained in a *smaller number* of more severe cycles.

The more severe cycles actually take more time than an equivalent baseline thermal cycle because lower temperatures have to be reached, but cracking is predicted to occur in fewer cycles and hence time is saved for a given amount of damage.

A 'target' crack density was established after a certain number of the baseline cycles (taken as 1000 cycles in our case). As can be seen in Figure 4.20, an equivalent amount of 'target' damage is predicted to occur in a much smaller number of more severe cycles, as shown by the thin horizontal line in Figure 4.20. For example, 1000 cycles which have a low temperature of -54°C (the baseline cycle) produce the same level of damage as about 250 cycles to a -150°C low, and only 150 cycles for a cycle with a low of -180°C. Hence, theoretically accelerated thermal cycles can produce the same damage after as little as 15% of the number of baseline cycles.

The accelerated thermal cycles used in this study went down to -180°C and -150°C: see Figure 4.20. These will be referred to as Accelerated thermal cycle 1 and Accelerated thermal cycle 2 respectively throughout the rest of this document. They were chosen as they were the most severe cycles that could be easily generated. They also had the largest theoretical affect on the thermal response of the material of any of the family of curves shown in Figure 4.19.

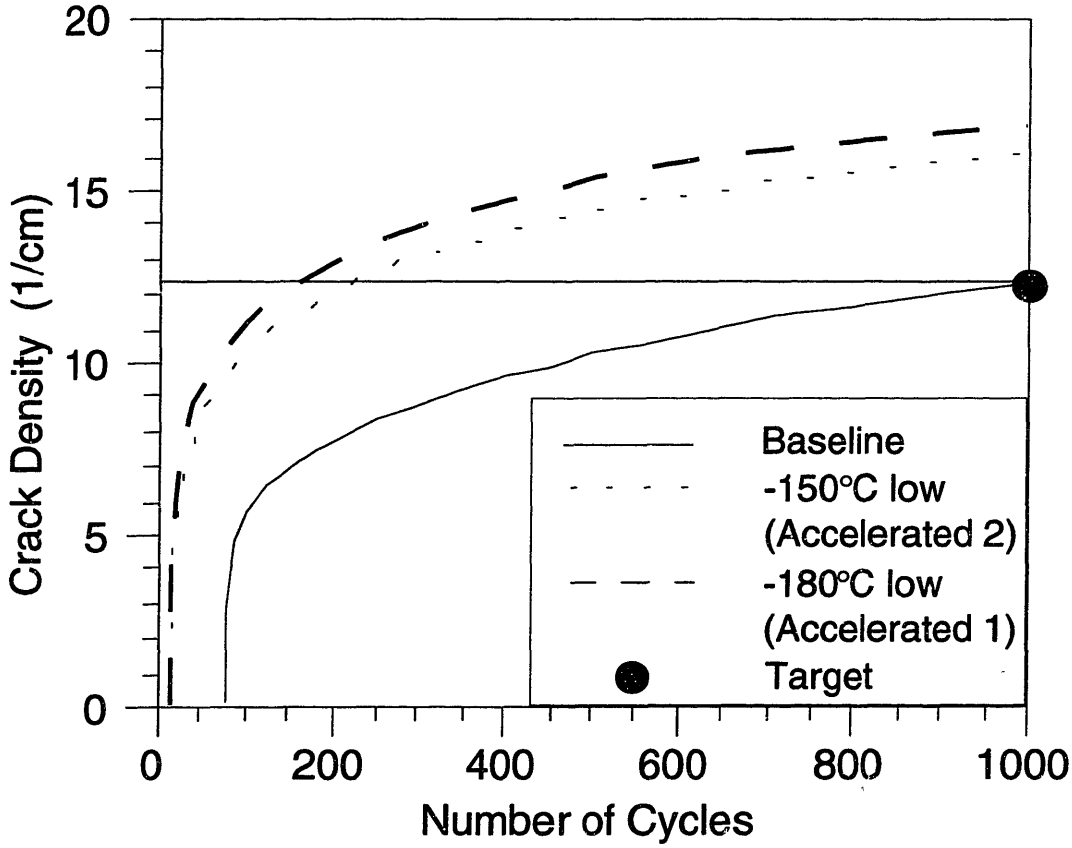

Figure 4.20: Accelerated thermal cycle design plot

CHAPTER 5

EXPERIMENTAL PROCEDURES

5.1 TEST MATRIX DESIGN

5.1.1 Stage I testing

A first phase of testing was undertaken by The Boeing Company. Specimens of four different materials with various layups were tested, as shown in Table 5.1. The materials chosen were those which were of prime interest to high temperature flight applications. For these initial tests, the layups were arbitrary and inconsistent between materials. This phase of testing was performed in order to show what range of damage responses could be expected from this class of materials.

Specimens were subjected to 0, 25, 100, 200, 500 and 1000 cycles of the baseline and isolated thermal environments. Crack damage was counted at Boeing and reduced at MIT. Some interior damage assessment was undertaken by cutting the specimens after exposure and polishing an interior surface which was well below the exposed edge during the test. However, this was only undertaken for one specimen at each cycle number.

The results of this set of tests are given in Appendix B.

Table 5.1: Stage I test program matrix (Boeing)

Material	Layups	Test types
R1-16	$[45/0/-45/90]_{2S}$ $[0_3/90_3]_S$ $[45/-45_2/45/0_4/90]_S$ $[45/-45/0_2/90/0_2/-45/45]_S$	Baseline environment Isolated thermal environment
PETI-5	$[45/0/-45/90]_{2S}$ $[90/0/90]_{2S}$ $[45/-45_2/45/0_4/90]_S$ $[45/-45/0_2/90/0_2/-45/45]_S$	Baseline environment Isolated thermal environment
K3B	$[45/-45/90/0]_{4S}$ $[-45/45/90/0]_{4S}$	Baseline environment Isolated thermal environment
PIXA	$[90/0/90]_{2S}$	Baseline environment Isolated thermal environment

5.1.2 Stage II testing

The second stage of testing was the main experimental program for this work. The testing was conducted both at The Boeing Company in Renton, WA and in the Technology Laboratory for Advanced Composites (TELAC) at MIT in Cambridge, MA.

Two materials which show promise for the application were tested: PETI-5 and PIXA-M. More details and references for these materials are given in Section 2.3.2. Three layups were chosen for testing:

- a 'research' layup of $[90_2/0_4/90_2]_S$
- a 'real' crossply layup of $[0/90/0]_{2S}$
- a 'real' quasi-isotropic layup of $[45/90/-45/0]_{2S}$

These layups will be referred to as 'research', 'crossply' and 'quasi-isotropic' respectively throughout the remainder of this document. Cracking from environmental (and other) damage is generally confined to a ply group (i.e. a number of plies stacked together with the same angle). The research layup was chosen because it contains thick 90_4 ply groups which had been shown in previous studies to damage more easily than thinner ply groups. This generated more data for this study. The two 'real' layups were chosen by Boeing as being realistic laminate layups which could be used for a flight application.

Specimens of each material and layup were exposed to a number of different conditions, designed to isolate one or more components of the baseline environment which potentially could be responsible for causing the damage. These components include:

- moisture cycling
- extended time at moisture
- thermal cycling

- extended time at temperature
- combinations of the above.

Tests were designed to expose specimens to the baseline environment and to isolate the exposure to the above mechanisms from the baseline environment. Parallel tests were also conducted which used the accelerated moisture and accelerated thermal cycles, the designs of which were discussed in the previous chapter. The tests performed exposed specimens to:

- full baseline cycle (combined response to all components)
- isolated thermal component of the baseline cycle (response to thermal only)
- isothermal aging (response to time at temperature)
- accelerated moisture cycling (to speed up response to pure moisture cycling)
- accelerated thermal cycling (to speed up response to pure thermal cycling)
- accelerated thermal cycling of previously isothermally-exposed specimens (to speed up visible damage to possibly degraded material)

This test program is summarized in the test matrix shown in Table 5.2.

Tests conducted by other researchers [55] investigated the effect of isomoisture exposure which showed response to long duration exposure to moisture.

In the operational environment, many other factors may be important, including mechanical stresses, chemical solvents, impacts, etc. The effect of mechanical stresses on these materials, both in isolation and coupled with moisture and temperature effects (so-called 'hygrothermomechanical' testing) are also being investigated [56] as an extension to this study.

Table 5.2: Stage II test program matrix

Material	Layups	Test types	No. of cycles	Notes
PETI-5	'Research' $[90_2/0_4/90_2]_S$ 'Crossply' $[0/90/0]_{2S}$ 'Quasi' $[45/90/-45/0]_{2S}$	Baseline	0, 50, 200, 500, 1000, 1500	2 different specimens at each cycle count
		Isolated thermal	0, 50, 200, 500, 1000, 1500	2 different specimens at each cycle count
		Isothermal	4250 hrs at 350°F only	Research: 8 spcmns Crossply: 4 spcmns Quasi: 7 spcmns
		Accel. moisture	0, 288, 500, 1000, 1500, 1960	2 different specimens at each cycle count
		Accel. thermal 1	0, 65, 100, 180, 300, 400, 540, 750	same 3 specimens used throughout
		Accel. thermal 2	0, 80, 170, 280, 410, 560, 750	same 3 specimens used throughout
		Accel. thermal 1 (isothermal specimens)	0, 50, 150, 300, 400	same 3 isothermal specimens used throughout
PIXA-M	'Research' $[90_2/0_4/90_2]_S$ 'Crossply' $[0/90/0]_{2S}$ 'Quasi' $[45/90/-45/0]_{2S}$	Baseline	0, 50, 200, 500, 1000, 1500	2 different specimens at each cycle count
		Isolated thermal	0, 50, 200, 500, 1000, 1500	2 different specimens at each cycle count
		Isothermal	4250 hrs at 350°F only	Research: 8 spcmns Crossply: 5 spcmns Quasi: 7 spcmns
		Accel. moisture	0, 288, 500, 1000, 1500, 1960	2 different specimens at each cycle count
		Accel. thermal 1	0, 65, 100, 180, 300, 400, 540, 750	same 3 specimens used throughout
		Accel. thermal 2	0, 80, 170, 280, 410, 560, 750	same 3 specimens used throughout
		Accel. thermal 1 (isothermal specimens)	0, 50, 150, 300, 400	same 3 isothermal specimens used throughout

5.2 MANUFACTURE AND TESTING PROCEDURES

5.2.1 Material manufacture (Boeing)

The plies were laid up into 12" by 12" flat plates according to the laminate configurations outlined above. The laminates were laid on a plate, vacuum-bagged and a 27" Hg vacuum was maintained during the cure. The PETI-5 material was cured at 750°F in an autoclave pressurized to 100 psi. The PIXA-M was cured at 700°F with 100 psi positive pressure. Exact dwell times and ramp rates were unavailable (proprietary data). After curing, the plates had 0.5" cut from all edges to remove resin-starved material, leaving plates of 11" square. These were then cut on a water-cooled diamond saw into specimens 2" long by 1" wide. The specimens were subsequently polished on all sides using Struers automatic polishers down to a 5μm finish. The specimens were then dried in a Blue-M electric oven for 5 days at 300°F to remove any internal moisture prior to testing.

5.2.2 Baseline environmental testing (Boeing)

A Thermotron Model F-7-CHM-5-5 environmental chamber was used with a Model 4800 microcontroller. This was pre-programmed to run the exact conditions of the baseline cycle. Wet and dry bulbs created the appropriate moisture environments, while electric heaters, forced-air mechanical refrigeration units and cryogenic attachments maintained the desired temperatures in the oven. Specimens were held in the oven in a rack assembly, with a controller feedback thermocouple situated next to these specimens. The specimens which were designated to experience only the thermal component of the cycle were wrapped in aluminum foil. This was to protect these specimens from the moisture in the environment without affecting the thermal exposure. However, there was evidence to suggest that this procedure did not actually shield the specimens from all of the moisture in the environment, the implications of which are discussed in Chapter 7.

5.2.3 Accelerated moisture cycling (Boeing)

A similar environmental chamber was used as for the baseline testing. It was programmed to conduct the accelerated moisture cycle as defined in the previous chapter. Unfortunately, equipment error meant that the actual cycle which the materials saw was different from the desired accelerated moisture cycle. All parameters were as detailed in Table 4.2, *except* the warm/wet hold temperature was 82°C (180°F) rather than the desired 93°C (200°F). This difference in warm/wet hold temperature had a non-trivial effect on the theoretical moisture distribution (see Figure 5.1). Of the two metrics, C_{eq} was 20% less and d was 25% less compared to the baseline cycle due to the error in the accelerated cycle parameters. Although the response to the accelerated moisture environment is further than desired from the baseline response, the C_{eq} and d parameters are sufficiently close as to not invalidate the usefulness of the tests. The moisture-thrashed peak is as high as in the baseline response, and hence the extreme edge layer sees a moisture environment similar to the baseline. The moisture-thrashed zone is a little less thick, so any moisture-thrashing-induced damage may not be expected to progress quite as far as in the material exposed to the baseline cycles.

Equipment failure during the course of the accelerated moisture cycling experiments left the specimens under unknown ambient conditions for several days. It is difficult to quantify the effect that this had on the response of the specimens (if any), but it is unlikely that this would significantly alter the damage response.

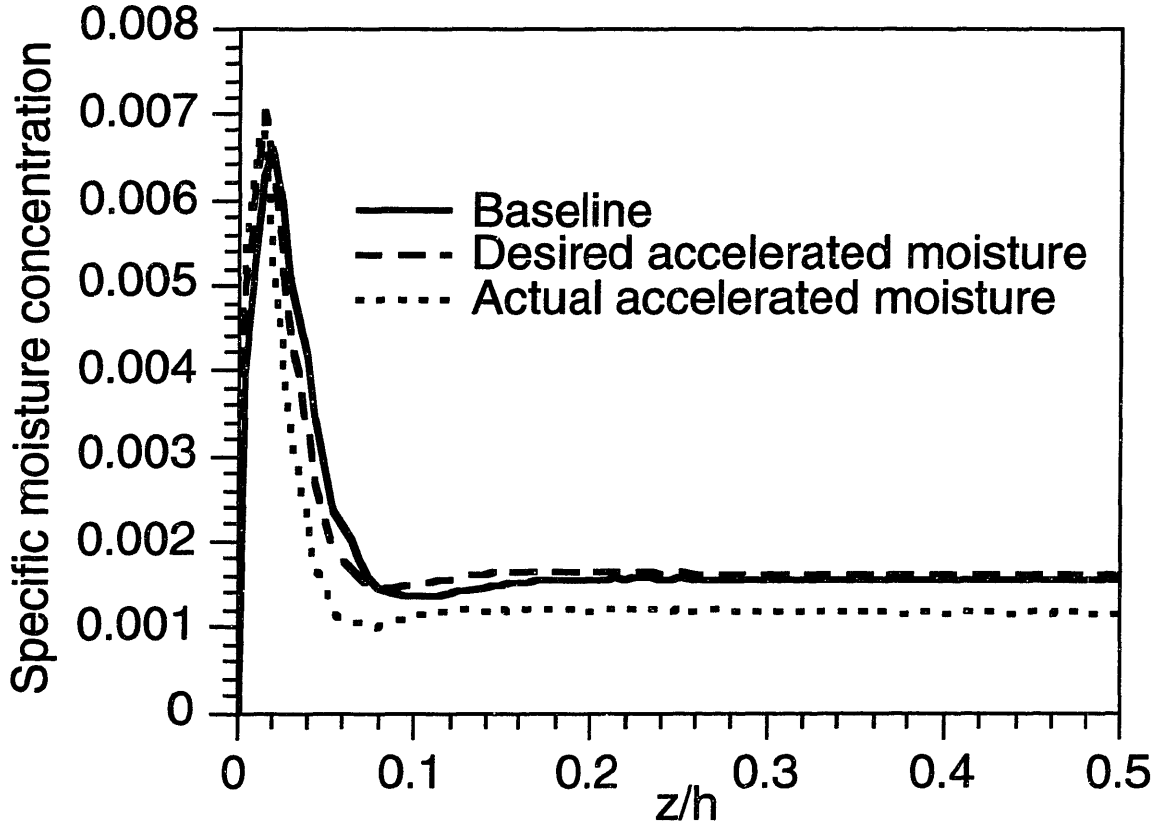

Figure 5.1: Moisture response from actual and desired accelerated moisture cycle

5.2.4 Accelerated thermal cycling (MIT)

Specimens were shipped from Boeing, precut and polished. The specimens were dried in a Blue-M electric post-cure oven at MIT for 5 days at 300°F to remove any internal moisture and stored in dessicant prior to testing. The testing chamber used was an Applied Test Systems Series 3610 Test Oven, with two 200W electric heaters and a liquid nitrogen injector assembly. Two 240 liter tanks of liquid nitrogen (pressurized to 22 psi) were connected to the chamber with the flow controlled by an Automatic Switch Co. 100 psi cryogenic valve. The desired temperature profile was entered into an Omega CN 2042 microprocessor-based controller which directly controlled the chamber heaters and cryogenic valve equipment. Specimens were held in a steel wire framework in the middle of the test oven, the framework being mounted in an aluminum frame. Feedback of the chamber temperature conditions was accomplished by a J-type thermocouple situated next to the specimen rack. See Figure 5.2.

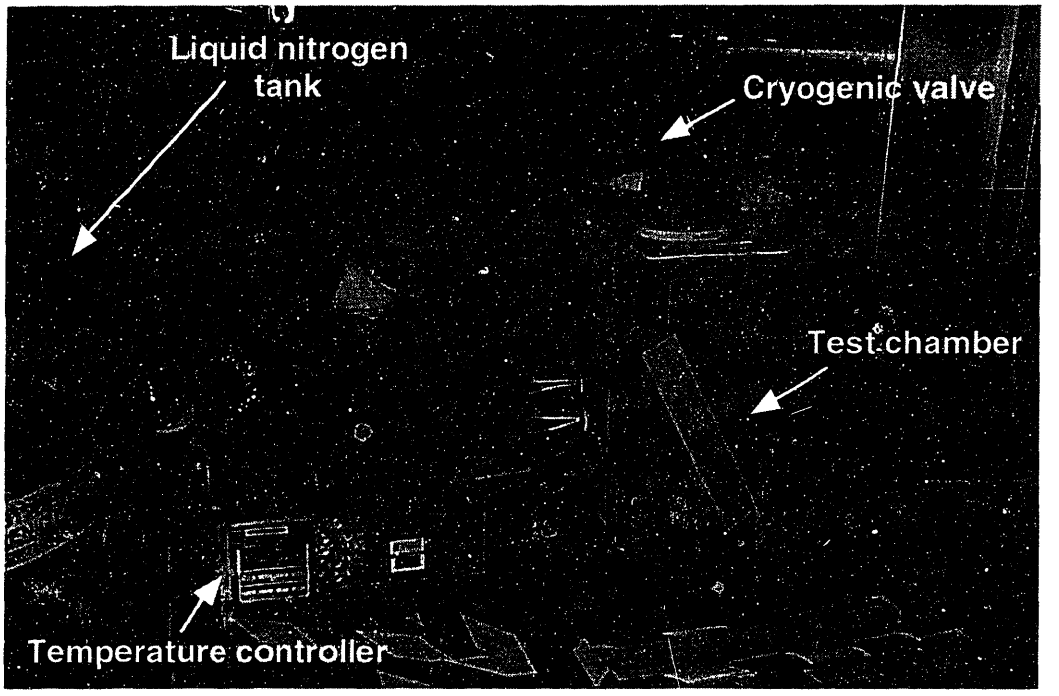

Figure 5.2: Accelerated thermal cycling equipment setup

5.2.5 Isothermal aging (Boeing)

Specimens were placed on a rack in a Blue-M electric oven. The oven was held at a constant temperature of 350°F and specimens were removed after 4250 hours of exposure.

5.3 DAMAGE ASSESSMENT TECHNIQUE (MIT)

5.3.1 Defining damage

The impact of the environment on the materials was measured by the amount of cracking damage that was visible on the polished edge of the specimens. In the research layup of $[90_2/0_4/90_2]_S$, it was the center 90_4 ply group which was chosen as the group of interest in this study as it was thick. A number of different crack configurations are possible: see Figure 5.3. A 'group' crack is defined as one which traverses the entire 90_4 ply group. 'Triple', 'double' and 'single' cracks traverse three, two and one ply from the group respectively. A crack was designated as a single if it traversed from half to one and a half plies, a double if it traversed one and a half to two and a half plies and as a triple if it traversed between two and a half and three and a half plies.

In the 'real' layups, the plies of interest were the single 90's (the other plies did not show significant damage). Hence, the only damage seen was of cracks spanning one ply: see Figures 5.4 and 5.5.

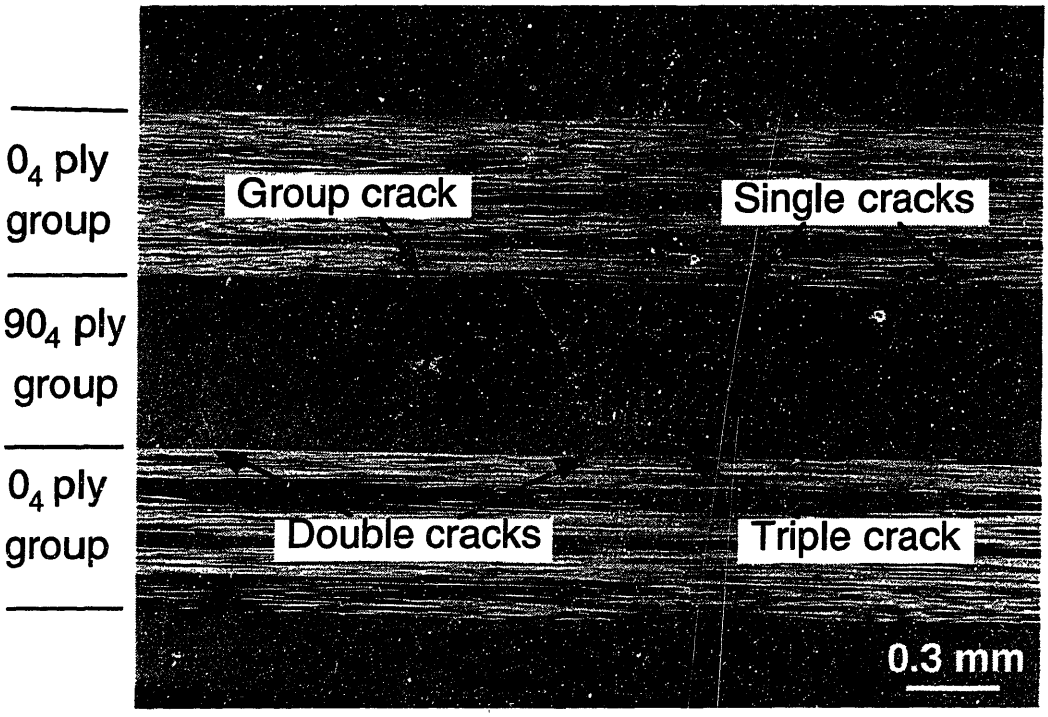

Figure 5.3: Crack types at the edge of the 'research' layup

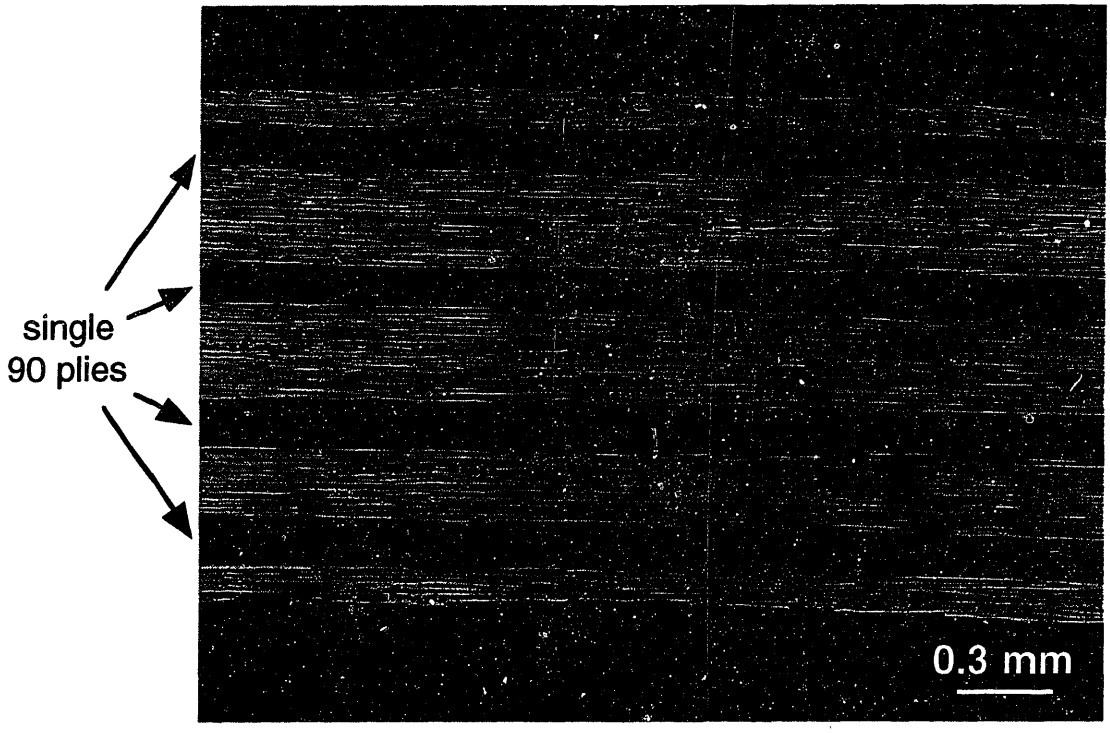

Figure 5.4: Cracking at the edge of the 'real' crossply layup

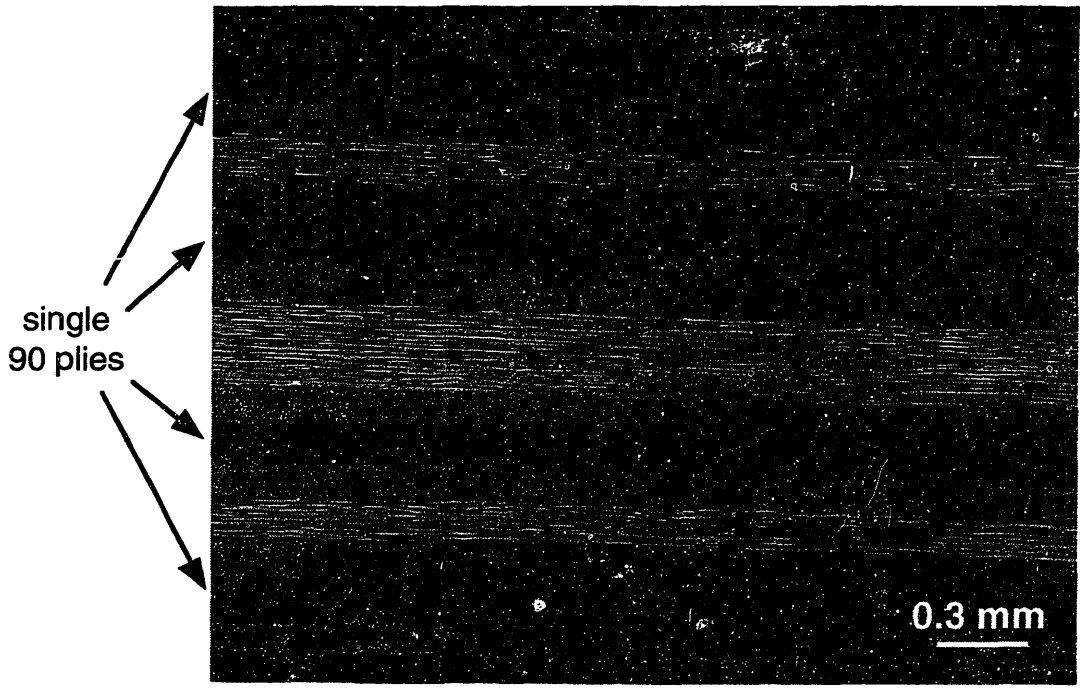

Figure 5.5: Cracking at the edge of the 'real' quasi-isotropic layup

5.3.2 Measuring edge damage

The edge damage was measured by counting the number of cracks in the ply groups of interest. For the research layup, the number of group, triple, double and single cracks on the entire length of each 2" side of all specimens were counted. For the real crossply and quasi-isotropic layups, the number of single cracks in each of the four 90° plies on each side were counted. The 45° plies were checked, but very few cracks were observed and were not useful for analysis purposes. Cracks were counted by viewing the specimens under an Olympus SZ stereoscope (see Figure 5.6), with a magnification of 20-40x as required. Light was brought onto the specimen using a 150W dual fiber optic halogen lamp. The polished surfaces of the specimen were cleaned with a water-soaked cotton-tipped applicator prior to viewing. Crack numbers were recorded using a hand tally counter as the specimen was moved across the field of view.

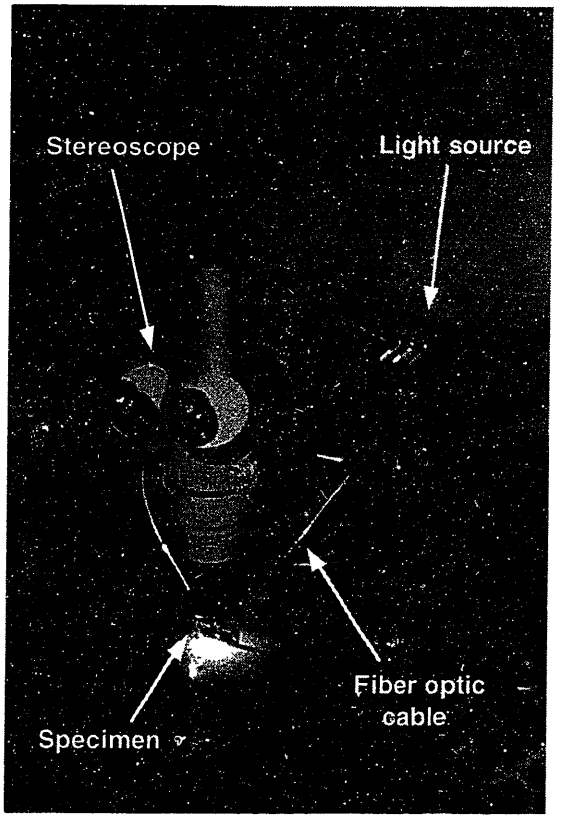

Figure 5.6: Crack-counting stereoscope equipment setup

Photographs of damage responses were taken using an Olympus BH-2 microscope with a 5x NeoSPlan lens coupled with an Olympus Polaroid film body. This gave a total magnification on the film of 38x. The film used was Polaroid 55 positive/negative 4x5 Instant Sheet Film, ISO 50/18°. The pictures used in this thesis were scanned directly from the print on an HP ScanJet 4c into a Power Macintosh, and then the sharpness was enhanced using Kodak PhotoEnhancer software to make the cracks more visible.

5.3.3 Tracking internal damage

To investigate the damage propagation in the interior, some specimens had surface layers removed by grinding down a known amount of material. This was achieved by the technique shown in Figure 5.7. Small 1" by 0.5" samples were cut from a corner of the

original 2" by 1" specimens using a Dremel Moto-Tool with No. 409 cut-off wheels. The polished edge whose damage depth was to be investigated was on the 1" side. A metal 'depth gage' was glued to the specimen with Ducco multipurpose cement such that the tip of the gage was directly in line with the polished edge of the specimen under investigation. It was very important to ensure that the gage was accurately aligned such that the two parallel edges of the gage were perpendicular to the polished edge. These procedures were achieved by viewing through the stereoscope and carefully positioning the metal gage while the cement was still compliant. The specimen was then stabilized with a Buehler stainless steel 'Sampl-Klip' support spring before placing in a Buehler 1.25" diameter plastic mold with the side to be polished facing down. 15g of Buehler Epo-Kwik resin was added to 3g of hardener and stirred slowly until the solution was clear. This was then added to the mold around the specimen and left to cure overnight. The result was the specimen mounted in a clear cylinder of epoxy resin, with the specimen at one end of the cylinder ready for grinding and polishing. Polishing was achieved on a Struers Rotopol-1 automatic polisher with Pedemat power heads capable of applying a predetermined force on up to 6 specimens simultaneously. Grinding took place with 500, 1200 and 2400 grit silicon carbide paper mounted on the wheels of the machine. Most grinding took place on the 500 grit paper, which was found to remove about 1 mm of material from the surface of the specimen with a force of 55N over 10 minutes. The other grit papers were used to remove the scratches left after the 500 grit was used. Final polishing to a suitable finish for photographic purposes was achieved with a force of 60N for 45 minutes using 4000 grit paper.

The depth, e, from the edge was found by measuring the length, l, of exposed 'depth gage' left on the new polished surface: see Figure 5.7. By knowing the angle at the tip of the depth gage (which is level with the initial surface prior to polishing), and the length, l, the depth below the initial exposed edge could easily be found. By performing a number of grinds, a three dimensional map of damage from the edge could be obtained.

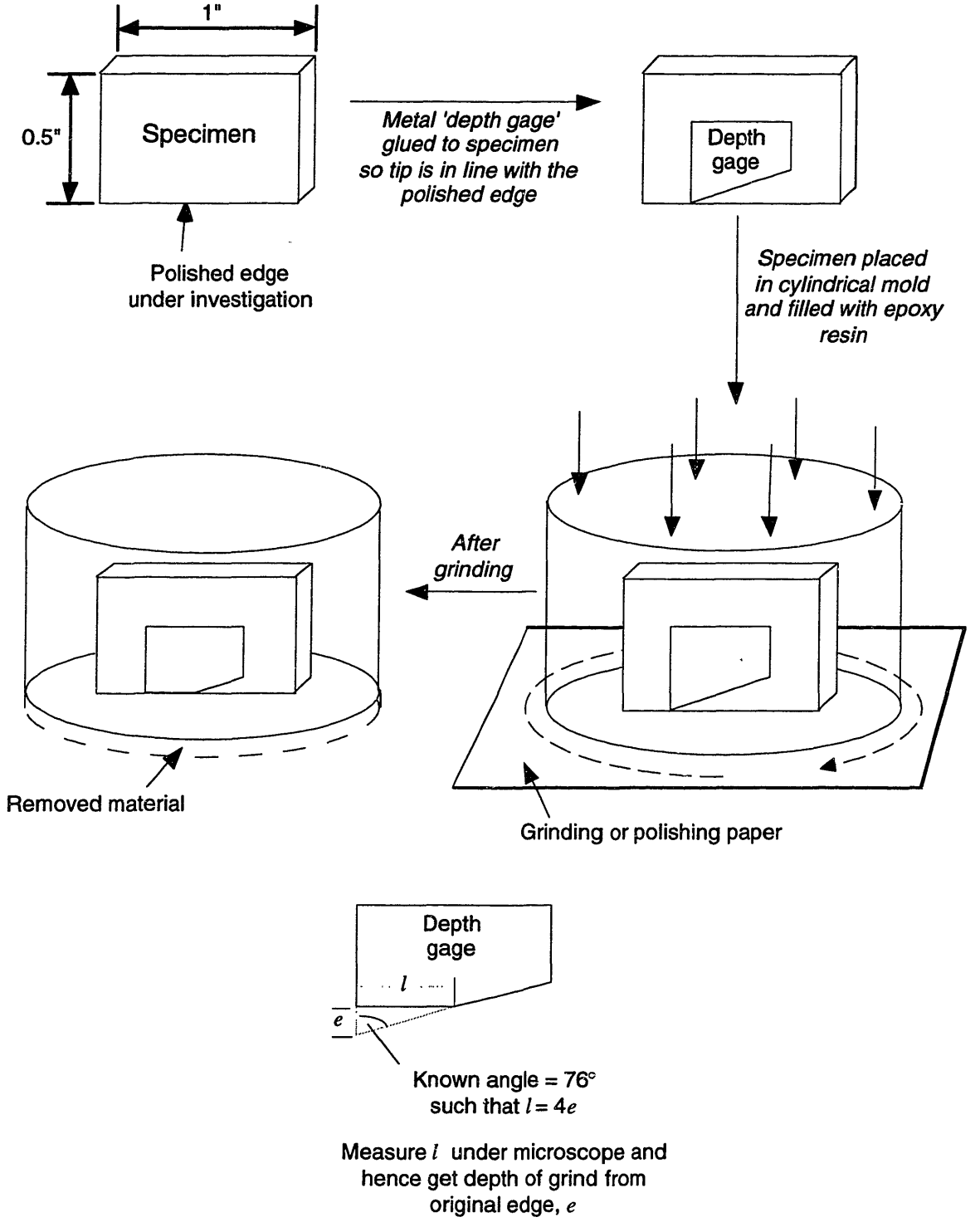

Figure 5.7: Grinding and polishing technique

5.4 DATA REDUCTION

5.4.1 Crack count data

The data obtained from these statistical methods is displayed in Appendix A.

5.4.1.1 Research layup

For the research layups, the number of group cracks were counted in the 90_4 group on both 2" sides of all three specimens at each condition. The average group crack density was calculated as:

$$Average\ group\ crack\ density\ (/cm) = \frac{\sum_{\substack{across\\ sides\ and\\ specimens}} (Group\ crack\ count)}{3\ specimens \times 2\ sides \times 5.08\ cm/side} \tag{5.1}$$

Counts of triple, double and single cracks were also taken and averaged in the same way. An 'aggregate' crack density was used as a measure of the overall level of cracking in these thick ply groups. The aggregate crack count in a given ply group was found from:

$$Aggregate\ crack\ count = \begin{bmatrix} (4 \times \#\ of\ groups) + (3 \times \#\ of\ triples) \\ + (2 \times \#\ of\ doubles) + (\#\ of\ singles) \end{bmatrix} \tag{5.2}$$

The average aggregate crack density was then calculated using:

$$Average\ aggregate\ crack\ density\ (/cm) = \frac{\sum_{\substack{across\\ sides\ and\\ specimens}} (Aggregate\ crack\ count)}{3\ specimens \times 2\ sides \times 5.08\ cm/side} \tag{5.3}$$

Standard deviations for a given crack type were calculated using the equation:

$$Standard\ deviation = \sqrt{\frac{\sum (crack\ count - average)^2}{(\#\ of\ count\ values\ - 1)}} \tag{5.4}$$

where 'crack count' is the number of cracks of a given type in each ply or ply group.

5.4.1.2 Crossply and quasi-isotropic layups

For these layups, the number of ply cracks were recorded for all four 90 plies on each 2" side of the three specimens at a given test condition. The average crack density was calculated using:

$$Average\ crack\ density\ (/cm) = \frac{\sum_{\substack{across\ plies,\\ sides\ and\\ specimens}} (\#\ of\ cracks\ in\ each\ ply)}{3\ specimens \times 2\ sides \times 4\ plies/side \times 5.08\ cm/side} \tag{5.5}$$

Standard deviations were calculated as in Eqn. 5.4.

5.4.2 CRACKOMATIC fits

Fits to select data sets were made using the CRACKOMATIC code. The fit to a G-N curve eliminates geometric and laminate effects and hence should reveal the *material* response to environmental cycling.

Material properties are input into the code (Appendix C). In all case, the shear lag parameter was taken as ξ=0.6 (consistent with that used in [43]). Assuming the material toughness drops as in Eqn. 4.17, a fit was obtained by adjusting G_0 and A and repeatedly running the analysis until cracking onset and growth rate were successfully simulated. The G_0 parameter has a dominant effect on the onset of cracking, while A dictates how quickly crack density increases thereafter. In some cases, Eqn. 4.17 was unsuitable and a more

general G-N curve (Eqn. 4.16) was determined by repeated analytical fits to the microcracking data.

The values obtained are representative of the properties of the material near the edges of the material which is cracking and not necessarily the material as a whole. But these values do give an indication as to the toughness of the material in the damaged layer and the susceptibility of the material to environmental cycling degradation. In cases where Eqn. 4.17 was usable, G_0 indicates the initial toughness of the material in the cracking area, while A reflects its sensitivity to the environment. A value of A close to 1 indicates a material which is resistant to degradation, while a value closer to zero indicates a material which is vulnerable to environmental damage.

CHAPTER 6

RESULTS

6.1 STAGE I TESTING

The first stage of testing (as outlined in Section 5.1.1) yielded some interesting qualitative data. Cracking which was observed on the edges was tracked into the specimen interior by the method described in Section 5.3.3. Figure 6.1 shows significant edge damage in the thick 0_6 ply group of the $[0_3/90_3]_S$ layup of the R1-16 material subjected to 500 baseline cycles. The smaller cracks were seen to disappear only a very short distance into the interior – Figure 6.2 shows the crack state 0.25 mm below the original edge. At 0.5 mm below the original edge, only 3 or 4 cracks were still visible (Figure 6.3), while at 0.8 mm virtually all the damage was gone (Figure 6.4). The same technique revealed that the more severe (group) cracking in this material was visible up to 2 mm below the original edge. Similar results were obtained for the other materials (except K3B) subjected to 500 baseline cycles, with no damage progressing further into the material than a very thin edge layer, with a depth of less than 2 mm.

Cutting and polishing of an interior surface (0.5" from the exposed edge) only revealed cracks in the 90° plies of the K3B quasi-isotropic specimens (see Figure 1.5). All the other specimens showed no damage at this internal location. The behavior displayed by the K3B material was consistent with that due to classical thermal microcracking. From the very limited amount of data available for K3B (only one specimen at each cycle number), an assessment with the classical thermal microcracking code CRACKOMATIC (see Section 4.4 and 5.4) was undertaken. An approximate fit to the data was obtained as shown in

Figure 6.5. The crack density variation is typical of thermal microcracking: delayed crack initiation followed by a rapid increase in the crack growth rate. The fracture toughness of these high temperature resin systems is proprietary, but it is generally believed to be around 1000 J/m^2. A value of 950 J/m^2 was suitable for capturing the onset of cracking at around 100 cycles, while a very low value of A (see Eqn. 4.17) was required to capture the level of cracking displayed thereafter. In order to achieve this, a value of 0.57 was needed for A, implying a 43% reduction in the fracture toughness of the material for each factor of ten increase in the number of exposure cycles.

The fit of the observed interior cracking behavior data to a classical thermal microcracking prediction suggests that the K3B material is more sensitive to the hygrothermal environment than the other materials tested. Even though the exact values may be approximate, using a realistic initial fracture toughness requires a very low value of A in order to fit to the data, suggesting that this material is *very* sensitive to hygrothermal fatigue. This is one of the reasons this material was not considered further for this application.

The data produced from this testing in contained in Appendix B.

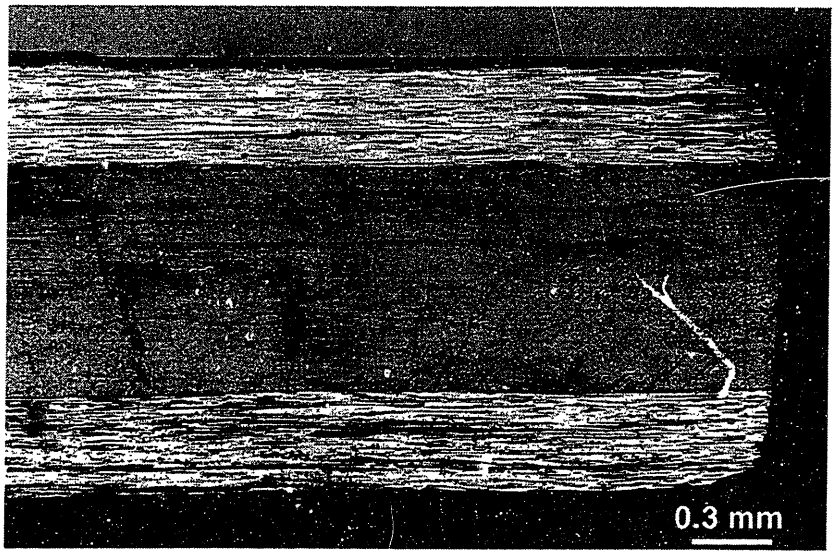

Figure 6.1: Edge damage in the $[0_3/90_3]_S$ R1-16 laminate subjected to 500 baseline cycles

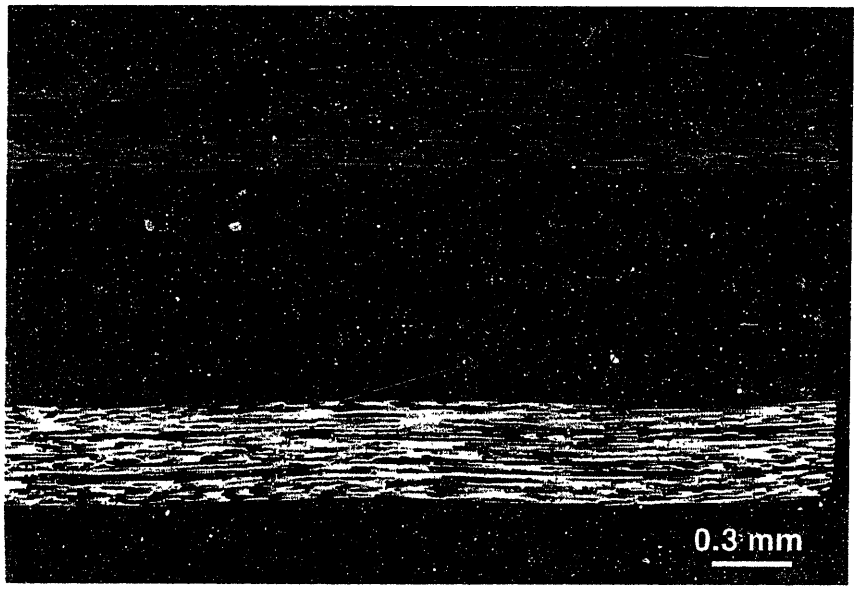

Figure 6.2: Damage at a depth of 0.25 mm from the original edge

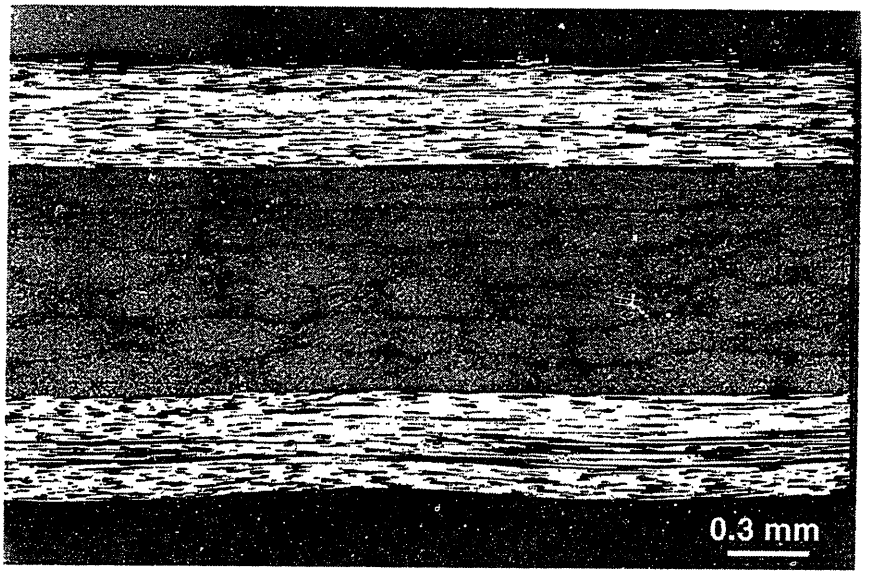

Figure 6.3: Damage at a depth of 0.5 mm from the original edge

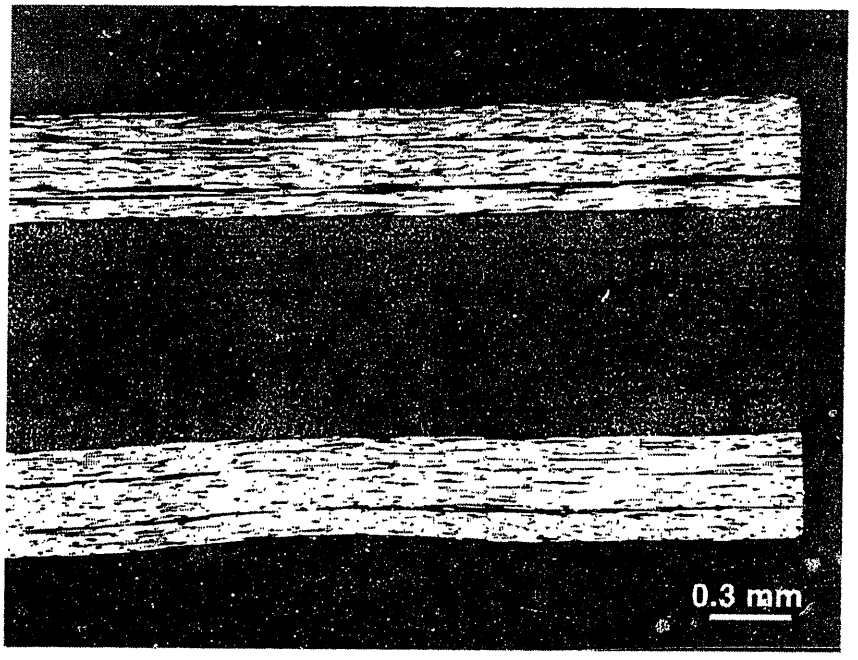

Figure 6.4: Damage at a depth of 0.8 mm from the original edge

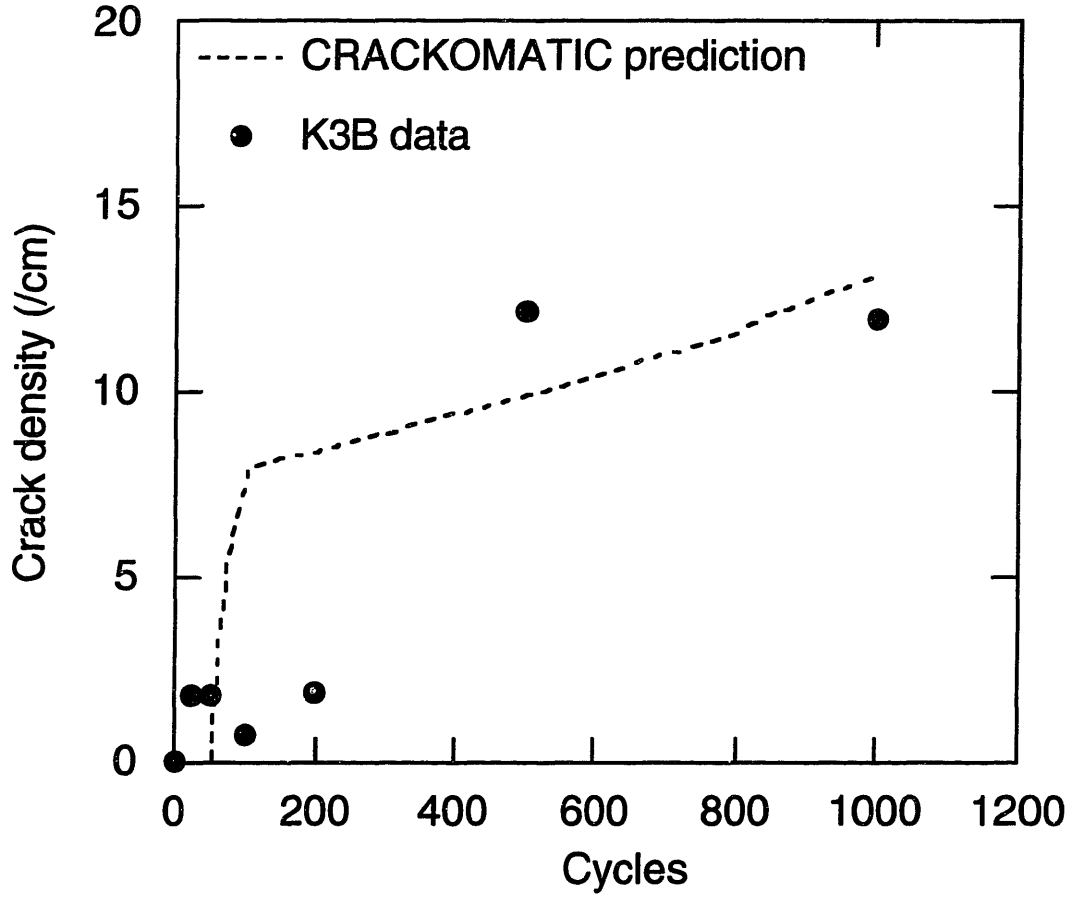

Figure 6.5: Comparison of classical thermal microcracking prediction with internal damage data in the K3B laminate subjected to the baseline environment

6.2 STAGE II TESTING – EDGE DAMAGE

6.2.1 General

Group, triple, double and single cracks were counted and recorded for all the 90_4 ply groups of the research specimens. The single crack counts were also taken for all the 90 ply groups of both the quasi-isotropic and crossply layups (see Appendix A). The data produced was reduced as discussed in Section 5.4.

The average crack densities and error bars showing one standard deviation from the average are plotted in the Figures which follow.

6.2.2 Baseline, isolated thermal and accelerated moisture edge data

6.2.2.1 PETI-5 results

The data for these tests can be found in Tables A.1, A.3 and A.5. Plots of the reduced data for the three tests for a given crack type (group and aggregate) and laminate are shown in Figures 6.6-6.9.

Figure 6.6 shows the number of group cracks in the 90_4 ply group of the PETI-5 research laminates for these three test conditions. Very little cracking is evident under any condition before 500 cycles have elapsed. Thereafter, the baseline cycle causes a rapid increase in group crack density after 1000 cycles. An additional 500 cycles causes no significant further increase in the group crack density average from that at 1000 cycles, but there is significant scatter in the 1500 cycle data. The data for specimens subjected to the isolated thermal environment shows a similar increase after 500 cycles to 30-50% of the baseline environment group crack values, but again there is a large amount of scatter in the 1500

cycle data. The data for specimens subjected to the accelerated moisture environment shows no group cracking occurs until after 1500 cycles have elapsed, and even then to only about 20% of the value caused by the baseline cycle after 1000 cycles.

Figure 6.7 shows the aggregate crack data for the same layup, ply group and conditions. Aggregate crack densities are uniformly higher than the corresponding group crack densities, by about a factor of 10. This indicates that there is extensive partial cracking, in addition to the large group cracks (see Eqn. 5.2 and Figure 5.3). The baseline environment causes a slow but steady increase in aggregate crack density up to 500 cycles. After this, the increase is more rapid until a pseudo-equilibrium level appears to be reached after 1000 cycles (at about 35 cracks/cm), much like that seen in the group crack data for the baseline environment. The isolated thermal environment causes a similar affect on the specimen's aggregate crack density as on the group cracks. Little response is shown up to 500 cycles, after which crack density rises steadily. The average crack density at 1000 cycles is about 50% of the value for the baseline environment, while the densities after 1500 cycles are almost identical (although there is much more scatter in the isolated thermal data). Again, the accelerated moisture environment causes little cracking until after 1500 cycles, although by 2000 cycles, the aggregate crack density has reached about 15 cracks/cm (albeit with a lot of scatter), which is about 50% of the 'pseudo-equilibrium' baseline value after 1000 cycles.

Similar behavior for all three environments is shown by the crossply laminate specimens (see Figure 6.8). The average cracking response of the specimens subjected to the baseline environment again displays a rapid increase to a pseudo-equilibrium level after 1000 cycles. Again, the response of specimens subjected to the isolated thermal environment is somewhat less severe than that due to the baseline environment before 1000 cycles. However, by 1500 cycles the averages are very similar and well within the scatter of data

from both environments. The cracking response of specimens subjected to the accelerated moisture cycle shows a more steady rise than before, but the values are about 30% of the corresponding baseline environment response, and much scatter is evident for the higher cycle counts.

The quasi-isotropic laminate response to the baseline and isolated thermal environments show similar trends (see Figure 6.9) as seen for the crossply specimens, although the crack densities are somewhat lower (final value of about 15/cm compared to about 25/cm in the crossply baseline response). However, the accelerated moisture environment now causes very little cracking, even after 2000 cycles.

6.2.2.2 PIXA-M results

The data for these tests can be found in Tables A.2, A.4 and A.6, and plotted in Figures 6.10-6.13.

Figure 6.10 shows the density of group cracks in the PIXA-M research specimens (compare with Figure 6.6). The baseline environment causes a steady rise in the group crack density average up to 1000 cycles, followed by a curious drop in the 1500 cycle average (although the scatter still encompasses all of the 1000 cycle data average and spread). Specimens exposed to the isolated thermal environment show similar behavior as seen in PETI-5: delayed crack initiation (to 500 cycles) followed by a steady increase thereafter, approaching the baseline values after 1500 cycles. Note that the baseline and isolated group crack densities are higher than the equivalent values in PETI-5 by approximately a factor of 2. The group data for specimens subjected to the accelerated moisture environment is also different from the PETI-5 response. Group cracking starts

immediately and produces crack densities comparable to those produced by the isolated thermal environment. Data scatter was very low for these specimens.

The trends for the aggregate crack densities in the research laminate (Figure 6.11) are remarkably similar to those displayed for the group crack densities for all three environments. Not surprisingly given the definition, the magnitudes are higher by a factor of about 7. Comparison of Figure 6.11 with Figure 6.7 shows that the response to the baseline cycle is somewhat more severe in the PIXA-M, but the response to the isolated thermal cycle is remarkably similar for the two materials, both having approximately 40 cracks/cm by the 1500 cycle point. The response to the accelerated moisture environment is much more severe in the PIXA-M than PETI-5, with aggregate crack density rising to about 30/cm by 1500 cycles, compared to only about 15/cm after 2000 cycles in the PETI-5.

Figure 6.12 shows the response of the PIXA-M crossply specimens to the three environments. Exposure to the baseline environment causes a fairly steady increase in crack density to 1500 cycles. Response to the isolated thermal environment shows the same delayed crack growth followed by an approach to the baseline environment values for 1500 cycles, as seen before for the other layups. Exposure to the accelerated moisture cycle causes cracking to a level of only about 50% of the response to the isolated thermal environment. Comparison with the PETI-5 response (Figure 6.8) shows the crack densities under all conditions are only slightly higher in PIXA-M than in PETI-5.

The behavior of the quasi-isotropic specimens is shown in Figure 6.13. The crack densities are very similar to those displayed by the crossplies for all environments up to 1000 cycles. However, after 1000 cycles the cracking from exposure to the baseline and isolated thermal environments show no further increase in average crack density. In fact, the response to the

baseline cycle to 1500 cycles shows a decrease in average crack density which cannot be fully explained by data scatter, which is relatively low in this case. Specimens subjected to the accelerated moisture environment show a similar slowing down of crack growth at larger cycle numbers. Comparison with the equivalent PETI-5 specimen results (Figure 6.9) show the baseline response gives very slightly more cracking in PIXA-M than PETI-5. The isolated thermal responses are very similar in behavior and crack density magnitude, while the accelerated moisture cracking response is much more significant in PIXA-M than in PETI-5.

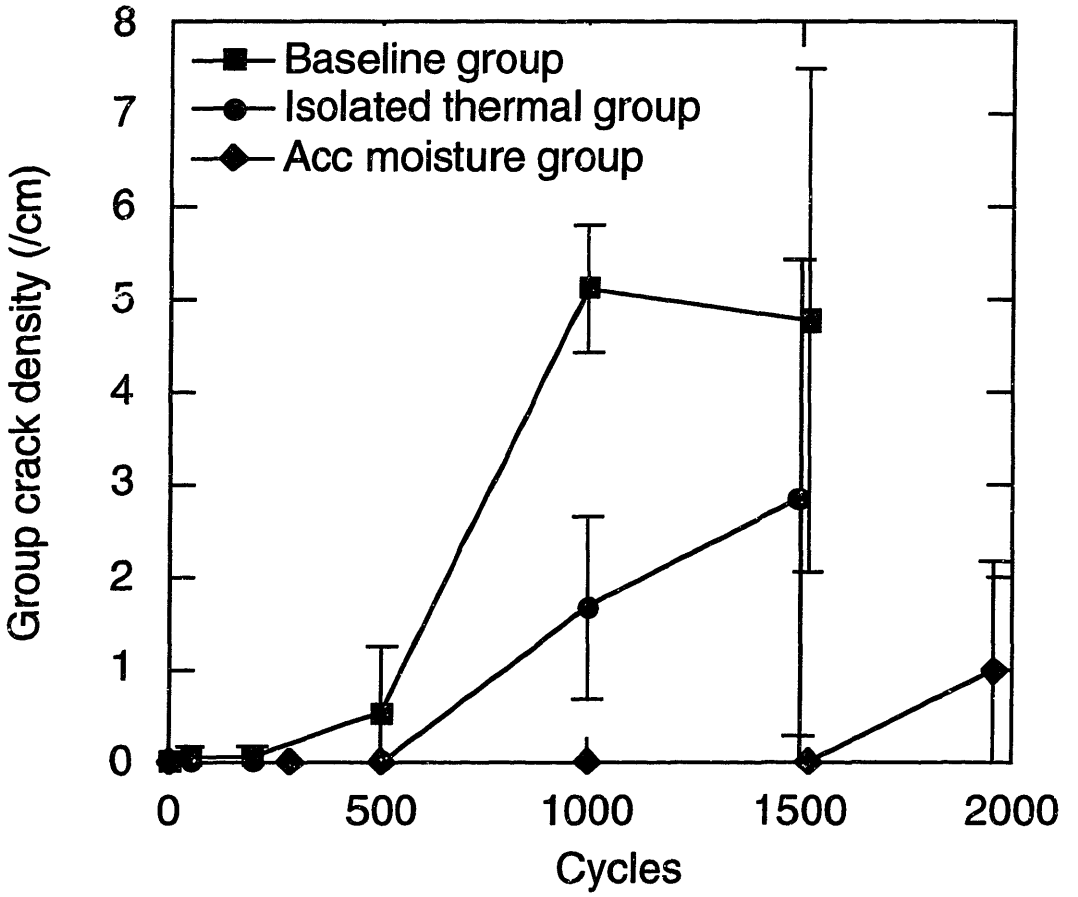

Figure 6.6: Group crack density at the edge in the 90_4 ply group for PETI-5 research specimens exposed to the baseline, isolated thermal and accelerated moisture environments

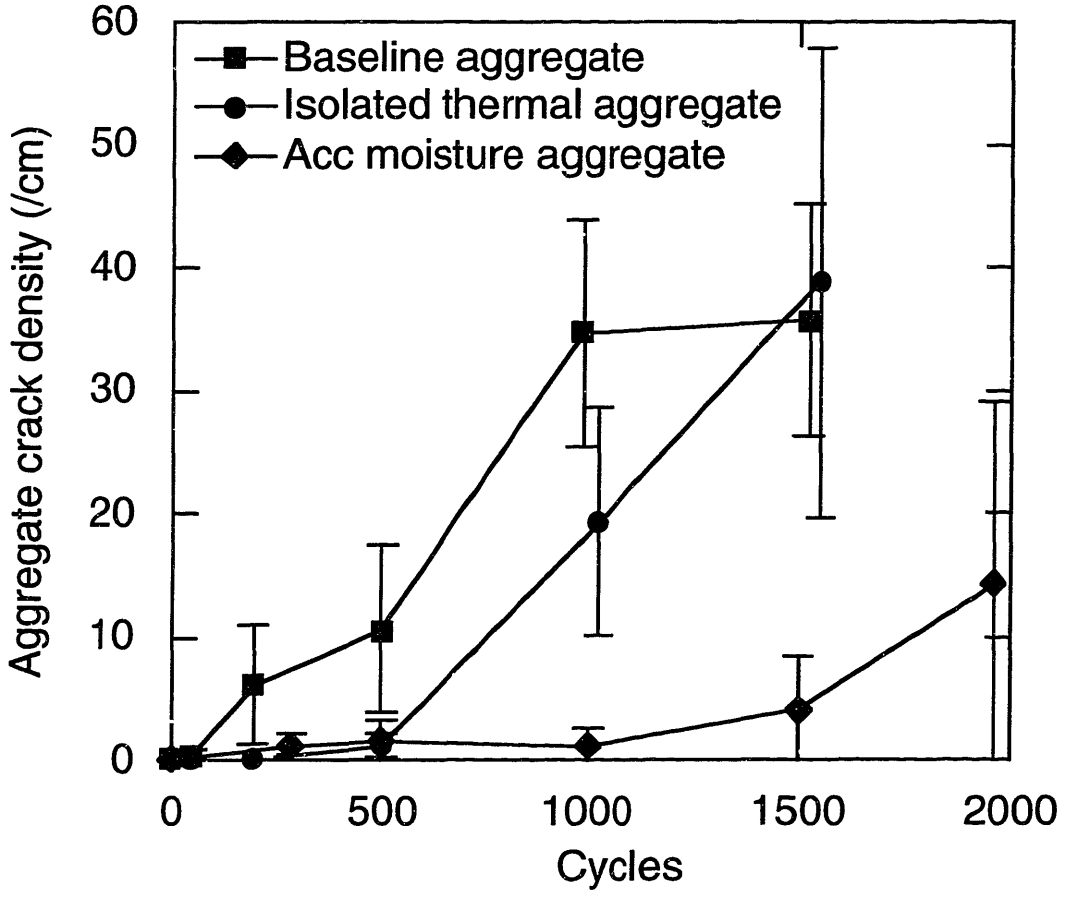

Figure 6.7: Aggregate crack density at the edge in the 90_4 ply group for PETI-5 research specimens exposed to the baseline, isolated thermal and accelerated moisture environments

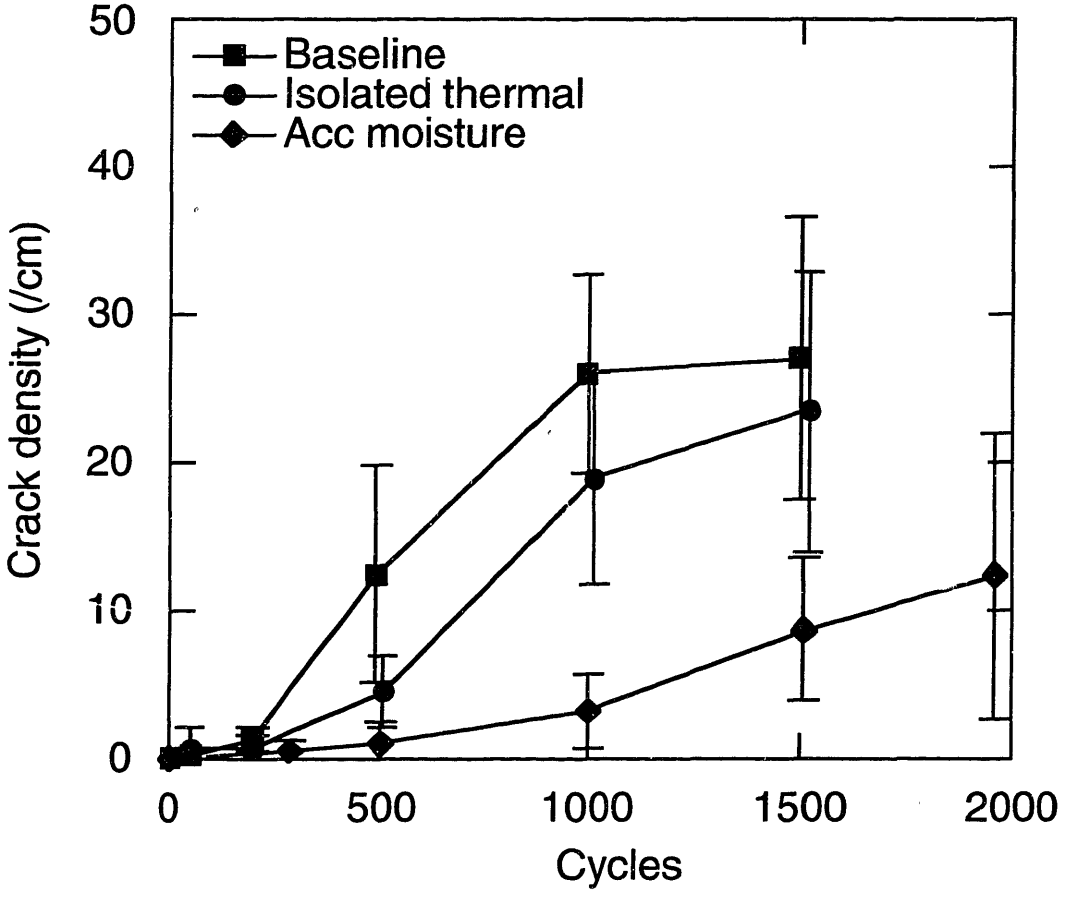

Figure 6.8: Averaged crack density at the edge for PETI-5 crossply specimens exposed to the baseline, isolated thermal and accelerated moisture environments

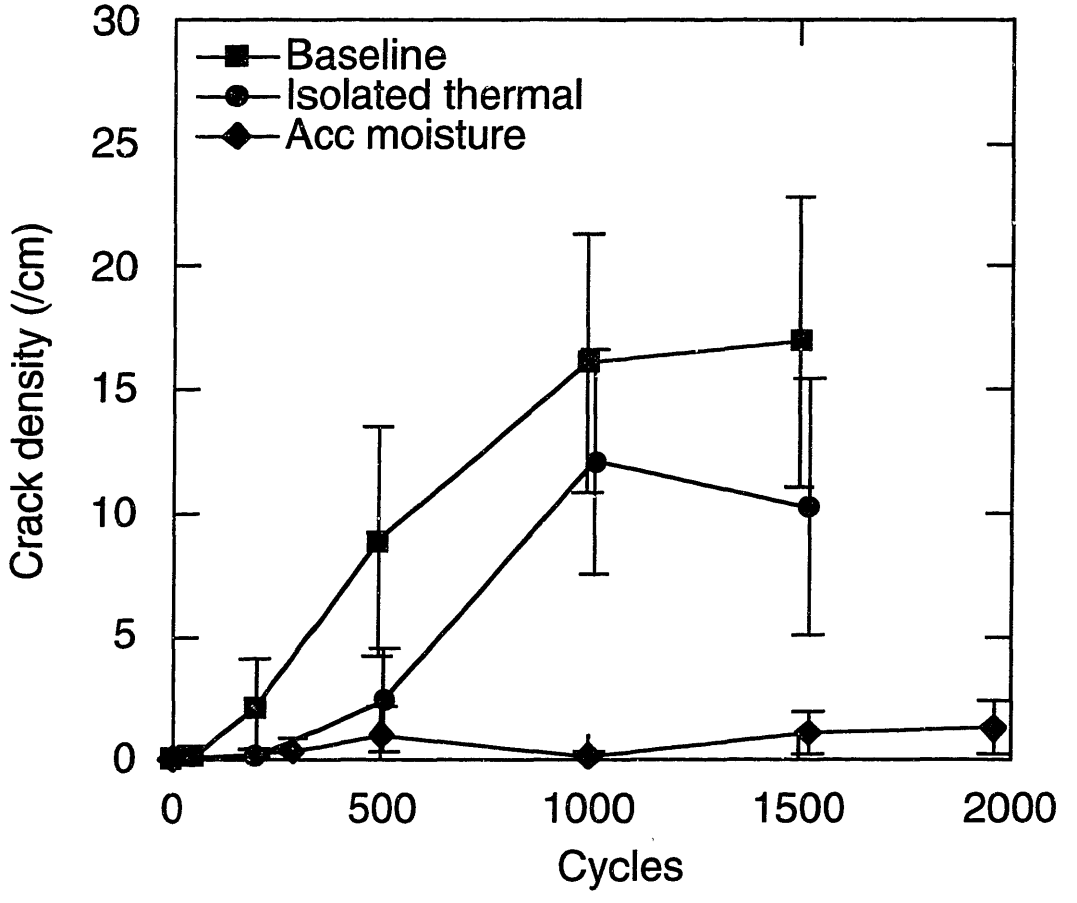

Figure 6.9: Averaged crack density at the edge for PETI-5 quasi-isotropic specimens exposed to the baseline, isolated thermal and accelerated moisture environments

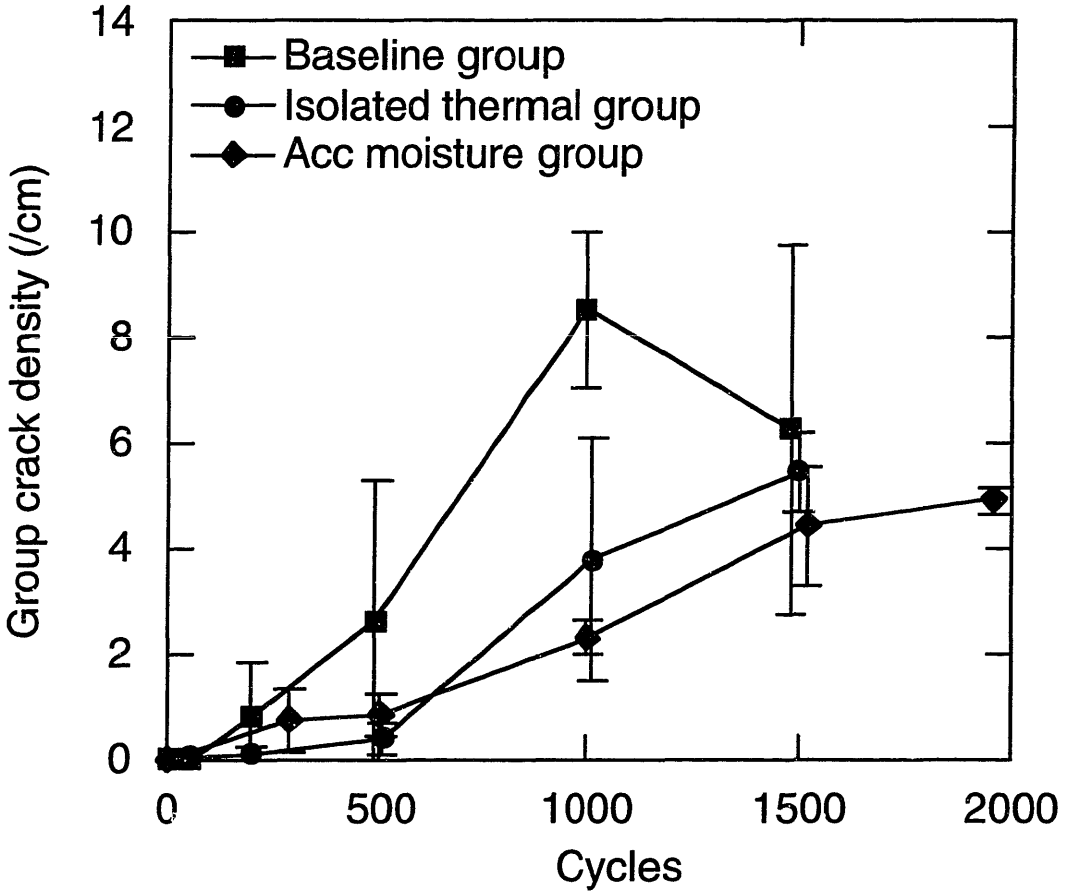

Figure 6.10: Group crack density at the edge in the 90_4 ply group for PIXA-M research specimens exposed to the baseline, isolated thermal and accelerated moisture environments

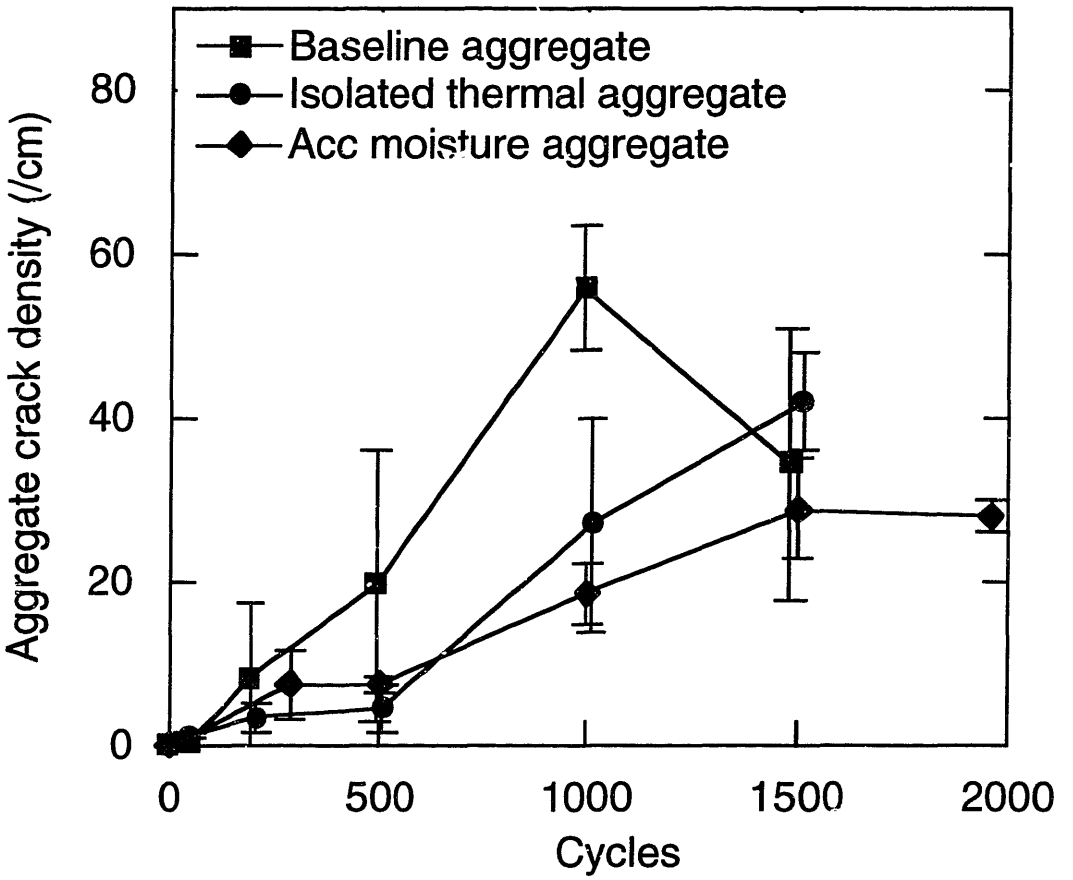

Figure 6.11: Aggregate crack density at the edge in the 90_4 ply group for PIXA-M research specimens exposed to the baseline, isolated thermal and accelerated moisture environments

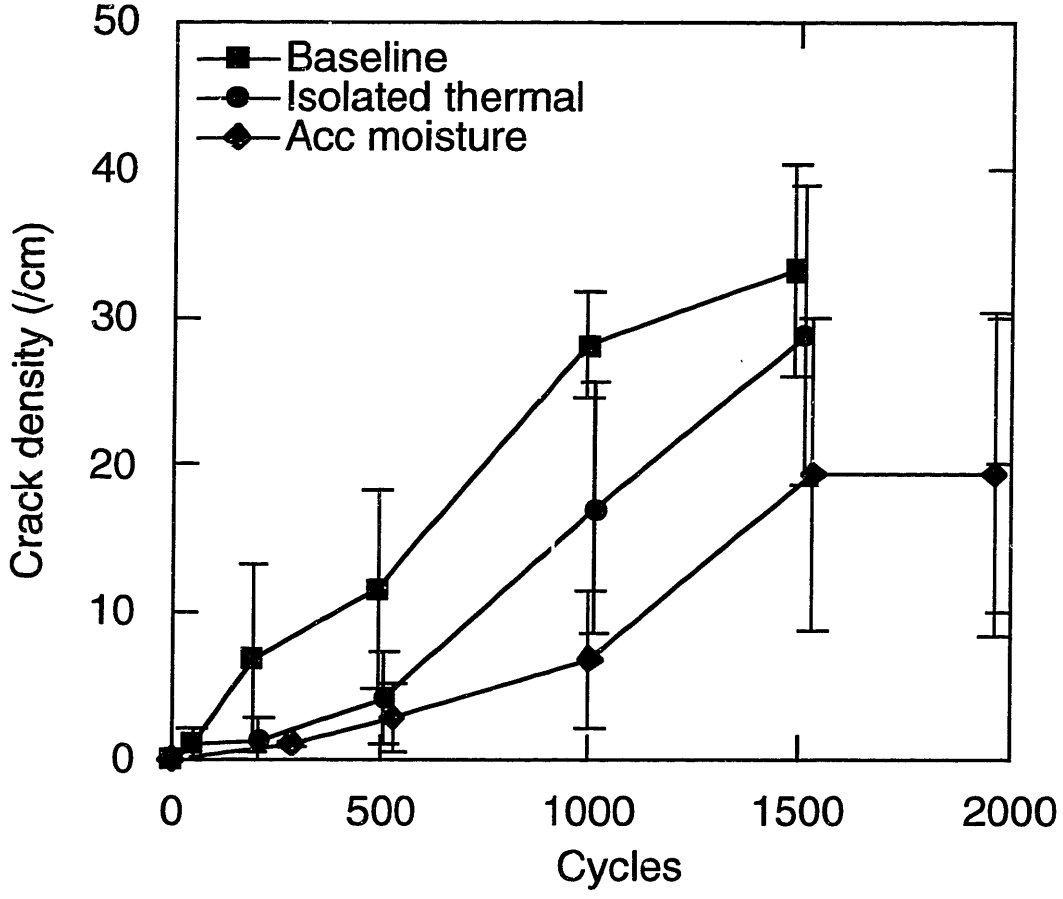

Figure 6.12: Averaged crack density at the edge for PIXA-M crossply specimens exposed to the baseline, isolated thermal and accelerated moisture environments

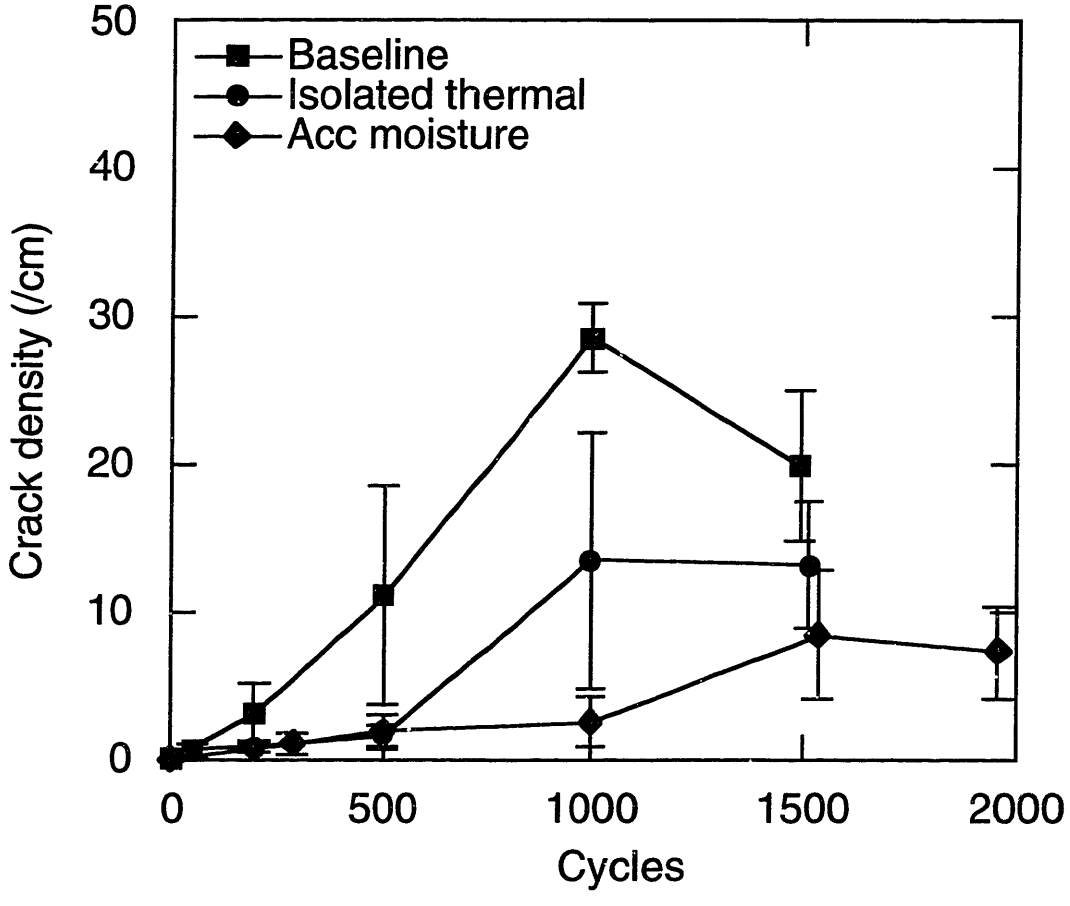

Figure 6.13: Averaged crack density at the edge for PIXA-M quasi-isotropic specimens exposed to the baseline, isolated thermal and accelerated moisture environments

6.2.3 Accelerated thermal 1 and 2 edge data

6.2.3.1 PETI-5 results

Data for these tests is contained in Tables A.7 and A.9. PETI-5 shows virtually zero cracking for all layups and crack types for both of the accelerated thermal cycles. The only non-zero readings were for the research aggregate crack counts for the accelerated thermal cycle to -180°C (Figure 6.14) and even these counts were trivially small.

6.2.3.2 PIXA-M results

Data for these tests is included in Tables A.8 and A.10, and presented in Figures 6.15-6.18.

Figure 6.15 shows the group crack response in the 90_4 ply group of PIXA-M research laminates subjected to both of the accelerated thermal cycles (down to -180°C and -150°C) and to the isolated thermal environment. Group cracking is very low in both accelerated environments up to 750 cycles (as it is for the isolated environment), and the more severe thermal environments do not appear to accelerate the group crack damage at this number of cycles.

Figure 6.16 shows the aggregate crack response in the research specimens. This time, exposure to the more severe accelerated cycle (Acc thermal 1 to -180°C) caused about 50% more average cracks than the isolated thermal environment up to 600 cycles, but the amount of scatter is non-trivial. The less severe accelerated cycle (Acc thermal 2 to -150°C) causes no more or less damage to the specimens than the isolated thermal environment up to 750 accelerated cycles.

Figure 6.17 shows the response for the crossply specimens. The response of the specimens exposed to the -180°C environment is more promising, with a rapid jump in average crack density at 100 cycles to a level which is not reached from exposure to the isolated thermal environment until about 700 cycles have elapsed. Up until about 500 cycles have elapsed, crack density due to the accelerated thermal 1 environment is about 3 times higher than that for the isolated thermal environment for a given number of cycles. The crack density rise after about 300 cycles is at a rate lower than for the isolated thermal environment. The damage response due to the -150°C environment does not show the rapid rise in average crack density seen for the more severe environment. However, the crack levels are about two times higher than the isolated environment response before the two responses converge at 750 cycles. It should be noted, however, that the scatter in the cracking responses for ALL environments is significant, thus making interpretation of the data difficult.

Figure 6.18 shows the equivalent graph for the quasi-isotropic specimens. Again the more severe accelerated environment causes a rapid rise in average crack density to a level after 100 cycles equivalent to 700 cycles of the isolated thermal environment (note: same as before). The responses to the accelerated thermal cycles and the baseline cycle converge after 800 cycles of both. This time the less severe accelerated cycle gives no benefit in shortening the number of cycles to duplicate the isolated thermal damage response, but it may still save time as the cycle is shorter. Again, the high scatter in the data should be noted.

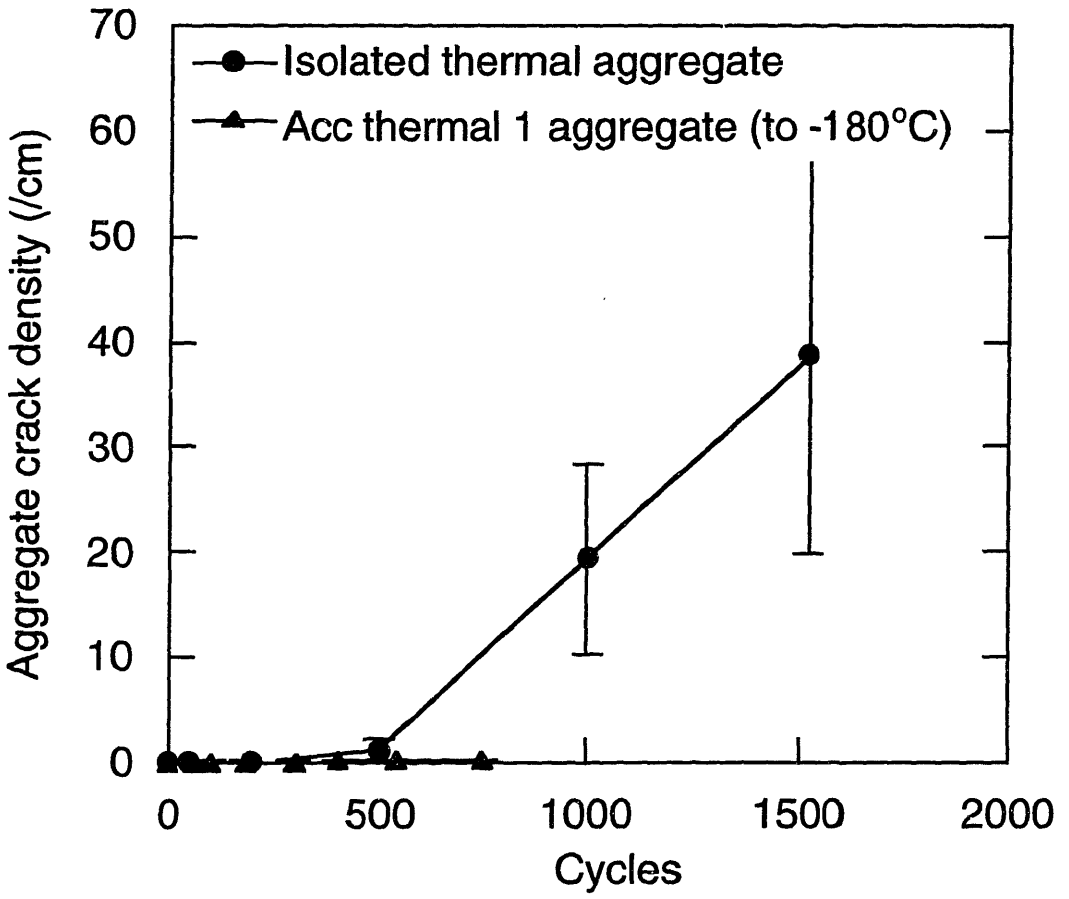

Figure 6.14: Aggregate crack density at the edge in the 90_4 ply group for PETI-5 research specimens exposed to the isolated thermal and accelerated thermal environments

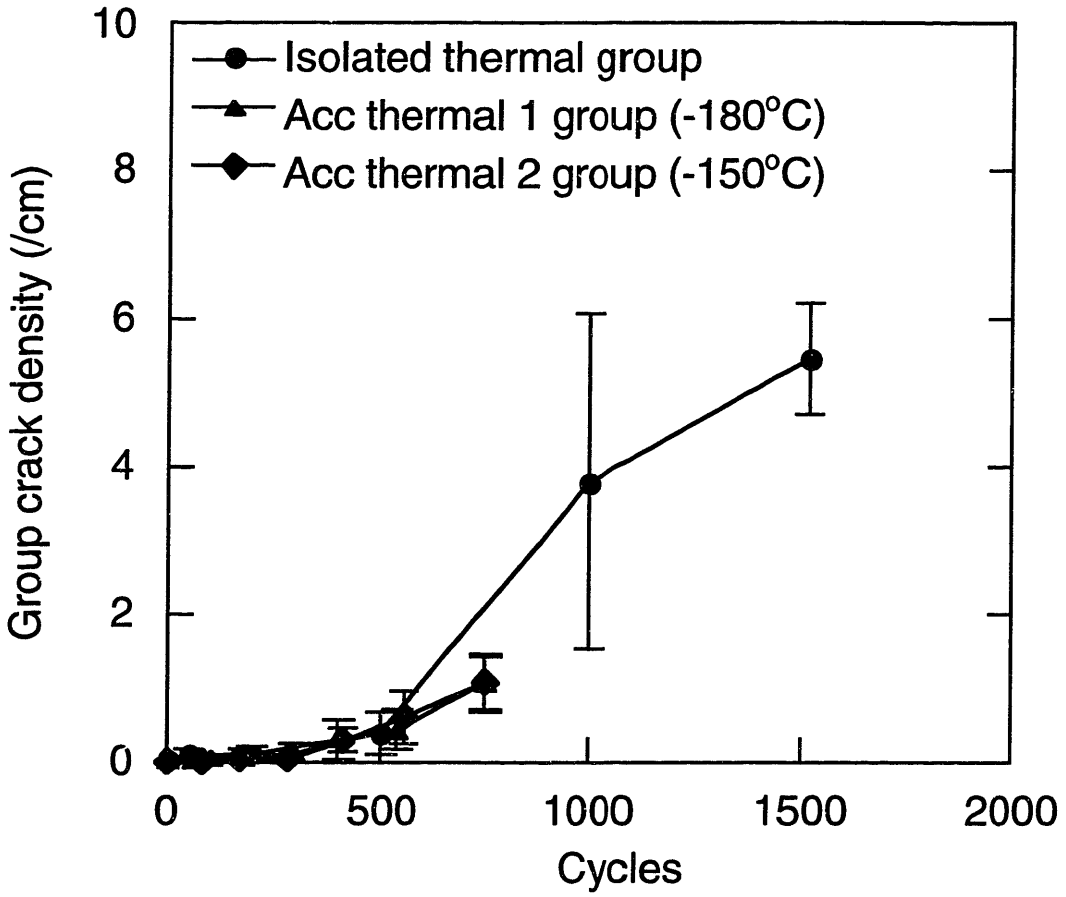

Figure 6.15: Group crack density at the edge in the 90_4 ply group for PIXA-M research specimens exposed to the isolated thermal and accelerated thermal environments

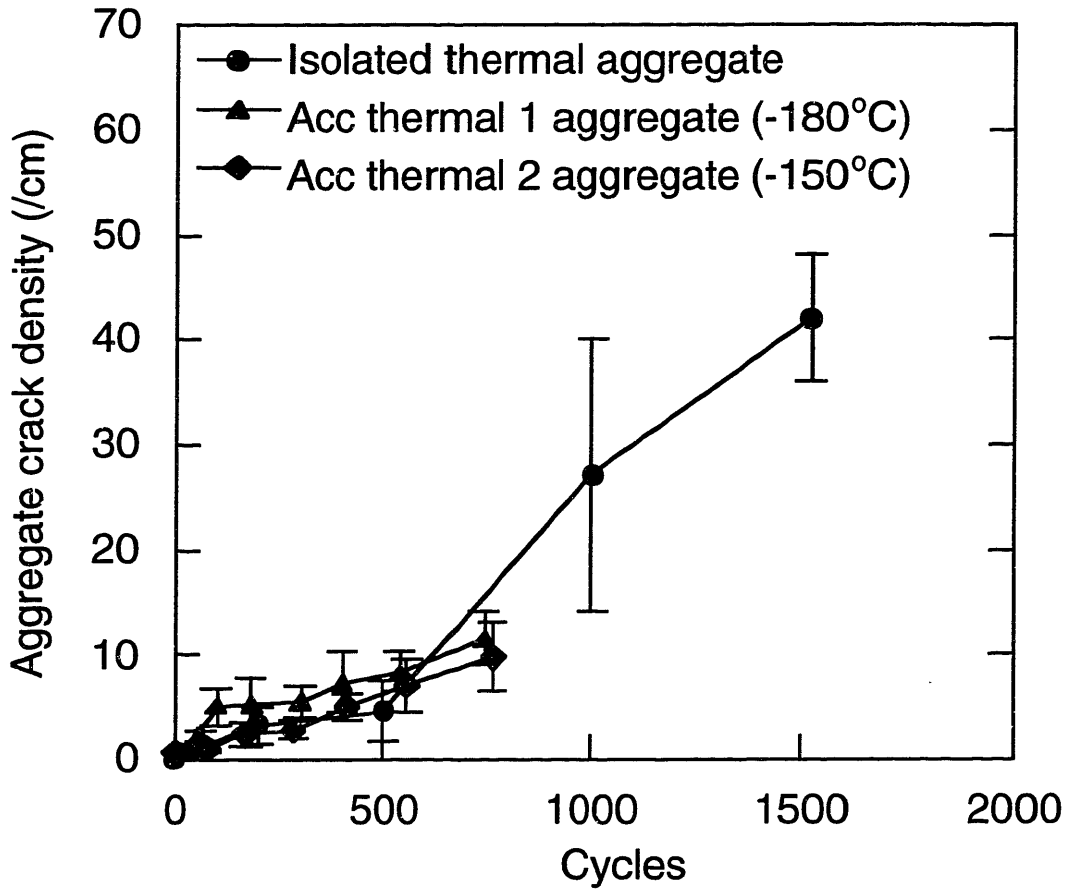

Figure 6.16: Aggregate crack density at the edge in the 90_4 ply group for PIXA-M research specimens exposed to the isolated thermal and accelerated thermal environments

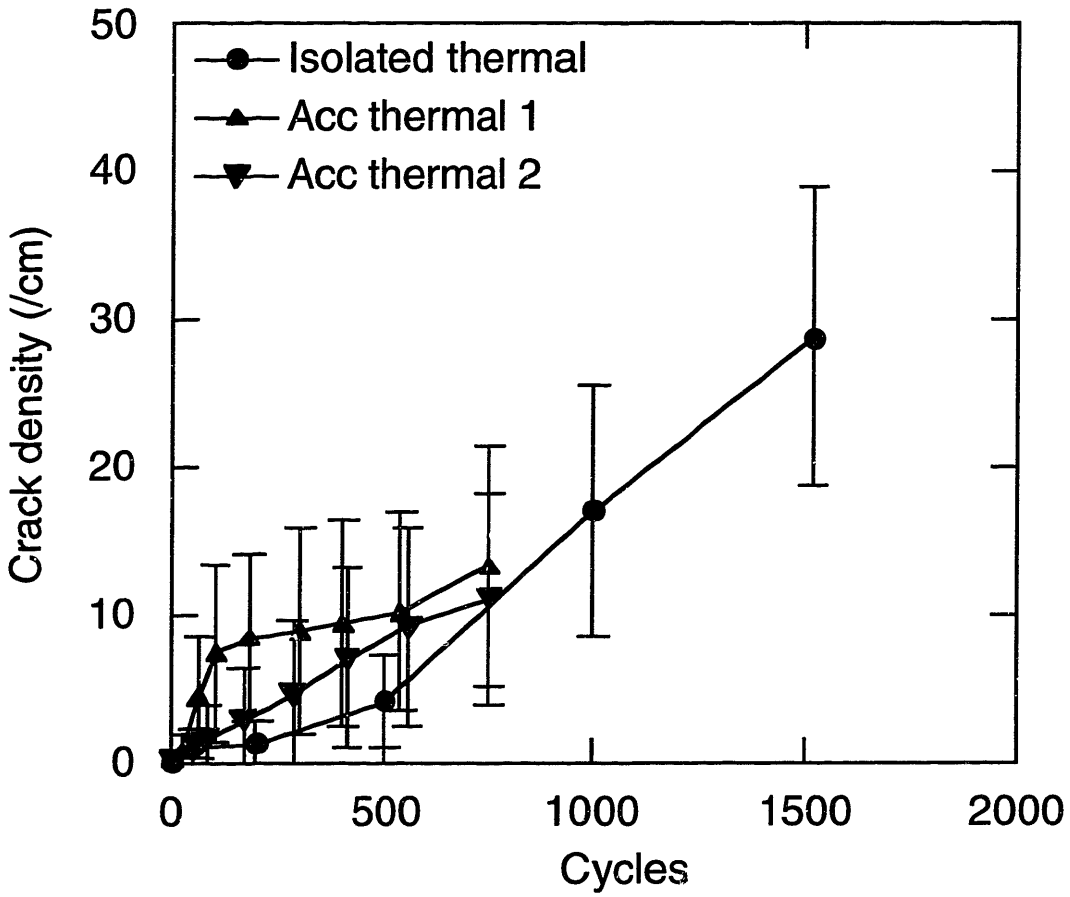

Figure 6.17: Averaged crack density at the edge for PIXA-M crossply specimens exposed to the isolated thermal and accelerated thermal environments

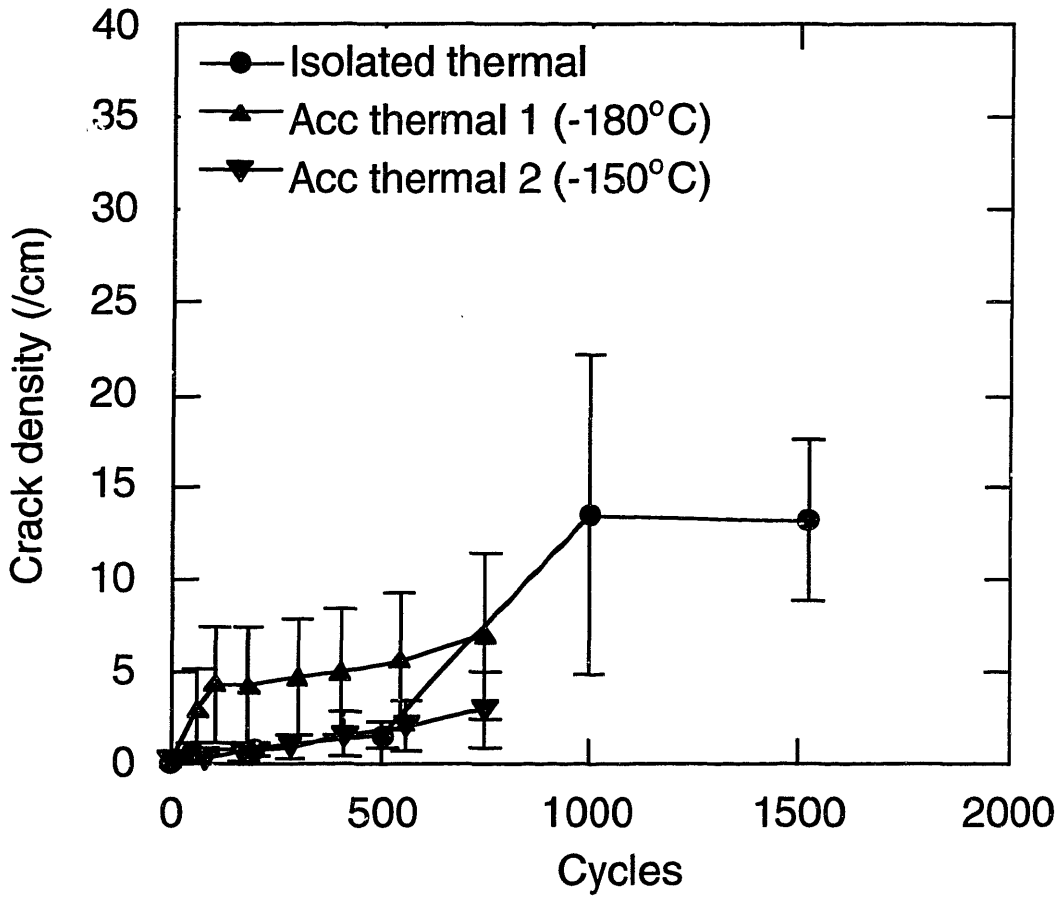

Figure 6.18: Averaged crack density at the edge for PIXA-M quasi-isotropic specimens exposed to the isolated thermal and accelerated thermal environments

6.2.4 Isothermal aging edge data

6.2.4.1 PETI-5 results

The PETI-5 specimens aged for 4250 hours at 350°F showed no cracking for any of the layups (see data under 0 cycle column of Table A.11).

6.2.4.2 PIXA-M results

The PIXA-M specimens aged for 4250 hours at 350°F showed minimal cracking for all of the layups (see data under 0 cycle column of Table A.12).

6.2.5 Accelerated thermal testing of isothermal specimens

6.2.5.1 PETI-5 results

The results of the PETI-5 isothermal specimens which were subsequently subjected to the accelerated thermal cycle down to -180°C are shown in Table A.11. These specimens did not show any significant damage as a result of the accelerated thermal testing.

6.2.5.2 PIXA-M results

The results of the PIXA-M isothermal specimens which were subsequently subjected to the accelerated thermal cycle down to -180°C are shown in Table A.12 and in Figures 6.19-6.21. These figures show a comparison of the response of the 'virgin' specimens and the specimens previously exposed to the isothermal environment to the accelerated thermal 1 cycle. Unlike the PETI-5 specimens, the PIXA-M material does crack when subjected to the accelerated thermal environment. In all cases, the isothermal specimens show a reduced tendency to crack compared to the virgin specimens, although as noted earlier, scatter in the data for the virgin specimens makes detailed interpretation difficult.

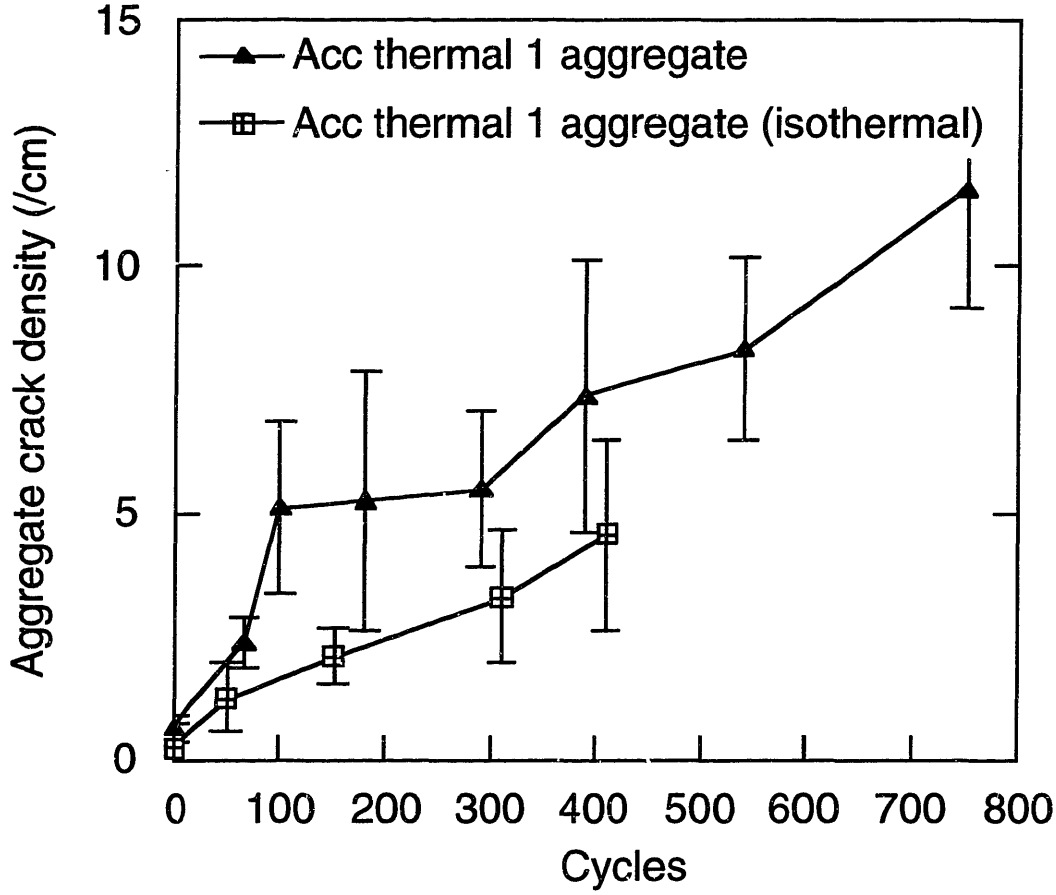

Figure 6.19: Comparison of aggregate crack density for virgin and isothermally-exposed PIXA-M research specimens exposed to the accelerated thermal environment (to -180°C)

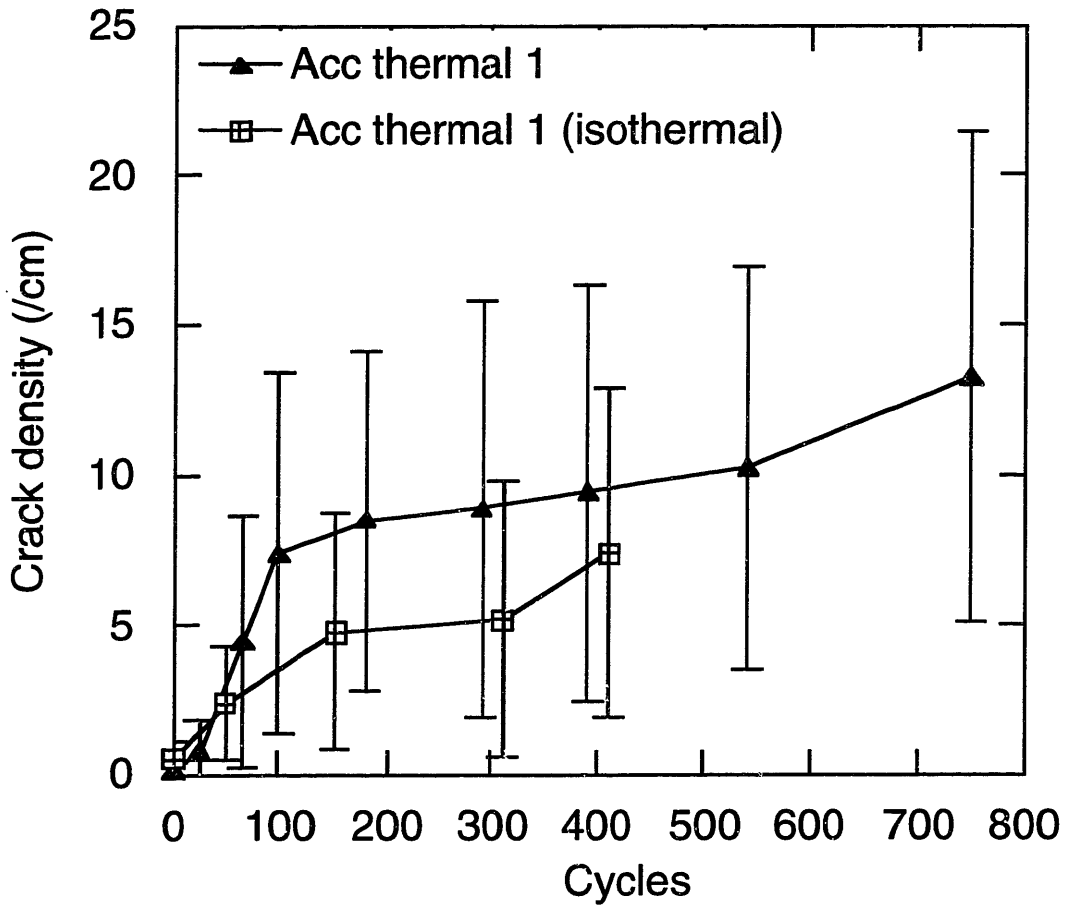

Figure 6.20: Comparison of crack density for virgin and isothermally-exposed PIXA-M crossply specimens exposed to the accelerated thermal environment (to -180°C)

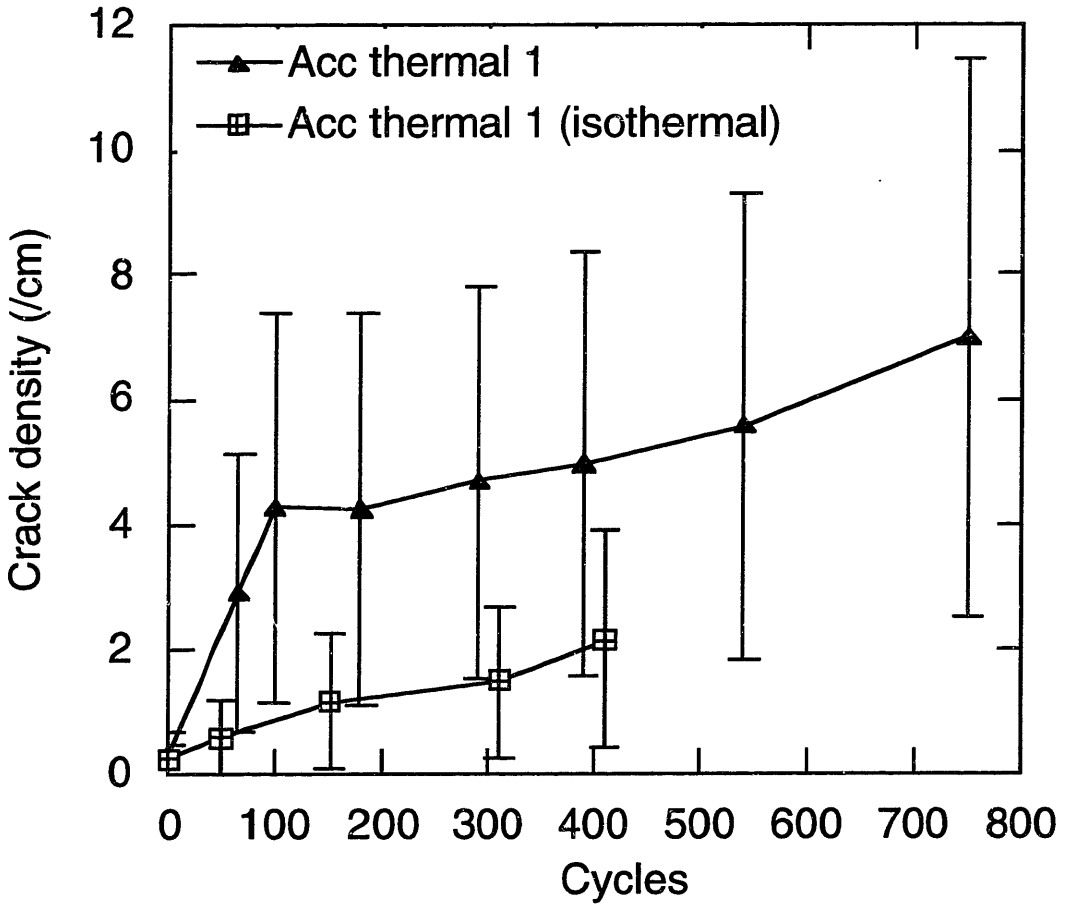

Figure 6.21: Comparison of crack density for virgin and isothermally-exposed PIXA-M quasi-isotropic specimens exposed to the accelerated thermal environment (to -180°C)

6.3 STAGE II TESTING - INTERIOR DAMAGE

6.3.1 General

The internal damage state was investigated as described in Section 5.3.3. The Stage I interior damage assessment tracked the damage at very small incremental steps (of about 0.1 mm) below the original edge (see Section 6.1). This investigation showed that, for most of the materials under investigation (except K3B), the damage only progressed a very small distance below the original edge (generally less than 1-2 mm). For the Stage II interior damage assessment, measurements were taken at 0.5-1 mm intervals until no more damage was visible. The process of grinding material away to take interior measurements is very time consuming, so minimizing the number of grinds is desirable. This gave a clear indication of whether damage was confined to an edge layer or went deeper, but did not provide enough resolution to establish how deep the damage went to the nearest tenth of a millimeter (as was achieved in Stage I).

6.3.2 PETI-5 results

6.3.2.1 Research specimens

Three PETI-5 research specimens were potted in epoxy and polished: one each of specimens subjected to 1500 cycles of the baseline and isolated thermal environments and 1000 cycles of the accelerated moisture environments. For all specimens, cracking other than group cracks were not visible after a grind to 1 mm below the original edge, while all group cracking subsequently disappeared when the grind was taken to 2 mm below the original edge. To investigate further depths, other samples were potted and polished but this time the *interior* edge was polished, rather than the exposed edge. This 'interior' surface (as it will be referred to throughout this section) would have been about 10 mm

from the exposed edge at the time of exposure. This is considered to be out of the region of influence of any edge effects. No damage was observed at the interior for any of these specimens.

6.3.2.2 Crossply specimens

One specimen from each of the baseline (1500 cycles), isolated thermal (1500 cycles) and accelerated thermal cycle 1 (to 750 cycles) were examined. The specimen subjected to the baseline environment showed some visible cracks at a depth of 0.7 mm, but these disappeared on subsequent grinding to a depth of 1.3 mm. The specimen subjected to the isolated thermal environment showed no damage deeper than 0.6 mm from the edge. The accelerated thermal cycling specimen showed no damage at any depth. No damage was seen at the interior for any of these specimens.

6.3.3 PIXA-M results

6.3.3.1 Research specimens

Three PIXA-M research specimens were potted in epoxy and polished: one each of specimens subjected to 1500 cycles of the baseline and isolated thermal and 1000 cycles of the accelerated moisture environments. In all cases, any damage less severe than a group crack disappeared after a grind to 1 mm. Group cracks, however, persisted to a depth of at least 3 mm. The baseline and isolated thermal environment specimens showed no damage after polishing the interior surface, implying that even the group cracks disappear at a depth between 3-10 mm below the original edge. However, two group cracks were faintly visible in the interior of the specimen subjected to the accelerated moisture cycle. This result is considered to be an anomaly with little significance since the accelerated moisture cycle was

not as severe as some of the other environments which universally caused zero internal damage.

6.3.3.2 Crossply specimens

One specimen from each of the baseline (1500 cycles), isolated thermal (1500 cycles) and accelerated thermal cycle 1 (to 750 cycles) were examined. For the specimen exposed to the baseline environment, crack were still clearly visible at 0.9 mm below the original edge, but they had disappeared at a depth of 1.5 mm. The isolated thermal environment specimen had cracks visible (although only barely) at a depth of 0.9 mm, but they had also disappeared at a depth of 1.5 mm. The accelerated thermal specimen showed no damage even on the first grind to 0.8 mm. Polishing of interior surfaces revealed no damage.

CHAPTER 7

DISCUSSION

7.1 INTRODUCTION & GENERAL OBSERVATIONS

In Section 5.1.2, the components of the baseline environment which were candidates for causing the observed damage were listed as:

- moisture cycling
- extended time at moisture
- thermal cycling
- extended time at temperature
- combinations of the above

The Stage II experimental program was designed to provide evidence as to the damage caused by each of the above. The results of this program were presented in Chapter 6, and are discussed here in the context of the list of candidates.

It is worth highlighting some of the more general observations of these results. One of the most striking observations is that the damage in all cases (bar only one specimen) was confined to a thin layer near the edge of specimens, usually less than 2 mm in depth. Cracking was also mainly seen in the 90° plies and only rarely in the 45° plies. Previous work [48] has shown that the transverse stresses responsible for microcracking are approximately the same near the edges in 90° plies as in the interior of a laminate. For 45° plies, the transverse stresses are *lower* near edges. Hence, the edge stress state can help explain the absence of cracks in 45° plies, but not the presence of cracks only near the

edges in the 90° plies. Therefore, the observation of damage only in this region suggests that the material near the edges has different properties from that in the interior of the specimen.

Since the cracks do not run all the way through the laminate, they cannot be considered as 'classical' microcracks. However, the cracks generally run to a depth about 5-10 times greater than their height within the edge layer zone. As a result, the theory used to understand microcrack behavior is valid if applied to these observed cracks. It is therefore reasonable to use microcracking analyses (CRACKOMATIC) to assess the cracking behavior in this region.

There is a large amount of scatter in the data, and this can be attributed to a number of different factors. Prior work [49] has shown that classical microcracking analyses predict considerable data scatter if one considers factors such as material variations. The current study was also limited in the number of specimens available for testing at each condition. Only three specimens were ultimately used for each test condition. The tests conducted at MIT tracked damage in the same specimens as they became progressively more damaged at each condition. In the Boeing tests, different specimens were used for each condition, adding more variation to the scatter. Overall, although the scatter is high, the trends in the data discussed here were all more significant than the data scatter.

Finally, some problems arose with the experimental setup, the effects of which are difficult to quantify. There was some evidence to suggest that the specimens subjected to the 'isolated' thermal environment were not actually fully isolated from the moisture component of the environment. The specimens subjected to the baseline environment had to be thoroughly cleaned prior to damage assessment to remove edge layers of dirt and mineral deposits. This contamination was presumed to be as a result of exposure to the

humid environment in the warm/wet phase of the cycle. Similar (although less pronounced) deposits were also found on many of the 'isolated' thermal specimens, leading to the suggestion that they did in fact encounter some of the moisture environment (i.e. the thermal blankets were not fully sealed). It is likely that the presence of the thermal blankets did lessen the impact of the moisture environment on these specimens. The blankets could have reduced the humidity inside the blanket, or shielded one side of the specimen from most of the moisture. The suggestion of a reduced humidity inside the blanket could account for the fact that the isolated thermal environment data generally mirrors the trends seen under the baseline environment, only at a lower level of damage (e.g. Figures 6.8, 6.9, 6.12 and 6.13). High data scatter would be a consequence of one edge being shielded from moisture while the other side was exposed.

Equipment failures and shutdowns (see Section 5.2.3) are an inevitable part of long term tests such as these. These problems also added to the overall uncertainty as to the environment that the specimens encountered.

7.2 MOISTURE CYCLING

The effect of moisture cycling can be seen by comparing the results of the baseline and accelerated moisture cycle. As discussed in Section 4.3.2, the accelerated moisture cycle was designed to give an almost identical theoretical moisture distribution in the material as the baseline cycle, only in a shorter cycle time. In particular, the characteristics of the 'moisture-thrashed' zone were matched between the two cycles. The actual accelerated cycle was subtly different from that designed (see Section 5.2.3), but the effect on changing the moisture distribution within the material was minimal (see Figure 5.1).

If moisture *cycling* had been the dominant parameter in causing the edge damage, the results from the two cycles would be expected to be very similar. The results for PETI-5 shown in Figures 6.6-6.9 show that this is clearly not the case. In all cases shown, the damage from the accelerated moisture cycle is very much lower than that seen under the baseline environment.

The equivalent results for the PIXA-M material are shown in Figures 6.10-6.13. Again, these plots show that the accelerated moisture cycling does not produce the same level of edge damage in PIXA-M as the baseline cycle. However, the damage levels are generally up to 50% of the damage due to the baseline environment. These crack levels are much greater than those displayed in PETI-5 under the same conditions. This indicates that the PIXA-M is more susceptible to one (or more) component of the accelerated moisture cycle than the PETI-5.

These results for both materials indicate that the moisture *cycling* component of the baseline cycle is unlikely to be the dominant factor responsible for the observed edge damage.

7.3 EXTENDED TIME AT MOISTURE

Extended time at moisture has been observed in previous studies to have very significant effects on the toughness of polymer matrix composites [55]. Moisture effects on K3B were seen to reduce the effective toughness of the resin to zero after only 500 hours of immersion in 80°C water. Immersion in 76% humidity air at 80°C was found to have a comparable effect. PETI-5 was seen to be less susceptible to isomoisture effects, but it too showed clear signs of decline in its fracture toughness before 2000 hours of exposure. The conditions used in [55] were very similar to those in the warm/wet segment of both the baseline and accelerated moisture cycles used in this study.

Although extended time under isomoisture conditions was not investigated directly in this study, insight into its effects can be gleaned from the data collected. In particular, comparison of the baseline and accelerated moisture cycle data reveals some interesting observations. The major difference in the accelerated cycle parameters from the baseline parameters was a 50% reduction in the warm/wet hold time—see Table 4.2. As noted in Section 5.2.3, the accelerated cycle parameters which were seen by the specimens were different from those detailed in Table 4.2: the warm/wet temperature was 82°C rather than the 93°C which was specified. This resulted in the specimens seeing exactly the same warm/wet conditions as the baseline, but only for half the time per cycle.

The accelerated moisture and baseline data are compared based on the time exposed to warm/wet conditions in Figures 7.1-7.4. This basis of comparison does not account for the depth of the zone affected by moisture, or the time moisture takes to diffuse into it. These considerations also tend to work against the accelerated cycle.

Figures 7.1 and 7.2 show this comparison for some PETI-5 specimens. Even corrected for time exposed to moisture, the accelerated cycles do *less* damage than the baseline, perhaps for some of the reasons given above. The correction works well for PIXA-M specimens, as can be seen in Figures 7.3 and 7.4. These results suggest that time at moisture may be more important than moisture *cycling*. Further evidence on this matter will be discussed in Section 7.6.

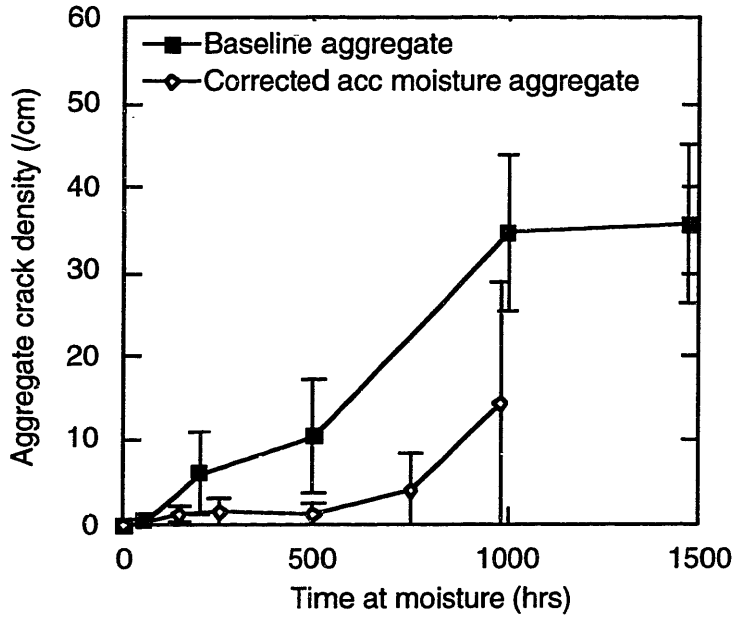

Figure 7.1: Corrected accelerated moisture aggregate crack data in PETI 5 research laminates

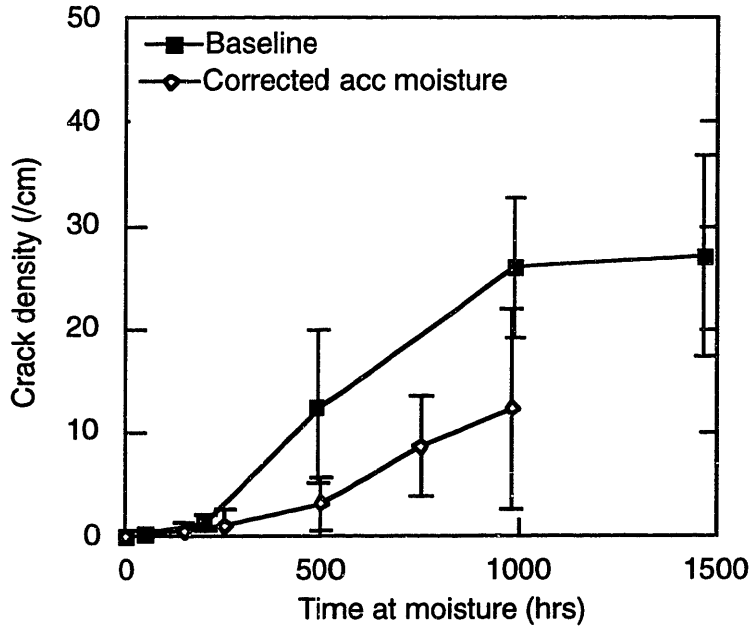

Figure 7.2: Corrected accelerated moisture crack data in PETI-5 crossply laminates

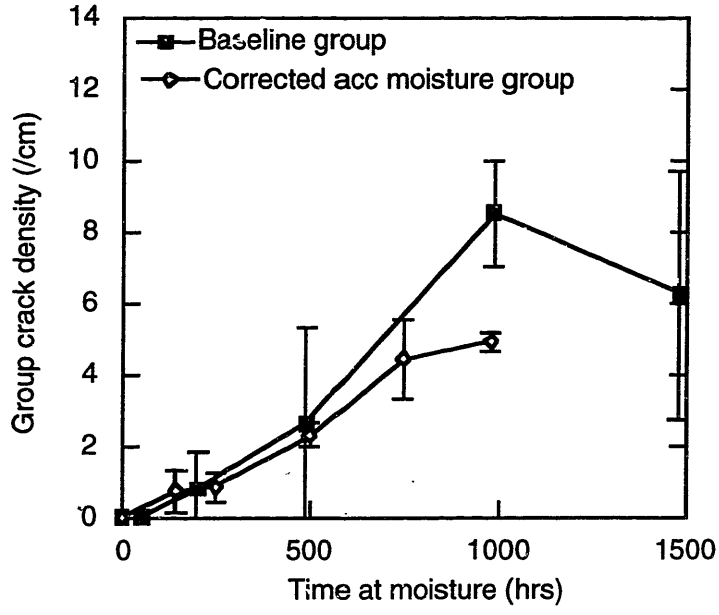

Figure 7.3: Corrected accelerated moisture group crack data in PIXA-M research laminates

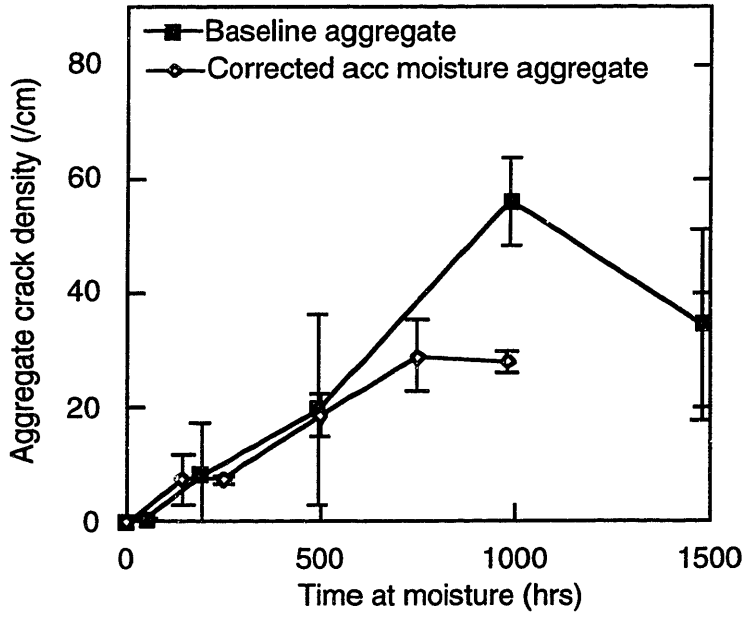

Figure 7.4: Corrected accelerated moisture aggregate crack data in PIXA-M research laminates

7.4 THERMAL CYCLING

The isolated thermal and the accelerated thermal environments were designed to isolate and accelerate respectively the effects of thermal cycling. As discussed in Section 7.1, there was evidence to suggest that the 'isolated' thermal environment specimens were not fully sealed from the moisture component of the environment. As a result, the only thermal cycling data discussed here will be from the accelerated thermal cycling experiments.

The results for PETI-5 (Section 6.2.3.1 and Figure 6.14) showed effectively zero damage up to 750 cycles under even the most severe accelerated thermal cycle (down to -180°C) for all specimens. This suggests that PETI-5 is not susceptible to damage from this severe thermal cycle up to 750 cycles. No evidence is available at this point to comment on its behavior beyond this number of cycles, but it should be noted that the accelerated thermal environment is *much* more severe than the thermal conditions in the baseline environment.

The results of the accelerated thermal cycle testing with PIXA-M (Section 6.2.3.2, Figures 6.15-6.18) shows that this material is more susceptible to thermal cycling effects than PETI-5. The damage is confined to a thin edge layer rather than behaving like classical thermal microcracks which propagate throughout the entire laminate. However, these edge cracks in the crossply laminates generally have aspect ratios (length/height) of about 10. This value is high enough for an evaluation with CRACKOMATIC to be viable. Figure 7.5 shows the result of best fit CRACKOMATIC plots to the data from the accelerated thermal 1 cycle (down to -180°C) and the accelerated thermal 2 cycle (down to -150°C) for the crossply layup.

A so-called 'G-N curve' (Eqn. 4.17) was fit to the data using the procedure outlined in Section 5.4. It illustrates how the material's effective fracture toughness is reduced by

cyclic exposure. For this plot, the parameters for the G-N curves are initial fracture toughness, G_0 = 508 J/m^2, A = 0.97 for Accelerated thermal 1 and G_0 = 508 J/m^2, A = 0.967 for Accelerated thermal 2. The other parameters were as for PETI-5 (see Appendix C). Only the A parameter had to be changed slightly (to 0.98) in order to get a best fit to the quasi-isotropic PIXA-M data—see Figure 7.6. On the other hand, the research layup did not microcrack in a classic fashion. Very few cracks were seen in the 90_4 ply group. Hence, no fit using CRACKOMATIC was attempted.

Given the scatter in the data (see Figure 7.6; error bars omitted from 7.5 for clarity), the fits are quite good in all cases, capturing the trends seen. In particular, the acceleration of damage at -180°C compared to -150°C (Figure 7.5) occurs as predicted. However, these fits apply only to the material near the edge of the specimens, where cracking was observed. The interior material is not damaged by thermal cycling. The reason why the edge material is vulnerable to damage is not known. Given that the transverse stresses in this region are no worse than in other parts of the laminate [48] and the susceptibility of the material to moisture already discussed, ambient moisture and/or some other environmental condition during cycling or in storage before the tests began is suspected.

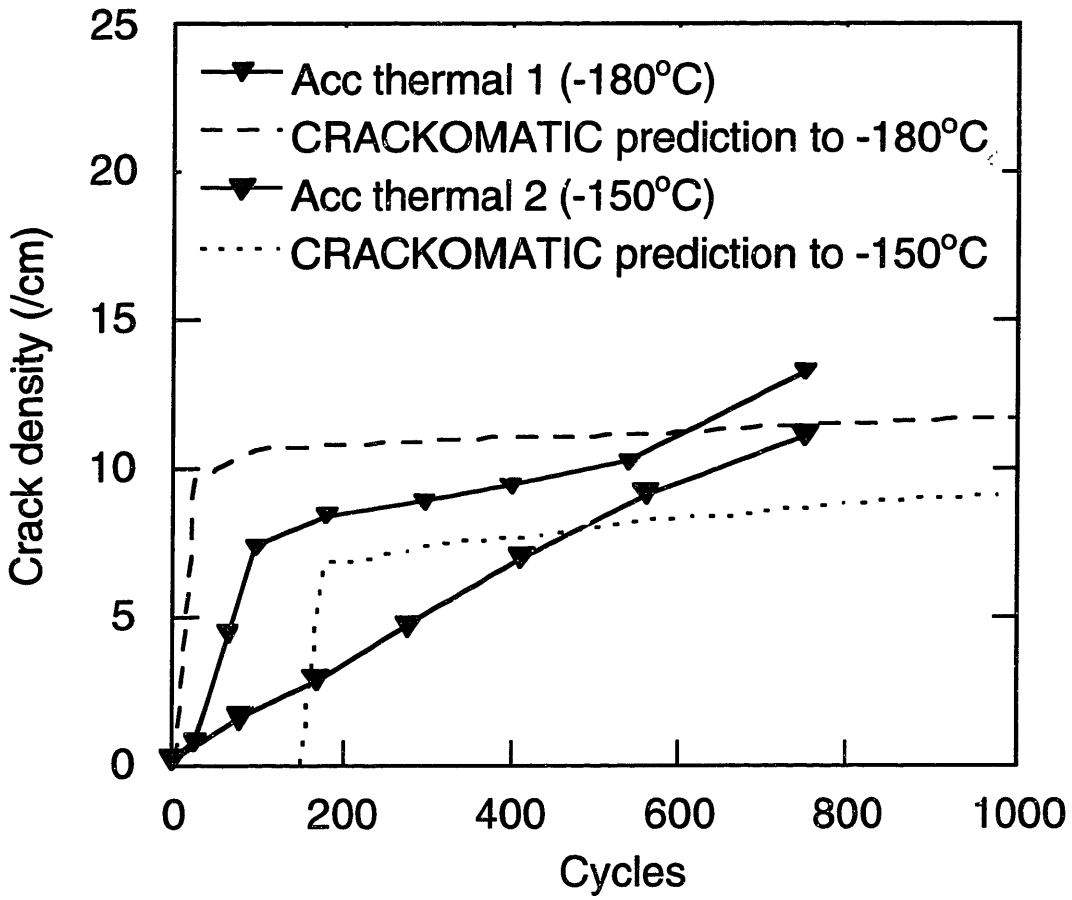

Figure 7.5: Fit of CRACKOMATIC output to accelerated thermal cycle data in IXA-M crossply

(Acc thermal 1: G_0 = 508 J/m^2, A = 0.97, Acc thermal 2: G_0 = 508 J/m^2, A = 0.967)

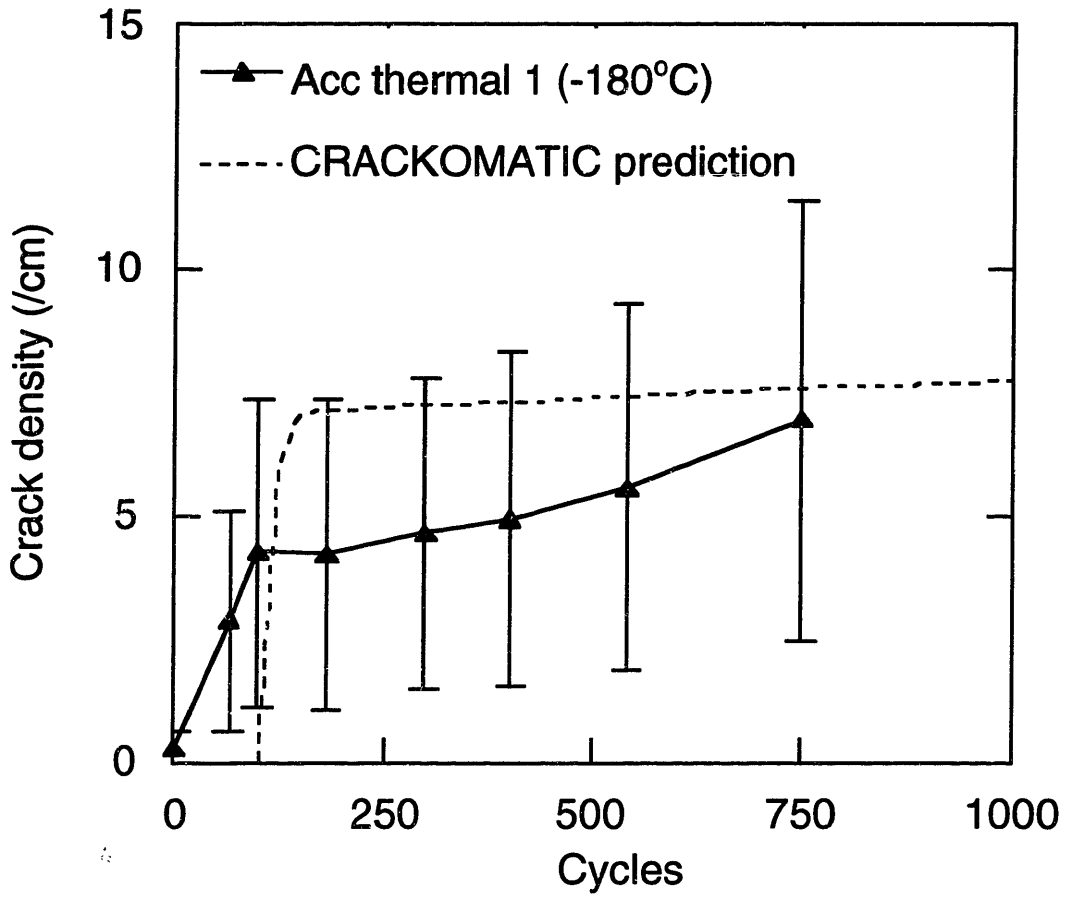

Figure 7.6: Fit of CRACKOMATIC output to the -180°C accelerated thermal cycle data in PIXA-M quasi-isotropic (G_0 = 508 J/m^2, A = 0.98)

7.5 EXTENDED TIME AT TEMPERATURE

The isothermal experiments directly tested the effects of extended time at temperature. After 4250 hours at 350°F, none of the laminates of either of the two materials showed any significant damage. This time at elevated temperature was considerably longer than any of the cycled specimens experienced. Therefore, the effect of time at temperature can be discounted as a direct causal factor in the observed damage behaviors in both materials.

Subsequent accelerated thermal cycling of these specimens resulted in no cracks in PETI-5 and a smaller number of cracks than seen in unaged specimens for a given number of cycles in PIXA-M (see Figures 6.19-6.21). This implies that the elevated temperature aging affected the edge layer of the material, making it *less* prone to cracking. This could be accounted for by either the aging reducing the laminate stresses at the edge, or the aging having a toughening effect on the edge layer.

7.6 COMBINATIONS OF ENVIRONMENTS

The results from the moisture cycling section shows that PETI-5 is not severely damaged by the moisture *cycling* component of the baseline environment. Accelerated moisture cycling produces *less* damage than the baseline environment. The level of damage which is observed can be partly explained by the time at moisture arguments. No damage was observed (either on the edge or internally) due to even the most severe accelerated thermal cycle. Similarly, extended time at elevated temperature was not seen to cause any damage. Hence, it is the time at moisture which seems to be the dominant environmental factor for PETI-5. However, it is not the *only* factor; the combined hygrothermal environment seems to have effects not accounted for simply by time at moisture.

CRACKOMATIC can be used to analyse the results of the baseline hygrothermal cycling since the cracks in the edge layer of the research laminates have an aspect ratio of at least 4. An 'effective' G-N curve for the hygrothermal environment can be developed based on fitting a CRACKOMATIC prediction to the baseline environment damage data for the research laminate.

The crossply and quasi-isotropic specimens had cracks that were very shallow (most cracking disappeared in these specimens on grinding off a very small amount of edge material). Therefore, CRACKOMATIC was not used to analyze these laminates.

The result for the research laminate is shown in Figure 7.7, with the G-N curve used to generate this plot illustrated in Figure 7.8. This is one of the 'general' G-N curves (Eqn. 4.16) discussed in Section 5.4.2. The G_0 value of around 1200 J/m^2 is consistent with other discussions, but the rapid drop off in G beyond 1000 cycles is interesting. Experiments (Section 6.2.3.1) proved that PETI-5 did not display this rapid decline in G when subjected to the pure thermal environment (or it would have cracked). This fit to the data indicates that the combined baseline environment is having a detrimental effect on the fracture toughness.

Similar arguments concerning moisture effects hold true for PIXA-M. Accelerated moisture cycling does not replicate the observed baseline damage, so moisture *cycling* is not the dominant environmental factor. Correcting the accelerated moisture data for time at moisture brings the data very much into line with the baseline damage data. Thermal cycling down to -180°C and -150°C does have an effect on edge material. But, using the CRACKOMATIC fit parameters from Section 7.4 to predict the response to the baseline thermal environment (which only went down to -54°C) indicates that even in the edge

zone, thermal cycling should not have a big effect at -54°C until at least 5000 cycles. As was the case for PETI-5, the prolonged exposure to elevated temperatures did not damage the material. This suggests that, for PIXA-M, the dominant environmental factor again is the time at moisture, but again this time at moisture may not be the *only* factor.

The best fit CRACKOMATIC plot to the research laminate baseline cycle group crack data is shown in Figure 7.9, with the associated G-N curve used to generate this plot shown in Figure 7.10. The initial toughness of the material for the combined environment is greater than that used in the thermal cycling fits (Section 7.4) and here it is more in line with the accepted value for PETI-5. This figure shows that the drop in G for PIXA-M after 100 cycles is more severe than it was in PETI-5. As was the case for PETI-5, this indicates that the combined environment degrades the effective fracture toughness of this material. Time at moisture and thermal cycling are the prime candidates for the combined effect.

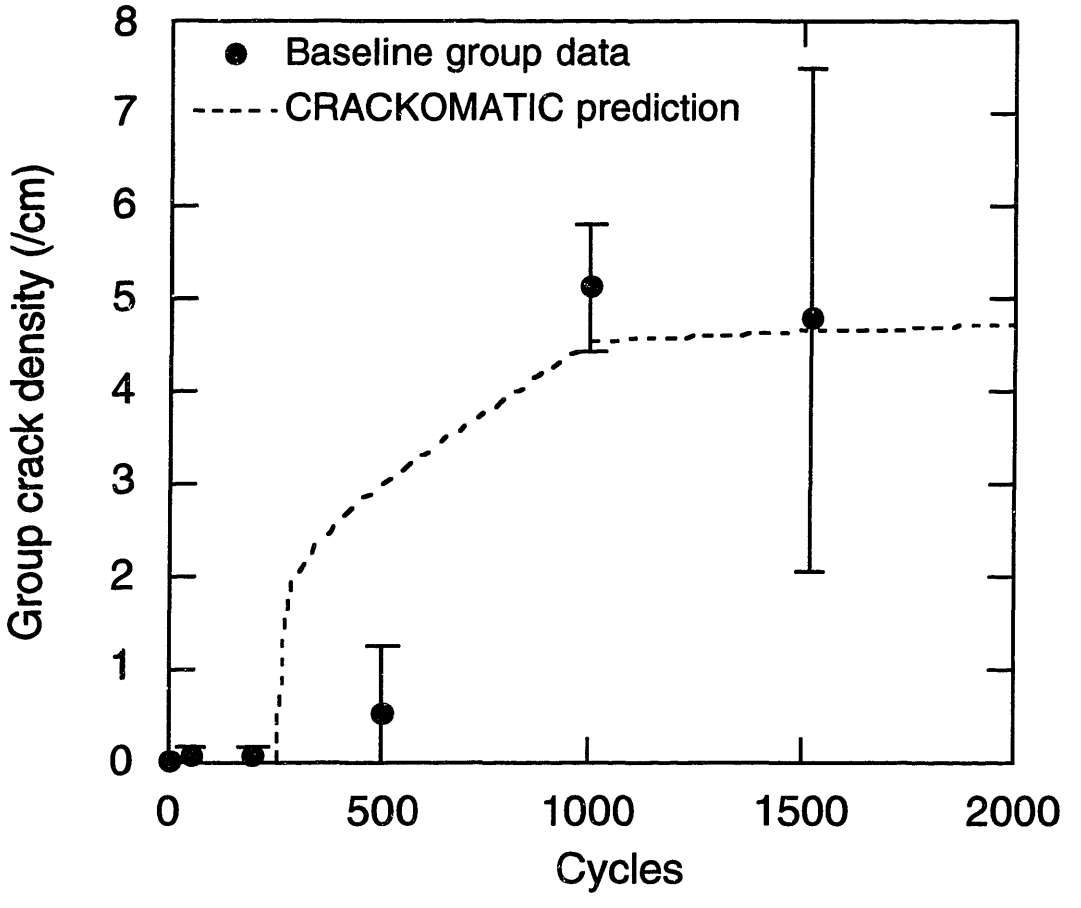

Figure 7.7: Fit of CRACKOMATIC output to baseline cycle group crack data in PETI-5 research laminates

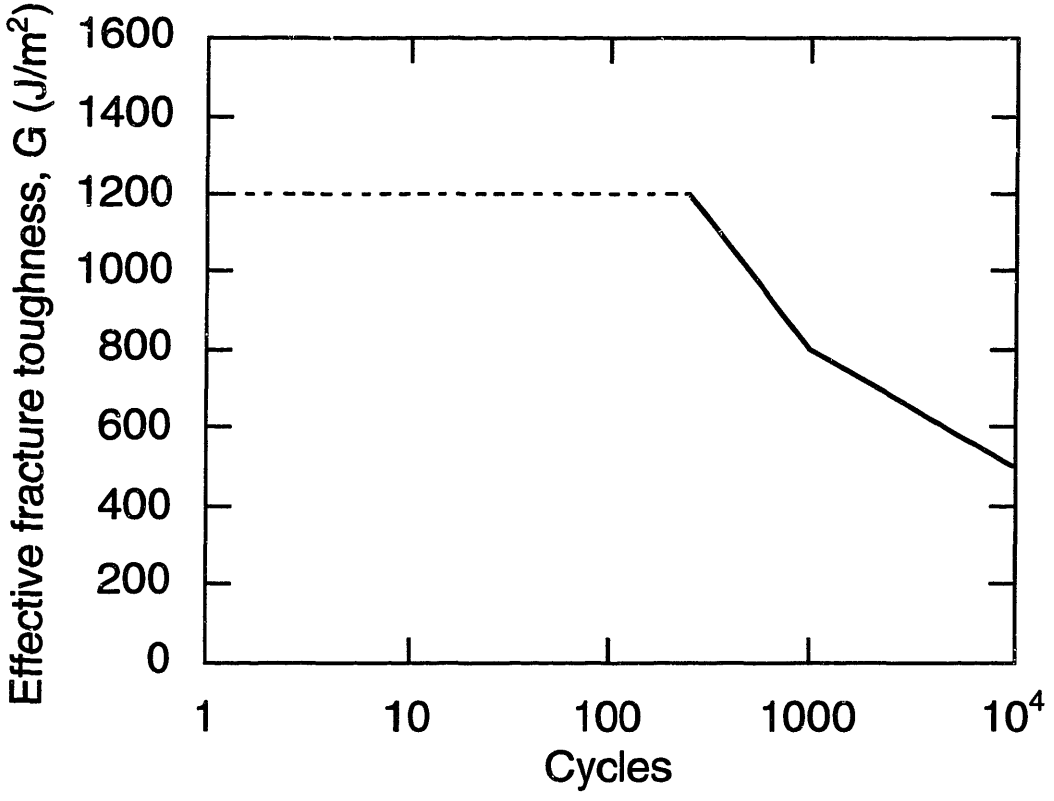

Figure 7.8: G-N curve used in Figure 7.7

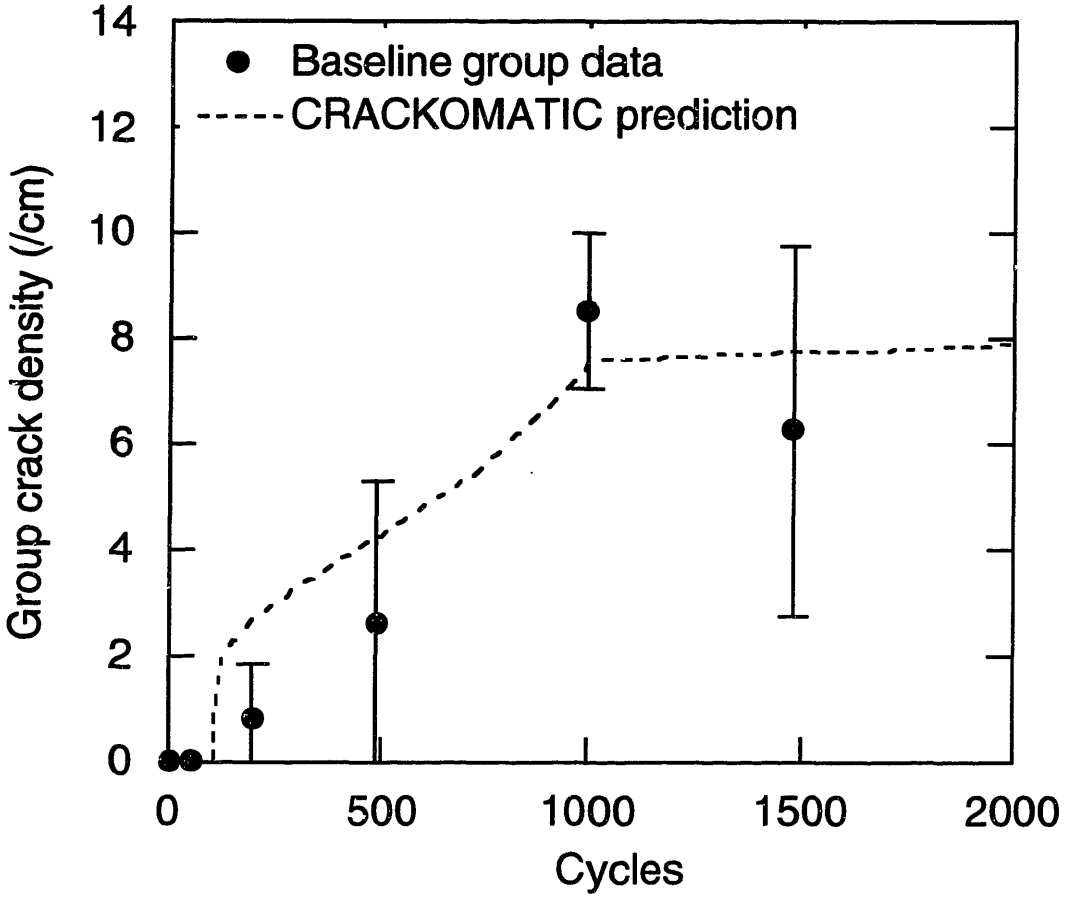

Figure 7.9: Fit of CRACKOMATIC output to baseline cycle group crack data in PIXA-M research laminates

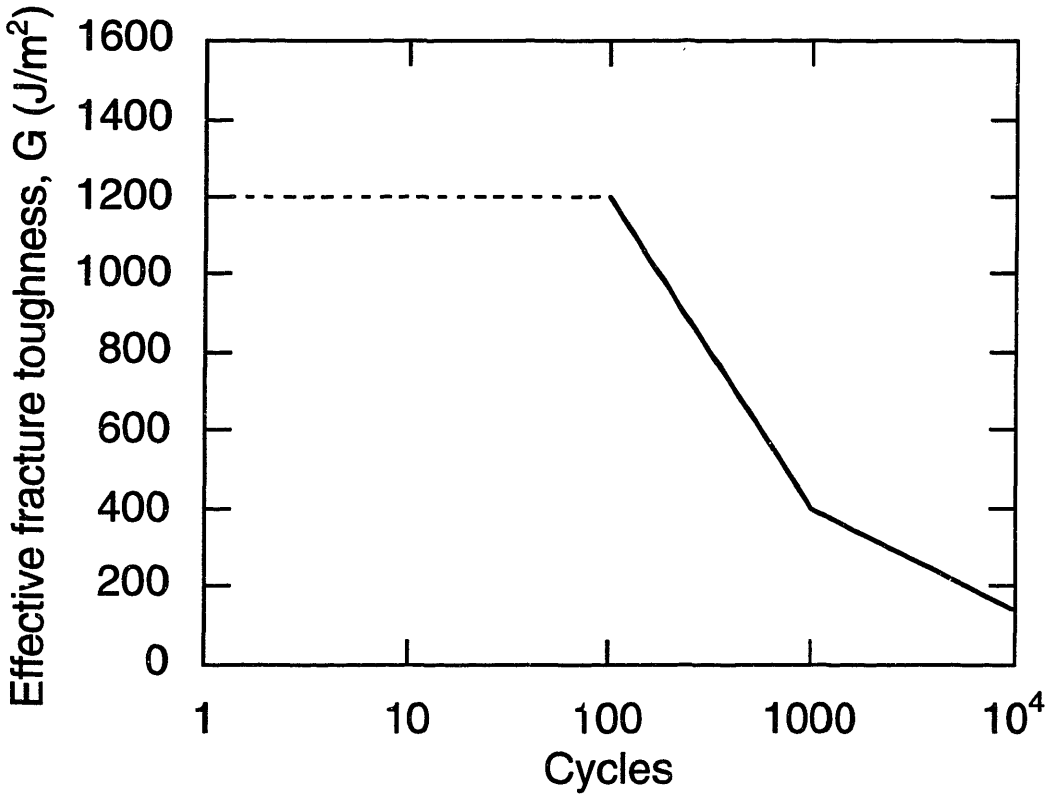

Figure 7.10: G-N curve used in Figure 7.9

Pure time at moisture studies are being carried out by Nairn as part of the HSR program. These differ from current studies in the fact that specimens are soaked, so all material is exposed to moisture and not just a thin surface/edge zone. There is no thermal cycling component in these tests, so no cyclic stresses are present. Mechanical loading is used to induce microcracking and data reduction similar to that in Section 5.4 was used to find the effects of time at moisture on the fracture toughness of the material.

Figure 7.11 shows the two G-N curves for hygrothermally-cycled PETI-5 and PIXA-M laminates, along with the experimental values obtained for a similar polyimide material after extended time under isomoisture conditions, as discussed in [55]. This data suggests that the *combined* environment degrades the edge material even more rapidly than simple time at moisture. PIXA-M seems to have a greater reduction in its toughness with the combined environment than PETI-5. The drop-off in effective fracture toughness occurs much sooner for the combined environment than in the isomoisture environment (100 cycles vs. 1500 cycles).

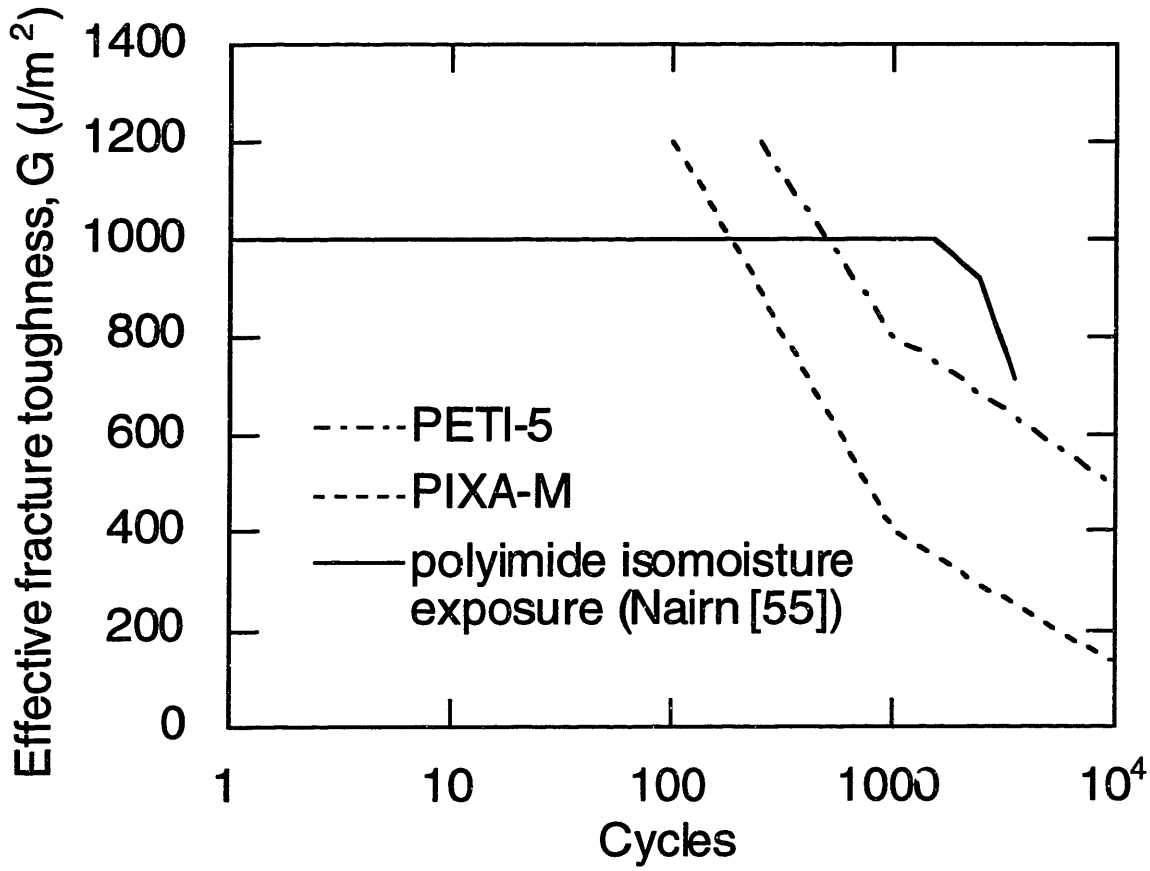

Figure 7.11: Combined G-N curves for PETI-5 & PIXA-M baseline environment exposure and isomoisture exposure of a similar polyimide material

CHAPTER 8

CONCLUSIONS

8.1 GENERAL

The effects of a realistic moisture and thermal environment on two high temperature polymer matrix composites (PETI-5 and PIXA-M) have been investigated. The response of the materials to this baseline environment and its individual components of time at moisture, moisture cycling, time at temperature and temperature cycling were studied. Models were used to design accelerated moisture cycles and accelerated thermal cycles in an attempt to speed up the response to these environmental factors.

The baseline environment was found to cause visible damage in the form of cracking in both materials. Some of the individual components of the environment also caused cracking, while other components caused no visible damage. When damage did occur, it was found to exist only in a thin layer of material next to the exposed edge, and did not progress beyond a few millimeters from that edge. This was the case for both materials. This suggests that the environmental exposure is reducing the effective fracture toughness of the material in this thin layer of material next to the exposed edge more than the material at the interior.

PIXA-M was seen to show more visible environmental damage than PETI-5. When cracking occurred in both materials at a given condition, PIXA-M displayed higher crack densities than PETI-5. In other cases, PIXA-M displayed cracking when exposed to environments which caused no visible damage in PETI-5.

8.2 INDIVIDUAL ENVIRONMENT COMPONENT EFFECTS

Time at temperature causes no visible damage in either material and appears to alter the material properties such that subsequent thermal cycling causes *less* damage in PIXA-M.

Severe thermal *cycling* (to -180°C and -150°C) has no effect on PETI-5. PIXA-M showed damage due to this severe thermal cycling, but not due to 'realistic' thermal cycling to the baseline cycle low of -54°C.

Time at moisture seems to be a dominant factor in damage of both materials.

Moisture *cycling* does not seem to be a principle component causing damage, as evidenced indirectly by the fact that the accelerated moisture cycling tests did not accelerate damage. However, it is believed to play an important role in setting up the depth of the damaged surface layer since it significantly affects the moisture distribution.

8.3 COMBINED ENVIRONMENT EFFECTS

The combined environments in the baseline cycle cause more visible damage to both materials than any one component of that cycle on its own. Time at moisture appears to be the dominant factor for both materials. Thermal cycling is known to cause cyclic internal stresses which can cause damage (and did in this case in PIXA-M). The mechanism by which moisture cycling affects the material is not fully understood, but evidence does not show it to be as large a factor in causing cracking as the thermal cycling component. Time at temperature is not seen to be a significant contributor to visible damage.

These observations point to the combined effects of time at moisture and thermal cycling as being the dominant parameters causing the visible damage in the baseline environment.

8.4 ACCELERATED CYCLES

The accelerated thermal cycles which were designed did cause some increased damage at low cycle numbers in the PIXA-M material and the more severe the cycle, the greater the observed damage. The accelerated moisture cycle was not seen to cause any acceleration of visible damage in either material. The goal of using these accelerated cycles to expedite the damage seen from the baseline environment was not achieved since they were not accelerating the dominant damage components of that cycle. However, the accelerated cycles were instrumental in providing data to establish what *were* the dominant parameters.

8.5 FURTHER ACCELERATED TESTING

The accelerated cycles which were used in this study did not accelerate the dominant parts of the baseline environment causing damage. In the light of the findings of the study, it is proposed that an isomoisture (extended time at moisture) environment combined with a thermal (or mechanical) cycling component would be a viable option for accelerating damage. Isomoisture exposure would expose specimens to the maximum amount of time at moisture for a given test time. The thermal or mechanical cycling component would introduce cyclic stresses throughout the laminate which are believed to play a role in causing visible damage when combined with isomoisture.

REFERENCES

1. Noor, A. K. and S. L. Venneri (Eds.), *Future Aeronautical and Space Systems*, AIAA Progress in Astronautics and Aeronautics, Vol. 172, AIAA, 1997, pp. 173-210.

2. Wilhite, A. W. and R. J. Shaw, "HSCT research picks up speed", *Aerospace America*, AIAA, August 1997, pp. 24-29, 41.

3. National Research Council, *U.S. Supersonic Commercial Aircraft: Assessing NASA's High Speed Research Program*, National Academy Press, 1997.

4. Thornton, E. A., *Thermal Structures for Aerospace Applications*, AIAA Education Series, AIAA, 1996, pp. 1-20.

5. Johnson, B., "Temperature Issues for a Mach 2.4 High Speed Civil Transport", SAE Technical Paper 942160, AEROTECH '94, Los Angeles, CA, October 1994.

6. Burianek, D., "Fatigue Damage in Titanium-Graphite Hybrid Laminates", AIAA-98-1965, 39th Structures, Structural Dynamics and Materials Conference, Long Beach, CA, April 1998.

7. Weitsman, Y., "Moisture in Composites: Sorption and Damage", *Fatigue in Composite Materials*, Elsevier Science Publishers, 1990, pp. 385-428.

8. Wolff, E. G., "Moisture Effects on Polymer Matrix Composites", *SAMPE Journal*, Vol. 29, No. 3, May/June 1990, pp. 11-19.

9. Shen, Chi-Hung and G. S. Springer, "Moisture Absorption and Desorption of Composite Materials", *Journal of Composite Materials*, Vol. 10, No. 1, 1976, pp. 2-20.

10. Springer, G. S., "Moisture Content of Composites Under Transient Conditions", *Journal of Composite Materials*, Vol. 11, No. 1, 1977, pp. 107-122.

11. McKague, Jr., E. L., J. E. Halkias and J. D. Reynolds, "Moisture in Composites: The Effect of Supersonic Service on Diffusion", *Journal of Composite Materials*, Vol. 9, No. 1, 1975, pp. 2-9.

12. Xiang, Z. D. and F. R. Jones, "Thermal-Spike-Enhanced Moisture Absorption by Polymer-Matrix Carbon-Fibre Composites", *Composites Science and Technology*, Vol. 57, 1997, pp. 451-461.

13. DeIasi, R. J., J. B. Whiteside and W. Wolter, "Effects of Varying Hygrothermal Environments on Moisture Absorption in Epoxy Composites", *Fibrous Composites in Structural Design*, E. M. Lenoe et al. (Eds.), Plenum Press, 1980, pp. 809-818.

14. Loos, A. C. and G. S. Springer, "Moisture Absorption of Graphite-Epoxy Composites Immersed in Liquids and in Humid Air", *Journal of Composite Materials*, Vol. 13, April 1979, pp. 131-147.

15. Whiteside, J. B., R. J. DeIasi and R. L. Schulte, "Distribution of Absorbed Moisture in Graphite/Epoxy Laminates After Real-Time Environmental Cycling", *Long-Term Behavior of Composites,* STP 813, ASTM, 1983, pp. 192-205.

16. Akay, M., S. Kong Ah Mun and A. Stanley, "Influence of Moisture on the Thermal and Mechanical Properties of Autoclaved and Oven-Cured Kevlar-49/Epoxy Laminates", *Composites Science and Technology*, Vol. 57, 1997, pp. 565-571.

17. Springer, G. S., "Environmental Effects on Epoxy Matrix Composites", *Composite Materials: Testing and Design*, STP 674, ASTM, 1979, pp. 291-312.

18. Shirrell, C. D. and J. Halpin, "Moisture Absorption and Desorption in Epoxy Composite Laminates", *Composite Materials: Testing and Design*, STP 617, ASTM, 1997, pp. 514-528.

19. Weitsman, Y., "A Rapidly Convergent Scheme to Compute Moisture Profiles in Composite Materials Under Fluctuating Ambient Conditions", *Journal of Composite Materials*, Vol. 15, July 1981, pp. 349-358.

20. Springer, G. S., *Environmental Effects on Composite Materials*, Technomic Publishing, Lancaster, PA, Vols. 1 and 2, 1981.

21. Foch, B. and H. L. McManus, "Modeling of Environmentally Induced Damage in Polymer Matrix Composites", 11th International Conference on Composite Materials, Gold Coast, Australia, July 1997.

22. Antoon, M. K. and J. L. Koenig, "Irreversible Effects of Moisture on the Epoxy Matrix in Glass-Reinforced Composites", *Journal of Polymer Science: Polymer Physics Edition*, Vol. 19, 1981, pp. 197-212.

23. Zhou, J. and J. P. Lucas, "Effects of Water on a Graphite/Epoxy Composite", *Journal of Thermoplastic Composite Materials*, Vol. 9, October 1996, pp. 316-328.

24. Upadhyay, P. C. and J. Prucz, "Parametric Damage Modeling of Composites due to Moisture Absorption", *Journal of Reinforced Plastics and Composites*, Vol. 11, 1992, pp. 198-210.

25. Davies, P. F. Pomies and L. A. Carlsson, "Influence of Water Absorption on Transverse Tensile Properties and Shear Fracture Toughness of Glass/Polypropylene", *Journal of Composite Materials*, Vol. 30, No. 9, 1996, pp. 1004-1019.

26. Flaggs, D. L. and F. W. Crossman, "Analysis of the Viscoelastic Response of Composite Laminates during Hygrothermal Exposure", *Journal of Composite Materials*, Vol. 15, January 1981, pp. 21-40.

27. Lee, Myung Cheon and N. A. Peppas, "Models of Moisture Transport and Moisture-Induced Stresses in Epoxy Composites", *Journal of Composite Materials*, Vol. 12, No. 12, 1993, pp. 1146-1171.

28. Harper, B. D. and Y. Weitsman, "On the Effects of Environmental Conditioning on Residual Stresses in Composite Laminates", *Int. Journal Solids Structures*, Vol. 21, No. 8, 1985, pp. 907-926.

29. Weitsman, Y., "Coupled Damage and Moisture-Transport in Fiber-Reinforced, Polymeric Composites", *Int. Journal Solids Structures*, Vol. 23, No. 7, 1987, pp. 1003-1025.

30. Milke, J. A. and A. J. Vizzini, "Thermal Response of Fire-Exposed Composites", *Journal of Composites Technology and Research*, Vol. 13, No. 3, pp. 145-151.

31. Crews, L. K. and H. L. McManus, "Modeling the High-Temperature Degradation of Graphite/Epoxy", *Proceedings of the American Society for Composites 12th Technical Conference on Composite Materials*, Detroit, MI, October 1997, pp. 1123-1132.

32. Chang, Win-Jin, Tei-Chen Chen and Cheng-I Weng, "Transient Hygrothermal Stresses in an Infinitely Long Annular Cylinder: Coupling of Heat and Moisture", *Journal of Thermal Stresses*, Vol. 14, 1991, pp. 439-454.

33. Cunningham, R. A. and H. L. McManus, "Coupled Diffusion-Reaction Models for Predicting the Distribution of Degradation in Polymer Matrix Composites", 1996 AMSE International Mechanical Engineering Congress and Exposition, Symposium on Composite Materials.

34. Nelson, J. B., "Thermal Aging of Graphite/Polyimide Composites", *Long-Term Behavior of Composites*, ASTM STP 813, T. K. O'Brien (Ed.), ASTM, 1983, pp. 206-221.

35. Harding, D. R., J. K. Sutter and D. S. Papadopoulos, "Protective Coatings for High Temperature Polymer Matrix Composites", 25th International SAMPE Conference, October 1993, pp. 514-527.

36. McManus, H. L. and C. C. Chamis, "Stress and Damage in Polymer Matrix Composite Materials due to Material Degradation at High Temperatures", NASA Technical Memorandum 4682, January 1996.

37. Tsuji, L. C., H. L. McManus and K. J. Bowles, "Mechanical Properties of Degraded PMR-15 Resin", ASTM Symposium on Time Dependent and Non-linear effects in Polymers and Composites, STP 1357, Atlanta, GA, May 1998.

38. Lo, Ying-Jin, Chung-Ho Liu, Diing-Guey Hwang, Jin-Fu Chang, Jong-Cheng Chen, Wen-Yin Chen and Shu-En Hsu, "High Temperature Behaviors of an Innovative Polymeric Matrix Composite", *High Temperature and Environmental Effects on Polymeric Composites*, STP 1174, C. E. Harris and T. S. Gates (Eds.), ASTM, 1993, pp. 66-77.

39. Meador, M. A., P. J. Cavano and D. C. Malarik, "High Temperature Polymer Matrix Composites for Extreme Environments", *Structural Composites: Design and Processing Technologies*, Proceedings of the 6th Annual ASM/ESD Advanced Composites Conference, Detroit, MI, October 1990, pp. 529-539.

40. Hou, T. H., B. J. Jensen and P. M. Hergenrother, "Processing and Properties of IM7/PETI Composites", *Journal of Composite Materials*, Vol. 30, No. 1, 1996, pp. 109-122.

41. Rommel, M. L., L. Konopka and P. M. Hergenrother, "Process Development and Mechanical Properties of IM7/LaRC PETI-5 Composites", 28th International SAMPE Technical Conference Proceedings, November 1996, pp. 1-13.

42. Hartness, J. T., "The Characterisation of a Thermoplastic Polyimide Composite", 28th International SAMPE Technical Conference, Vol. 28, 1996, pp. 48-62.

43. Maddocks, J. R., "Microcracking in Composite Laminates under Thermal and Mechanical Loading", Master of Science Thesis, Massachusetts Institute of Technology, 1995.

44. Tompkins, S. S. and S. L. Williams, "Effects of Thermal Cycling on Mechanical Properties of Graphite Polyimide", *Journal of Spacecraft*, Vol. 21, No. 3, 1984, pp. 274-280.

45. Adams, D. S., D. E. Bowles and C. T. Herakovich, "Thermally-Induced Transverse Cracking in Graphite-Epoxy Cross-Ply Laminates", *Journal of Reinforced Plastics and Composites*, Vol. 5, July 1986, pp. 152-169.

46. McManus, H. L., D. E. Bowles and S. S. Tompkins, "Prediction of Thermal Cycling Induced Matrix Cracking", *Journal of Reinforced Plastics and Composites*, Vol. 15, February 1996, pp. 124-140.

47. McManus, H. L. and J. R. Maddocks, "On Microcracking in Composite Laminates Under Thermal and Mechanical Loadings", *Polymers & Polymer Composites*, Vol. 4, No. 5, 1996, pp. 305-314.

48. Park, C. H. and H. L. McManus, "Thermally Induced Damage in Composite Laminates: Predictive Methodology and Experimental Investigation", *Composites Science and Technology*, Vol. 56, 1996, pp. 1209-1219.

49. Michii, Y. and H. L. McManus, "Prediction of Microcracking Distributions in Composite Laminates Using a Monte Carlo Simulation Method", *Journal of Reinforced Plastics and Composites*, Vol. 16, No. 13, pp. 1220-1230.

50. Clifton Furrow, A. P., D. A. Dillard, T. L. St. Clair and J. Hinkley, "Dye Penetrant Induced Microcracking in High Performance Thermoplastic Polyimide Composites", *Journal of Composite Materials*, Vol. 32, No. 1, 1998, pp. 31-48.

51. McManus, H. L., B. J. Foch and R. A. Cunningham, "Mechanism-based Modeling of Long-term Degradation", DURACOSYS 97: Progress in Durability Analysis of Composite Systems, Blacksburg, VA, September 1997.

52. Sriram, P., Y. Khourchid, S. J. Hooper and R. H. Martin, "Experimental Development of a Mixed-Mode Fatigue Delamination Criterion", *Composite Materials Fatigue and Fracture*, STP 1230, ASTM, 1995, pp. 3-18.

53. Foch, B. J., "Integrated Degradation Models for Polymer Matrix Composites", Master of Science Thesis, Massachusetts Institute of Technology, May 1997.

54. Bradai, M., "Microcracking in Composite Laminates Under Thermal Cycling", Technology Laboratory for Advanced Composites, TELAC Report 97-9, Massachusetts Institute of Technology, March 1997.

55. Nairn, J., Polyimide isomoisture data, personal communication with R. Cunningham, The Boeing Co., October 1997.

56. Hygrothermomechanical testing document, in preparation, TELAC, MIT.

APPENDIX A

STAGE II TESTING EDGE DAMAGE DATA

A.1 DEFINITIONS

Laminate/Material type
P5 = PETI-5
PM = PIXA-M

cycle number

specimen number

RESEARCH P5-R		50 cycles		200 cycles		500 cycles		1000 cycles		1520 cycles	
		-1	-2	-3	-4	-5	-6	-7	-8	-9	-10
side 1	90_2 group	0	0	16g 8(1)	6g 9(1)	18g 3(1)	21g 4(1)	45g 6(1)	44g	36g 2(1)	38g 2(1)
	90_4 group	2(2)	0	1g 4(2) 50(1)	2(3) 3(2) 27(1)	2g 2(3) 3(2) 47(1)	1g 1(3) 4(2) 38(1)	24g 8(3) 9(2)	26g 8(3) 17(2)	12g 1(3) 10(2) 52(1)	33g 5(3) 12(2) 44(1)
side 2	90_2 group	0	0	6g 14(1)	2g 5(1)	32g 2(1)	12g 4(1)	45g 6(1)	47g	37g	42g
	90_4 group	0	1g	15(1)	2(2) 4(1)	8g 2(3) 14(2) 22(1)	1(2) 5(1)	31g 9(3) 19(2) 55(1)	23g 9(3) 20(2)	39g 4(3) 10(2) 37(1)	13g 6(3) 16(2) 60(1)

side of specimen under consideration

ply group under consideration

number of cracks:
g = group
(3) = triple
(2) = double
(1) = single

A.2 DATA

Table A.1: Baseline environment damage data (PETI-5)

RESEARCH P5-R		50 cycles		200 cycles		500 cycles		1000 cycles		1520 cycles	
		-1	-2	-3	-4	-5	-6	-7	-8	-9	-10
side 1	90_2 group	0	0	16g 8(1)	6g 9(1)	18g 3(1)	21g 4(1)	45g 6(1)	44g	36g 2(1)	38g 2(1)
	90_4 group	2(2)	0	1g 4(2) 50(1)	2(3) 3(2) 27(1)	2g 2(3) 3(2) 47(1)	1g 1(3) 4(2) 38(1)	24g 8(3) 9(2)	26g 8(3) 17(2)	12g 1(3) 10(2) 52(1)	33g 5(3) 12(2) 44(1)
side 2	90_2 group	0	0	6g 14(1)	2g 5(1)	32g 2(1)	12g 4(1)	45g 6(1)	47g	37g	42g
	90_4 group	0	1g	15(1)	2(2) 4(1)	8g 2(3) 14(2) 22(1)	1(2) 5(1)	31g 9(3) 19(2) 55(1)	23g 9(3) 20(2)	39g 4(3) 10(2) 37(1)	13g 6(3) 16(2) 60(1)
Group Avg.		0.05		0.05		0.54		5.12		4.77	
Group SD		0.10		0.10		0.71		0.70		2.72	
Aggr. Avg.		0.39		6.10		10.58		34.60		35.68	
Aggr. SD		0.45		4.84		6.76		9.20		9.38	

CROSSPLY P5-C		50 cycles		200 cycles		500 cycles		1000 cycles		1520 cycles	
		-1	-2	-3	-4	-5	-6	-7	-8	-9	-10
side 1	90	0	0	3	bp	55	25	57	171	157	173
	90	0	0	3?	bp	21	bp	88	159	121	115
	90	5	0	?	bp	27	bp	109	162	166	131
	90	6	0	5	bp	50	25	157	127	158	146
side 2	90	bp	0	10	10	77	102	158	bp	102	196
	90	bp	0	3	1	21	62	121	bp	50	184
	90	1	0	8	4	92	106	129	bp	54	183
	90	0	0	8	14	86	137	147	bp	65	195
Average		0.17		1.23		12.46		26.00		27.02	
SD		0.39		0.79		7.40		6.75		9.63	

Table A.1 (cont.)

QUASI P5-Q		50 cycles		200 cycles		500 cycles		1000 cycles		1520 cycles	
		-1	-2	-3	-4	-5	-6	-7	-8	-9	-10
side 1	90	0	0	24	22	69	72	bp	41	109	124
	90	0	0	10	16	40	28	bp	bp	48	39
	90	0	0	6	26	77	56	94	67	92	63
	90	0	6	15	28	77	35	87	65	99	66
side 2	90	0	0	0	2	29	80	65	123	103	156
	90	1	0	1	0	7	24	57	bp	47	84
	90	0	0	4	1	19	38	112	bp	80	84
	90	3	0	7	8	26	45	106	bp	93	89
Average		0.12		2.09		8.88		16.08		16.93	
SD		0.32		1.95		4.64		5.26		5.92	

Table A.2: Baseline environment damage data (PIXA-M)

RESEARCH PM-R		50 cycles		200 cycles		500 cycles		1000 cycles		1520 cycles	
		-1	-2	-3	-4	-5	-6	-7	-8	-9	-10
side 1	90_2 group	2g	3(1)	8g 6(1)	9g 2(1)	19g 15(1)	19g 16(1)	42g 20(1)	38g 24(1)	39g 25(1)	33g 13(1)
	90_4 group	1(1)	6(1)	5g 2(3) 5(2) 12(1)	11g 2(3) 12(2) 32(1)	29g 6(3) 13(2) 28(1)	20g 10(3) 8(2) 28(1)	36g 17(3) 15(2) 54(1)	bp	45g 4(3) 7(2) 33(1)	48g 6(3) 9(2) 18(1)
	90_2 group	5g 4(1)	4g 3(1)	12g 8(1)	16g 12(1)	24g 12(1)	27g 9(1)	46g 27(1)	40g 18(1)	41g 17(1)	39g 3(1)
side 2	90_2 group	0	0	1g	1g	2g 0(1)	8g 1(1)	47g 20(1)	43g 14(1)	19g 8(1)	32g 8(1)
	90_4 group	1(1)	3(1)	1(1)	2(3) 1(2) 4(1)	3g 4(3) 6(2) 15(1)	1g 1(2) 1(1)	43g 6(3) 3(2) 52(1)	51g 8(3) 22(2) 54(1)	11g 2(2) 19(1)	23g 6(3) 6(2) 26(1)
	90_2 group	1g	0	5g 3(1)	12g 3(1)	31g 12(1)	20g 2(1)	44g 19(1)	43g 16(1)	37g 4(1)	40g 5(1)
Group Avg.		0.00		0.79		2.61		8.53		6.25	
Group SD		0.00		1.03		2.66		1.48		3.50	
Aggr. Avg.		0.54		8.22		19.69		55.97		34.45	
Aggr. SD		0.47		9.31		16.75		7.73		16.68	

CROSSPLY PM-C		50 cycles		200 cycles		500 cycles		1000 cycles		1520 cycles	
		-1	-2	-3	-4	-5	-6	-7	-8	-9	-10
side 1	90	6	9	70	70	98	119	149	143	187	189
	90	0	0	25	24	21	59	150	131	152	169
	90	0	2	39	50	35	73	146	142	121	182
	90	14	18	73	115	86	96	138	163	210	197
side 2	90	5	5	20	16	101	70	166	144	bp	186
	90	0	2	5	2	14	18	103	137	144	144
	90	0	4	5	2	11	40	128	122	167	77
	90	13	12	27	18	47	48	148	179	218	180
Average		1.11		6.90		11.52		28.16		33.11	
SD		1.16		6.36		6.81		3.53		7.15	

Table A.2 (cont.)

QUASI PM-Q		50 cycles		200 cycles		500 cycles		1000 cycles		1520 cycles	
		-1	-2	-3	-4	-5	-6	-7	-8	-9	-10
side 1	90	0	4	14	5	96	97	142	161	116	105
	90	0	1	15	8	72	62	133	148	98	111
	90	0	5	26	28	90	76	157	160	120	111
	90	4	9	31	37	97	92	154	167	146	131
side 2	90	3	2	5	3	6	17	130	131	72	110
	90	2	2	7	5	4	5	133	132	77	52
	90	2	6	14	14	12	24	151	142	96	66
	90	4	2	17	16	95	58	138	145	125	77
Average		0.57		3.01		11.11		28.59		19.84	
SD		0.48		2.03		7.52		2.37		5.09	

Table A.3: Isolated thermal environment damage data (PETI-5)

RESEARCH P5-R		50 cycles		200 cycles		500 cycles		1000 cycles		1520 cycles	
		-11	-12	-13	-14	-15	-16	-17	-18	-19	-20
side 1	90_2 group	0	0	2(1)	1g 6(1)	7g 8(1)	7g 4(1)	35g 17(1)	29g 14(1)	27g 5(1)	48g 8(1)
	90_4 group	6g 1(3) 2(2)	0	0	0	2(1)	1(2) 11(1)	14g 5(3) 19(2) 56(1)	8g 3(3) 11(2)	12g 8(3) 9(2) 111(1)	33g 9(3) 29(2) 108(1)
side 2	90_2 group	0	1g 2(3) 1(2) 1(1)	1g 3(1)	2(1)	3g 6(1)	5g 6(1)	34g 5(1)	30g 10(1)	34g 4(1)	20g 6(1)
	90_4 group	0	0	0	0	6(1)	2(1)	2g 4(3) 5(2) 39(1)	10g 6(3) 19(2)	11g 5(3) 11(2) 89(1)	2g 2(3) 5(2) 68(1)
Group Avg.		0.00		0.00		0.00		1.67		2.85	
Group SD		0.00		0.00		0.00		0.98		2.58	
Aggr. Avg.		0.00		0.00		1.13		19.34		38.78	
Aggr. SD		0.00		0.00		1.02		9.20		19.07	

CROSSPLY P5-C		50 cycles		200 cycles		500 cycles		1000 cycles		1520 cycles	
		-11	-12	-13	-14	-15	-16	-17	-18	-19	-20
side 1	90	0	0	1	0	47	bp	bp	bp	195	166
	90	0	0	0	0	14	bp	bp	bp	130	81
	90	0	0	8	0	16	bp	bp	bp	129	76
	90	0	0	17	4	35	bp	bp	bp	123	52
side 2	90	0	0	0	0	31	16	130	125	bp	bp
	90	0	0	0	0	9	4	57	49	bp	bp
	90	0	26	0	4	20	22	81	85	bp	bp
	90	0	20	9	9	37	24	88	153	bp	bp
Average		0.57		0.64		4.51		18.90		23.43	
SD		1.56		0.99		2.47		7.21		9.41	

Table A.3 (cont.)

QUASI P5-Q		50 cycles		200 cycles		500 cycles		1000 cycles		1520 cycles	
		-11	-12	-13	-14	-15	-16	-17	-18	-19	-20
side 1	90	0	0	1	0	36	28	46	51	119	99
	90	0	0	1	0	6	13	52	19	45	48
	90	0	0	0	1	19	13	51	51	68	52
	90	7	1	0?	3	24	21	63	59	48	46
side 2	90	0	0	1	0	4	5	113	60	52	50
	90	0	0	0	0	0	0	61	38	27	18
	90	0	0	0	0	2	4	81	84	30	22
	90	1	0	1	3	9	11	91	bp	44	63
Average		0.11		0.14		2.40		12.07		10.22	
SD		0.34		0.20		2.11		4.54		5.19	

Table A.4: Isolated thermal environment damage data (PIXA-M)

RESEARCH PM-R		50 cycles		200 cycles		500 cycles		1000 cycles		1520 cycles	
		-11	-12	-13	-14	-15	-16	-17	-18	-19	-20
side 1	90_2 group	2g	1g 3(1)	2g 2(1)	3g 3(1)	5g 3(1)	5g 3(1)	33g 9(1)	31g 8(1)	27g 22(1)	33g 9(1)
	90_4 group	1g 1(1)	6(1)	1g 1(3) 3(2) 4(1)	1g 4(3) 2(2) 8(1)	1g 2(2) 7(1)	2g 1(3) 5(1)	27g 3(3) 6(2) 31(1)	28g 10(3) 13(2) 27(1)	32g 6(3) 21(2) 47(1)	25g 11(3) 14(2) 37(1)
	90_2 group	6g	2g	3g 4(1)	7g 5(1)	13g 5(1)	13g 7(1)	38g 20(1)	44g 22(1)	48g 8(1)	40g 9(1)
side 2	90_2 group	0	0	1g 1(1)	1(1)	4g 5(1)	4g 6(1)	29g 17(1)	8g 11(1)	27g 14(1)	19g 16(1)
	90_4 group	1(2) 6(1)	5(1)	2(3) 3(2) 6(1)	1(2) 3(1)	1g 3(2) 8(1)	4g 2(3) 5(2) 13(1)	19g 9(3) 13(2) 23(1)	3g 3(3) 2(2) 17(1)	24g 4(3) 15(2) 41(1)	30g 10(3) 17(2) 58(1)
	90_2 group	1(1)	1g 1(1)	7g 1(1)	1g 3(1)	16g 8(1)	12g 9(1)	26g 15(1)	27g 6(1)	30g 18(1)	40g 12(1)
Group Avg.		0.05		0.10		0.39		3.79		5.46	
Group SD		0.10		0.11		0.28		2.28		0.76	
Aggr. Avg.		1.18		3.35		4.63		27.02		42.03	
Aggr. SD		0.28		1.85		2.83		13.03		5.91	

CROSSPLY PM-C		50 cycles		200 cycles		500 cycles		1000 cycles		1520 cycles	
		-11	-12	-13	-14	-15	-16	-17	-18	-19	-20
side 1	90	6	7	6	9	33	24	139	131	217	206
	90	0	0	1	8	5	7	101	60	133	153
	90	2	1	3	2	24	8	117	117	134	126
	90	9	21	21	26	41	14	153	104	196	189
side 2	90	5	5	5	3	47	13	83	67	215	146
	90	1	2	0	2	8	2	23	30	57	84
	90	0	4	0	2	9	16	22	31	92	71
	90	8	14	7	12	41	48	101	107	156	166
Average		1.05		1.32		4.18		17.05		28.80	
SD		1.13		1.47		3.13		8.46		10.08	

Table A.4 (cont.)

QUASI PM-Q		50 cycles		200 cycles		500 cycles		1000 cycles		1520 cycles	
		-11	-12	-13	-14	-15	-16	-17	-18	-19	-20
side 1	90	2	2	5	4	11	12	98	114	64	75
	90	1	4	3	3	7	4	61	93	50	73
	90	3	1	4	1	6	3	104	117	36	39
	90	3	2	8	6	6	6	120	147	58	59
side 2	90	3	1	6	5	12	13	34	15	70	110
	90	2	0	4	2	6	12	17	12	59	107
	90	7	4	0	6	8	2	30	28	44	82
	90	9	6	5	4	12	9	62	47	55	91
Average		0.62		0.81		1.59		13.52		13.19	
SD		0.48		0.40		0.71		8.74		4.34	

Table A.5: Accelerated moisture environment damage data (PETI-5)

RESEARCH P5-R		288 cycles		500 cycles		1000 cycles		1500 cycles		1960 cycles	
		-33	-34	-35	-36	-37	-38	-39	-40	-41	-42
side 1	90_2 group	5(1)	1g 4(1)	1g 10(1)	3g 6(1)	1g 4(1)	4(1)	18g 8(1)	5g 7(1)	34g 16(1)	10g 2(1)
	90_4 group	6(1)	5(1)	20(1)	6(1)	16(1)	1(1)	4(2) 37(1)	1(3)	8g 4(3) 16(2) 59(1)	2(3) 6(1)
side 2	90_2 group	1g 2(1)	5(1) 1(2) 10(1)	7(1) 2(1)	3(1) 4(1)	1g 6(1) 2(1)	1g 10(1) 6(1)	4g 3(1) 0	14g 16(1) 1(3) 3(2) 24(1)	14g 2(1) 4(1)	18g 4(1) 12g 4(3) 12(2) 55(1)
	90_4 group										
Group Avg.		0.00		0.00		0.00		0.00		0.98	
Group SD		0.00		0.00		0.00		0.00		1.18	
Aggr. Avg.		1.23		1.57		1.23		3.99		14.27	
Aggr. SD		0.83		1.61		1.35		4.38		14.68	

CROSSPLY P5-C		288 cycles		500 cycles		1000 cycles		1500 cycles		1960 cycles	
		-38	-39	-40	-41	-42	-43	-44	-45	-46	-47
side 1	90	bp	0	1	11	11	25	46	78	137	29
	90	0	0	0	1	8	12	9	23	56	8
	90	3	1	1	3	6	15	21	47	80	8
	90	12	5	0	23	9	44	65	62	120	27
side 2	90	bp	bp	bp	bp	bp	bp	bp	bp	bp	101
	90	bp	bp	bp	bp	bp	bp	bp	bp	bp	bp
	90	0?	bp	bp	bp	bp	bp	bp	bp	bp	bp
	90	2?	bp	bp	bp	bp	bp	bp	bp	bp	43
Average		0.50		0.98		3.20		8.64		12.38	
SD		0.78		1.60		2.49		4.78		9.60	

Table A.5 (cont.)

QUASI P5-Q		288 cycles		500 cycles		1000 cycles		1500 cycles		1960 cycles	
		-2	-3	-4	-5	-39	-40	-42	-43	-44	-45
side 1	90	1	0	18	3	1	0	6	4	13	13
	90	0	0	2	0	0	2	3	3	5	0
	90	1	0	1	1	0	0	5	17	17	2
	90	4	7	14	5	0	d	4	11	14	7
side 2	90	1	0	7	d	0	3	4	2	8	4
	90	0	0	1	d	0	0	2	0	2	0
	90	0	0	2	d	0	1	9	2	3	4
	90	6	6	5	d	0	1	8	5	4	4
Average		0.32		0.97		0.10		1.05		1.23	
SD		0.50		1.11		0.18		0.83		1.04	

Table A.6: Accelerated moisture environment damage data (PIXA-M)

RESEARCH PM-R		288 cycles		500 cycles		1000 cycles		1500 cycles		1960 cycles	
		-36	-37	-38	-39	-40	-41	-42	-43	-44	-45
side 1	90_2 group	3g 3(1)	6g 6(1)	8g 3(1)	6g 3(1)	12g 6(1)	9g 3(1)	16g 12(1)	18g 4(1)	24g 13(1)	20g 6(1)
	90_4 group	1g 2(3) 4(2) 3(1)	8g 2(3) 4(2) 20(1)	6g 3(2) 13(1)	6g 1(3) 3(2) 7(1)	11g 3(3) 9(2) 16(1)	13g 6(3) 5(2) 15(1)	22g 6(3) 11(2) 44(1)	30g 6(3) 7(2) 23(1)	24g 1(3) 4(2) 30(1)	24g 2(3) 6(2) 20(1)
	90_2 group	10g 5(1)	11g 3(1)	18g 4(1)	20g 4(1)	24g 7(1)	21g 11(1)	27g 18(1)	23g 6(1)	29g 17(1)	24g 8(1)
side 2	90_2 group	1g 3(1)	9g 4(1)	8g 2(1)	8g 2(1)	12g 7(1)	13g 5(1)	15g 9(1)	11g 7(1)	23g 14(1)	15g 5(1)
	90_4 group	3g 9(1)	3g 1(3) 5(2) 18(1)	2g 1(3) 5(2) 17(1)	3g 3(3) 1(2) 9(1)	13g 10(3) 8(2) 21(1)	10g 3(3) 6(2) 14(1)	16g 6(3) 4(2) 20(1)	22g 4(3) 6(2) 20(1)	26g 1(3) 7(2) 23(1)	26g 6(3) 2(2) 29(1)
	90_2 group	8g 4(1)	11g 7(1)	18g 3(1)	23g 3(1)	20g 7(1)	18g 5(1)	20g 5(1)	23g 9(1)	24g 8(1)	22g 7(1)
Group Avg.		0.74		0.84		2.31		4.43		4.92	
Group SD		0.59		0.41		0.30		1.13		0.23	
Aggr. Avg.		7.43		7.53		18.50		28.99		28.05	
Aggr. SD		4.23		0.91		3.66		6.23		1.84	

CROSSPLY PM-C		288 cycles		500 cycles		1000 cycles		1500 cycles		1960 cycles	
		-38	-39	-40	-41	-42	-43	-44	-45	-46	-47
side 1	90	10	14	21	19	54	41	132	159	153	180
	90	3	2	1	4	15	14	68	48	45	32
	90	1	1	1	1	14	28	46	49	61	58
	90	16	9	24	35	69	71	128	173	168	156
side 2	90	9	7	23	30	63	41	148	bp	115	135
	90	4	0	5	4	4	15	29 bp	bp	23	61
	90	0	1	4	7	9	14	36	bp	55	48
	90	9	4	25	27	62	40	169	bp	124	166
Average		1.11		2.84		6.82		19.43		19.44	
SD		0.10		2.37		4.61		10.63		10.95	

Table A.6 (cont.)

QUASI PM-Q		288 cycles		500 cycles		1000 cycles		1500 cycles		1960 cycles	
		-36	-37	-38	-39	-40	-41	-42	-43	-44	-45
side 1	90	6	6	14	12	9	16	40	44	32	42
	90	4	5	7	7	4	9	28	28	28	29
	90	3	8	12	11	13	8	42	41	23	30
	90	5	16	26	14	26	25	74	64	67	53
side 2	90	7	0	6	3	15	20	24	bp	31	61
	90	1	2	0	3	3	4	12	79	13	38
	90	4	9	4	11	6	1	7	65	13	32
	90	7	5	6	14	29	17	32	67	41	56
Average		1.09		1.85		2.52		8.49		7.25	
SD		0.73		1.24		1.73		4.39		3.12	

Table A.7: Accelerated thermal environment 1 (-180°C) damage data (PETI-5)

RESEARCH P5-R		0 cycles			65 cycles			100 cycles			180 cycles		
		-22	-24	-25	-22	-24	-25	-22	-24	-25	-22	-24	-25
side 1	90_2 group	3(1)	2(1)	3(1)	1g 5(1)	13(1)	3g 3(1)	2g 3(1)	2g 8(1)	4g 4(1)	2g 5(1)	5g 7(1)	5g 3(1)
	90_4 group	0	0	0	0	0	1(1)	0	1(1)	1(1)	0	0	1(1)
side 2	90_2 group	0	0	0	2(1)	2(1)	4(1)	1g 1(1)	4g 4(1)	1g 5(1)	1g 2(1)	4g 3(1)	1g 3(1)
	90_4 group	0	0	0	0	1(1)	0	0	1(1)	0	0	2(1)	0
Group Av.		0.00			0.00			0.00			0.00		
Group SD		0.00			0.00			0.00			0.00		
Aggr. Av.		0.00			0.07			0.10			0.10		
Aggr. SD		0.00			0.10			0.11			0.16		

RESEARCH P5-R		300 cycles			400 cycles			540 cycles			750 cycles		
		-22	-24	-25	-22	-24	-25	-22	-24	-25	-22	-24	-25
side 1	90_2 group	3g 4(1)	5g 7(1)	6g 1(1)	4g 4(1)	7g 8(1)	5g 2(1)	4g 3(1)	8g 6(1)	8g	6g 4(1)	10g 2(1)	8g
	90_4 group	0	0	1(1)	1(1)	1(1)	1(1)	0	1(1)	1(1)	1(1)	1(1)	1(2)
side 2	90_2 group	2g 3(1)	7g 2(1)	3g 3(1)	2g 1(1)	10g 1(1)	3g 3(1)	3g 4(1)	10g 3(1)	5g 3(1)	3g 5(1)	12g 2(1)	10g 1(1)
	90_4 group	0	2(1)	0	0	1(1)	0	0	1(1)	0	0	1(1)	0
Group Av.		0.00			0.00			0.00			0.00		
Group SD		0.00			0.00			0.00			0.00		
Aggr. Av.		0.10			0.16			0.16			0.16		
Aggr. SD		0.16			0.15			0.15			0.15		

P5-C and P5-Q all zeros.

Table A.8: Accelerated thermal environment 1 (-180°C) damage data (PIXA-M)

RESEARCH PM-R		0 cycles			65 cycles			100 cycles			180 cycles		
		-23	-24	-25	-23	-24	-25	-23	-24	-25	-23	-24	-25
side 1	90_2 group	1(1)	0	0	1g 1(1)	4g 1(1)	1g 1(1)	3g 1(1)	7g 2(1)	1g 2(1)	3g 1(1)	7g 2(1)	3g 1(1)
	90_4 group	4(1)	1(1)	1(2) 1(1)	3(2) 9(1)	1(2) 9(1)	3(2) 10(1)	3(3) 5(2) 21(1)	3(2) 11(1)	4(2) 15(1)	1g 4(3) 5(2) 25(1)	2(2) 12(1)	4(2) 12(1)
	90_2 group	3(1)	0	1(1)	10g 2(1)	3g 7(1)	6g 3(1)	11g 3(1)	7g 5(1)	9g 1(1)	12g 3(1)	9g 2(1)	9g 1(1)
side 2	90_2 group	0	1(1)	2(1)	2g	1g 1(1)	2g	3g 4(1)	3g 1(1)	3g	3g 3(1)	3g 1(1)	3g
	90_4 group	3(1)	1(2) 2(1)	5(1)	10(1)	2(2) 6(1)	11(1)	1g 2(3) 3(2) 17(1)	2(3) 4(2) 5(1)	3(2) 18(1)	1g 2(3) 3(2) 17(1)	3(3) 4(2) 3(1)	1(3) 3(2) 11(1)
	90_2 group	0	0	2(1)	3g 3(1)	1g 4(1)	2g 3(1)	11g 4(1)	3g 4(1)	3g 4(1)	13g 2(1)	6g 3(1)	3g 4(1)
Group Av.		0.00			0.00			0.03			0.07		
Group SD		0.00			0.00			0.08			0.10		
Aggr. Av.		0.66			2.40			5.12			5.25		
Aggr. SD		0.27			0.52			1.73			2.76		

RESEARCH PM-R		300 cycles			400 cycles			540 cycles			750 cycles		
		-23	-24	-25	-23	-24	-25	-23	-24	-25	-23	-24	-25
side 1	90_2 group	3g 1(1)	7g	3g	3g 2(1)	7g 1(1)	3g	4g 2(1)	8g 1(1)	3g	7g	12g	4g
	90_4 group	2g 3(3) 5(2) 22(1)	2(3) 1(2) 14(1)	5(2) 13(1)	4g 2(3) 5(2) 33(1)	1g 1(3) 2(2) 17(1)	1g 1(3) 3(2) 15(1)	4g 3(3) 6(2) 22(1)	1g 1(3) 6(2) 16(1)	1g 6(3) 3(2) 17(1)	6g 4(3) 8(2) 23(1)	2g 1(3) 11(2) 15(1)	8g 2(3) 6(2) 15(1)
	90_2 group	12g 1(1)	9g 3(1)	9g 1(1)	12g 4(1)	9g 3(1)	10g 1(1)	14g 2(1)	12g 2(1)	10g	13g 5(1)	13g 1(1)	13g 3(1)
side 2	90_2 group	3g 2(1)	3g 2(1)	3g	4g 1(1)	3g 1(1)	3g 1(1)	5g 5(1)	4g 2(1)	5g	7g 2(1)	5g 1(1)	4g 1(1)
	90_4 group	1g 2(3) 5(2) 15(1)	3(3) 3(2) 5(1)	2(3) 2(2) 30(1)	1g 4(3) 4(2) 15(1)	2g 3(3) 1(2) 12(1)	3(3) 1(2) 23(1)	1g 4(3) 6(2) 15(1)	3g 2(3) 2(2) 11(1)	3g 1(3) 4(2) 16(1)	6g 4(3) 4(2) 16(1)	5g 1(3) 3(2) 12(1)	5g 5(3) 4(2) 20(1)
	90_2 group	14g 2(1)	8g 1(1)	6g 4(1)	14g 3(1)	8g 1(1)	6g 3(1)	16g 3(1)	11g 2(1)	9g 4(1)	18g 2(1)	13g	10g 3(1)
Group Av.		0.10			0.30			0.43			1.05		
Group SD		0.16			0.27			0.26			0.39		
Aggr. Av.		5.48			7.38			8.33			11.55		
Aggr. SD		1.57			2.77			1.84			2.42		

Table A.8 (cont.)

CROSSPLY PM-C		0 cycles			65 cycles			100 cycles			180 cycles		
		-23	-24	-25	-23	-24	-25	-23	-24	-25	-23	-24	-25
side 1	90	0	1	0	22	15	47	31	50	67	30	50	
	90	1	0	0	7	4	9	10	8	18	10	6	
	90	1	0	1	8	1	10	14	5	18	12	5	
	90	1	2	0	52	50	67	82	82	85	79	76	
side 2	90	0	1	0	29	12	44	43	34	68	40	32	
	90	0	0	0	7	2	6	13	7	14	13	6	
	90	0	0	0	8	3	6	13	6	9	12	5	
	90	2	6	2	65	28	40	88	73	65	89	62	
Average		0.15			4.45			7.41			8.48		
SD		0.26			4.19			5.99			5.64		

CROSSPLY PM-C		300 cycles			400 cycles			540 cycles			750 cycles		
		-23	-24	-25	-23	-24	-25	-23	-24	-25	-23	-24	-25
side 1	90	34	65	79	38	61	85	46	74	93	60	118	103
	90	13	12	28	17	12	24	23	19	30	29	31	38
	90	14	8	24	20	11	25	23	14	27	36	18	43
	90	88	80	89	101	92	87	99	95	92	118	127	109
side 2	90	53	41	78	74	45	82	78	54	81	94	65	104
	90	16	11	17	18	10	19	21	16	25	26	24	38
	90	15	6	14	19	7	19	19	11	27	25	15	39
	90	106	113	78	115	82	85	109	78	94	125	112	122
Average		8.87			9.42			10.24			13.28		
SD		6.94			6.97			6.72			8.16		

Table A.8 (cont.)

CROSSPLY PM-Q		0 cycles			65 cycles			100 cycles			180 cycles		
		-23	-24	-25	-23	-24	-25	-23	-24	-25	-23	-24	-25
side 1	90	0	0	0	5	17	20	16	21	29	12	25	25
	90	0	0	1	0	3	14	1	3	19	0	4	18
	90	3	0	2	6	5	16	10	6	28	9	10	26
	90	4	5	4	32	26	32	52	33	42	53	33	43
side 2	90	0	0	0	18	8	9	35	10	10	30		
	90	0	bp	0	8	bp	1	19	bp	6	14		
	90	5	bp	0	17	bp	4	33	bp	4	29		
	90	3	4	3	39	bp	17	50	29	24	52		
Average		0.31			2.89			4.27			4.23		
SD		0.38			2.20			3.11			3.14		

CROSSPLY PM-Q		300 cycles			400 cycles			540 cycles			750 cycles		
		-23	-24	-25	-23	-24	-25	-23	-24	-25	-23	-24	-25
side 1	90	19	28	31	16	26	35	15	28	37	22	36	53
	90	1	5	29	1	5	29	1	6	28	2	9	47
	90	9	7	27	8	12	31	10	19	38	10	20	41
	90	53	34	42	55	35	49	59	41	57	59	50	75
side 2	90	31	bp	22	34	bp	18	34	bp	23	42		33
	90	20	bp	13	20	bp	10	17	bp	16	26		26
	90	29	bp	5	32	bp	5	35	bp	7	34		10
	90	50	bp	26	54	bp	34	57	bp	44	56		54
Average		4.68			4.95			5.56			6.96		
SD		3.14			3.38			3.72			4.48		

Table A.9: Accelerated thermal environment 2 (-150°C) damage data (PETI-5)

RESEARCH P5-R		0 cycles			80 cycles			170 cycles			280 cycles		
		-26	-27	-28	-26	-27	-28	-26	-27	-28	-26	-27	-28
side 1	90_2 group	2(1)	3(1)	1(1)	3(1)	3(1)	1(1)	3(1)	3(1)		1g 2(1)	3(1)	1g 1(1)
	90_4 group	0	0	0	0	0	0	0	0		0	0	0
side 2	90_2 group	0	1(1)	0	2(1)	2(1)	0	2(1)			4(1)	1g 3(1)	1(1)
	90_4 group	0	0	0	0	0	0	0			0	0	0
Group Av.		0.00			0.00			0.00			0.00		
Group SD		0.00			0.00			0.00			0.00		
Aggr. Av.		0.00			0.00			0.00			0.00		
Aggr. SD		0.00			0.00			0.00			0.00		

RESEARCH P5-R		410 cycles			560 cycles			750 cycles		
		-26	-27	-28	-26	-27	-28	-26	-27	-28
side 1	90_2 group	1g 4(1)	2g 1(1)	1g 1(1)	2g 3(1)	2g 1(1)	1g 1(1)	3g 3(1)	2g 1(1)	2g 2(1)
	90_4 group	0	0	0	0	0	0	0	0	0
side 2	90_2 group	1g 5(1)	2g 3(1)	1g 1(1)	2g 4(1)	2g 3(1)	1g 1(1)	4g 4(1)	4g 2(1)	4g 1(1)
	90_4 group	0	0	0	0	0	0	0	0	0
Group Av.		0.00			0.00			0.00		
Group SD		0.00			0.00			0.00		
Aggr. Av.		0.00			0.00			0.00		
Aggr. SD		0.00			0.00			0.00		

P5-C and P5-Q all zeros.

Table A.10: Accelerated thermal environment 2 (-150°C) damage data (PIXA-M)

RESEARCH PM-R		0 cycles			80 cycles			170 cycles			280 cycles		
		-27	-28	-29	-27	-28	-29	-27	-28	-29	-27	-28	-29
side 1	90_2 group	3(1)	0	2(1)	1g 2(1)	1(1)	3(1)	1g 2(1)	4(1)	2g 1(1)	1g 2(1)	3(1)	3g
	90_4 group	2(1)	6(1)	2(1)	2(1)	8(1)	4(1)	2(2) 3(1)	1(3) 1(2) 10(1)	5(1)	2(3) 7(1)	2(3) 2(2) 9(1)	9(1)
	90_2 group	d	0	1(1)	d	1g 1(1)	1g 3(1)	6g 1(1)	3g 2(1)	6g 2(1)	7g	6g 2(1)	7g 1(1)
side 2	90_2 group	0	3(1)	1(1)	0	1g 2(1)	1g	1g 1(1)	2g	1g 1(1)	1g 2(1)	3g	2g
	90_4 group	3(1)	4(1)	2(1)	4(1)	6(1)	7(1)	1g 1(2) 3(1)	10(1)	3(2) 6(1)	1g 3(2) 2(1)	1(2) 12(1)	2(3) 1(2) 12(1)
	90_2 group	0	1g	3(1)	1(1)	2g 4(1)	5g 4(1)	6g	5g 6(1)	10g 2(1)	6g	9g 2(1)	12g 1(1)
Group Av.		0.00			0.00			0.03			0.03		
Group SD		0.00			0.00			0.08			0.08		
Aggr. Av.		0.62			1.02			2.26			2.72		
Aggr. SD		0.32			0.44			1.13			0.98		

RESEARCH PM-R		410 cycles			560 cycles			750 cycles		
		-27	-28	-29	-27	-28	-29	-27	-28	-29
side 1	90_2 group	3g	2g 4(1)	4g 2(1)	4g	4g 5(1)	7g 2(1)	4g 2(1)	8g 4(1)	10g 3(1)
	90_4 group	2g 1(3) 1(2) 7(1)	2g 3(3) 3(2) 8(1)	1(3) 3(2) 13(1)	3g 2(2) 6(1)	6g 1(3) 3(2) 9(1)	1g 2(3) 4(2) 16(1)	3g 3(2) 9(1)	8g 1(3) 5(2) 9(1)	5g 1(3) 9(2) 12(1)
	90_2 group	8g 2(1)	8g 4(1)	8g 1(1)	10g 3(1)	9g 8(1)	10g 1(1)	13g 2(1)	14g 5(1)	13g 3(1)
side 2	90_2 group	2g 3(1)	5g 2(1)	2g 1(1)	2g 3(1)	7g 1(1)	3g 1(1)	3g 3(1)	9g 2(1)	4g
	90_4 group	2g 2(3) 4(1)	1g 1(3) 3(2) 20(1)	2g 3(2) 15(1)	4g 7(1)	2g 4(3) 6(2) 23(1)	2g 4(3) 4(2) 10(1)	4g 1(3) 2(2) 8(1)	6g 3(3) 11(2) 16(1)	7g 4(3) 3(2) 14(1)
	90_2 group	7g 6(1)	15g 4(1)	14g	8g 6(1)	14g 5(1)	14g 2(1)	11g 2(1)	16g 4(1)	18g 4(1)
Group Av.		0.30			0.59			1.08		
Group SD		0.16			0.35			0.37		
Aggr. Av.		3.84			4.66			5.38		
Aggr. SD		1.41			2.95			2.45		

Table A.10 (cont.)

CROSSPLY PM-C		0 cycles			80 cycles			170 cycles			280 cycles		
		-26	-27	-28	-26	-27	-28	-26	-27	-28	-26	-27	-28
side 1	90	0	0	0	3	d	1	10	10	10	19	22	25
	90	0	3	1	1	6	5	2	13	8	6	16	17
	90	1	1	3	1	9	14	3	13	15	6	24	20
	90	2	3	0	6	28	48	15	55	71	25	78	100
side 2	90	0	0	0	2	0	5	7	9	11	11	6	33
	90	0	0	0	2	3	0	2	7	2	5	12	4
	90	0	0	1	1	4	1	4	6	1	7	7	1
	90	1	1	6	2	9	37	11	20	49	16	36	74
Average		0.19			1.56			2.90			4.68		
SD		0.29			2.42			3.51			4.99		

CROSSPLY PM-C		410 cycles			560 cycles			750 cycles		
		-26	-27	-28	-26	-27	-28	-26	-27	-28
side 1	90	29	41	53	51	62	78	57	76	90
	90	11	34	26	16	49	32	25	66	34
	90	15	34	35	23	55	38	30	67	46
	90	35	99	125	42	113	139	54	121	140
side 2	90	20	17	42	34	26	51	45	51	66
	90	7	18	10	10	28	14	10	41	22
	90	11	13	5	14	19	7	16	21	8
	90	25	54	97	33	70	110	45	90	130
Average		7.02			9.14			11.08		
SD		6.12			6.81			7.22		

Table A.10 (cont.)

CROSSPLY PM-Q		0 cycles			80 cycles			170 cycles			280 cycles		
		-26	-27	-29	-26	-27	-29	-26	-27	-29	-26	-27	-29
side 1	90	0	0	0	0	0	1	1	1	2	1	3	6
	90	0	0	0	1	1	2	1	2	3	1	3	5
	90	2	2	0	2	2	1	1	3	2	2	4	3
	90	0	0	0	1	0	2	4	4	6	6	6	9
side 2	90	0	0	1	0	0	0	0	0	3	1	0	5
	90	0	0	0	0	0	0	2	1	4	4	1	5
	90	4	1	1	4	1	0	4	2	3	7	3	6
	90	2	1	4	4	3	6	8	5	11	13	5	12
Average		0.15			0.25			0.60			0.91		
SD		0.24			0.32			0.50			0.65		

CROSSPLY PM-Q		410 cycles			560 cycles			750 cycles		
		-26	-27	-29	-26	-27	-29	-26	-27	-29
side 1	90	2	4	10	5	9	15	7	14	18
	90	2	3	6	5	3	9	6	4	11
	90	4	5	8	5	6	11	6	11	17
	90	12	15	19	16	22	24	17	33	35
side 2	90	2	1	12	4	1	15	9	4	21
	90	4	2	6	7	3	8	10	3	12
	90	8	4	9	9	3	11	10	6	15
	90	17	14	23	20	16	25	34	21	34
Average		1.57			2.07			2.94		
SD		1.20			1.39			1.99		

Table A.11: Accelerated thermal environment 1 damage data (PETI-5 isothermal specimens)

RESEARCH P5-R		0 cycles			50 cycles			150 cycles			300 cycles		
		-43	-44	-45	-43	-44	-45	-43	-44	-45	-43	-44	-45
side 1	90_4 group	0	1g	0	2(2) 2(1)	0	0	2(2) 4(1)	5(1)	1(1)	1(3) 1(2) 6(1)	5(1)	1(1)
side 2	90_4 group	0	0	0	0	1(2)	0	2(1)	1(3)	2(1)	3(1)	1g	3(1)
Group Av.		0.00			0.00			0.00			0.03		
Group SD		0.00			0.00			0.00			0.08		
Aggr. Av.		0.13			0.26			0.33			0.89		
Aggr. SD		0.32			0.48			0.63			0.68		

RESEARCH P5-R		400 cycles		
		-43	-44	-45
side 1	90_4 group	1g 1(2) 6(1)	1(2) 3(1)	1(1)
side 2	90_4 group	6(1)	1g	3(1)
Group Av.		0.07		
Group SD		0.10		
Aggr. Av.		1.02		
Aggr. SD		0.74		

Table A.11 (cont.)

CROSSPLY P5-C		0 cycles			50 cycles			150 cycles			300 cycles		
		-34	-35	-36	-34	-35	-36	-34	-35	-36	-34	-35	-36
side 1	90	0	0	0	0	0	0	4	1	0	5	0	0
	90	0	0	0	0	0	0	0	0	0	0	0	0
	90	0	0	0	0	0	0	1	0	0	0	0	0
	90	d	d	d	d	d	d	d	d	d	d	d	d
side 2	90	0	0	0	0	0	0	3	0	1	2	0	0
	90	0	0	0	1	0	0	1	0	0	1	0	0
	90	0	0	0	2	0	0	3	1	0	3	2	0
	90	d	d	d	d	d	d	d	d	d	d	d	d
Average		0.00			0.02			0.12			0.11		
SD		0.00			0.09			0.22			0.22		

CROSSPLY P5-C		400 cycles		
		-34	-35	-36
side 1	90	4	0	0
	90	0	0	0
	90	1	0	0
	90	d	d	d
side 2	90	2	0	3
	90	1	0	0
	90	5	1	0
	90	d	d	d
Average		0.17		
SD		0.28		

Table A.11 (cont.)

QUASI P5-Q		0 cycles			50 cycles			150 cycles			300 cycles		
		-36	-37	-38	-36	-37	-38	-36	-37	-38	-36	-37	-38
side 1	90	0	0	0	1	0	1	0	0	1	0	0	2
	90	0	0	0	0	0	0	0	0	0	0	0	0
	90	0	0	0	0	1	0	0	2	0	0	2	0
	90	0	d	0	0	d	0	0	d	0	0	d	1
side 2	90	0	0	0	0	1	1	0	3	0	0	3	0
	90	0	0	0	0	0	0	0	2	0	0	1	0
	90	0	0	0	0	0	0	0	0	0	0	0	0
	90	0	0	0	1	0	0	1	2	0	1	5	0
Average		0.00			0.05			0.09			0.12		
SD		0.00			0.09			0.17			0.24		

QUASI P5-Q		400 cycles		
		-36	-37	-38
side 1	90	3	0	4
	90	0	0	0
	90	0	0	2
	90	1	d	1
side 2	90	0	3	1
	90	0	2	0
	90	0	0	0
	90	1	d	2
Average		0.12		
SD		0.24		

Table A.12: Accelerated thermal environment 1 damage data (PIXA-M isothermal specimens)

RESEARCH PM-R		0 cycles			50 cycles			150 cycles			300 cycles		
		-33	-34	-35	-33	-34	-35	-33	-34	-35	-33	-34	-35
side 1	90_4 group	0	1(2) 4(1)	0	7(1)	1(2) 11(1)	4(1)	12(1)	1(2) 13(1)	1(2) 8(1)	14(1)	1(3) 26(1)	1(2) 10(1)
side 2	90_4 group	1(1)	0	0	6(1)	5(1)	3(1)	11(1)	10(1)	6(1)	1(2) 14(1)	1(2) 18(1)	1(2) 8(1)
Group Avg.		0.00			0.00			0.00			0.00		
Group SD		0.00			0.00			0.00			0.00		
Aggr. Avg.		0.23			1.25			2.10			3.31		
Aggr. SD		0.47			0.70			0.58			1.35		

RESEARCH PM-R		400 cycles		
		-33	-34	-35
side 1	90_4 group	2(2) 19(1)	2(3) 1(2) 23(1)	2(3) 8(1)
side 2	90_4 group	1g 1(2) 14(1)	6(2) 26(1)	1g 1(2) 7(1)
Group Avg.		0.07		
Group SD		0.10		
Aggr. Avg.		4.56		
Aggr. SD		1.93		

Table A.12 (cont.)

CROSSPLY PM-C		0 cycles			50 cycles			150 cycles			300 cycles		
		-33	-34	-35	-33	-34	-35	-33	-34	-35	-33	-34	-35
side 1	90	0	1	7	7	18	21	19	46	24	24	53	27
	90	0	1	1	6	4	10	13	8	11	15	10	9
	90	1	1	1	6	4	4	7	6	5	8	6	5
	90	4	10	4	16	33	18	44	57	37	57	78	36
side 2	90	2	2	4	9	16	15	26	34	24	34	30	23
	90	0	1	3	4	6	5	9	15	7	10	12	7
	90	3	1	0	4	2	0	7	4	3	9	3	5
	90	12	4	3	32	27	22	62	62	52	82	43	47
Average		0.54			2.37			4.77			5.19		
SD		0.61			1.89			3.93			4.56		

CROSSPLY PM-C		400 cycles		
		-33	-34	-35
side 1	90	37	62	41
	90	15	9	16
	90	9	6	8
	90	73	75	50
side 2	90	45	53	41
	90	13	22	13
	90	10	6	10
	90	93	72	78
Average		7.38		
SD		5.50		

Table A.12 (cont.)

QUASI PM-Q		0 cycles			50 cycles			150 cycles			300 cycles		
		-34	-35	-X1	-34	-35	-X1	-34	-35	-X1	-34	-35	-X1
side 1	90	0	1	0	2	3	0	2	4	1	2	5	3
	90	1	1	1	1	1	0	1	3	3	2	8	3
	90	1	3	1	4	7	2	7	16	6	7	15	11
	90	0	3	1	4	5	4	7	16	9	9	16	14
side 2	90	2	0	2	3	1	1	4	1	3	4	1	6
	90	0	1	0	3	1	1	3	1	4	4	4	5
	90	1	0	4	5	0	5	6	2	7	6	2	8
	90	0	2	3	2	2	14	4	7	24	5	12	28
Average		0.23			0.58			1.16			1.48		
SD		0.23			0.59			1.10			1.20		

QUASI PM-Q		400 cycles		
		-34	-35	-X1
side 1	90	5	14	6
	90	4	18	6
	90	11	28	16
	90	12	24	31
side 2	90	7	4	6
	90	4	4	7
	90	7	4	17
	90	14	15	32
Average		2.15		
SD		1.74		

APPENDIX B

STAGE I TESTING EDGE DAMAGE DATA

Material	Layup	Ply Group	Crack density (/cm) at number of cycles shown					
			25	50	100	200	500	1000
R1-16	Quasi	90_2	0	-	0	0.4	0.4	9.4
R1-16	$[0_3/90_3]_s$	90_6	0.4	-	15.7	9.4	9.4	13
R1-16	$[+45/-45_2/+45/0_4/90]_s$	90_2	0	-	18.5	9.8	15.7	33.5
R1-16	$[+45/-45/0_2/90/0_2/-45/+45]_s$	avg. 90's	0	-	0	1.4	0.8	21.3
PETI-5	Quasi	90_2	0	0	0	0.4	0.8	5.1
PETI-5	$[0/90/0]_{2s}$	avg. 90's	0	0	0	0	0	0.4
PETI-5	$[+45/-45_2/+45/0_4/90]_s$	90_2	0	0	2.8	2.4	8.3	18.1
PETI-5	$[+45/-45/0_2/90/0_2/-45/+45]_s$	avg. 90's	0	0	0	3.0	16.1	17.3
K3B	$[+45/-45/90/0]_{4s}$	90_2	1.9	1.9	0.8	1.57	12.2	12.2
PIXA	$[0/90/0]_{2s}$	avg. 90's	0.6	7.1	4.4	0	0.6	1.0

APPENDIX C

CRACKOMATIC & MODCOD INPUTS

C.1 CRACKOMATIC INPUTS (PETI-5 & PIXA-M)

E_x	longitudinal ply modulus	(157.3 GPa)
E_y	transverse ply modulus	(9.7 GPa)
ν	major Poisson's ratio	(0.33)
G_{xy}	shear modulus	(4.20 GPa)
α_1	longitudinal ply CTE	(-0.7 με/K)
α_2	transverse ply CTE	(36.9 με/K)
T_o	laminate stress free temperature	(400°C)
ξ	shear lag factor	(0.6)

C.2 MODCOD INPUTS (based on PETI-5 data)

t	ply thickness	(0.125 mm)
D_i	moisture diffusivity	(1.108 mm^2/s)
Temperature Profile Description		(time, temperature, RH)

THESIS PROCESSING SLIP

FIXED FIELD: ill. _____ name _____

index _____ biblio _____

COPIES: (Archives) (Aero) Dewey Eng Hum

Lindgren Music Rotch Science

TITLE VARIES: ▶ ☐ _____

_____

_____

NAME VARIES: ▶ ☐ _____

_____

IMPRINT: (COPYRIGHT) _____

_____

COLLATION: 176 ℓ

_____

ADD: DEGREE: _____ ▶ DEPT.: _____

SUPERVISORS: _____

_____

_____ ___ _____

_____ ___ _____

_____ ___ _____

_____ ___ _____

_____ ___ _____

_____ ___ _____

_____ ___ _____

NOTES:

_____ cat'r: _____ date:

page: 535

▶ DEPT: Aero

▶ YEAR: 1998 ▶ DEGREE: [redacted] S.M.

▶ NAME: REYNOLDS, Tom George

_____